Università degli Studi di Cagliari

DOTTORATO DI RICERCA

Ingegneria Industriale

Ciclo XXVIII

TITOLO TESI

Study and achievement of organic-inorganic innovative materials through electrochemical techniques

Settore/i scientifico disciplinari di afferenza

ING-IND/25

Presentata da: Simone Rizzardini

Coordinatore Dottorato: Prof. Roberto Baratti

Tutor: Prof. Michele Mascia

Esame finale anno accademico 2014 – 2015

Study and achievement of organic-inorganic innovative materials through electrochemical techniques

Simone Rizzardini

Supervisor: Professor Michele MASCIA
University of Cagliari, Italy

Dottorato di Ricerca in Ingegneria Industriale
Università degli Studi di Cagliari
XXVIII Ciclo

Simone Rizzardini gratefully acknowledges Sardinia Regional Government for the financial support of her Ph.D. scholarship (P.O.R. Sardegna F.S.E. Operational Programme of the Autonomous Region of Sardinia, European Social Fund 2007-2013 - Axis IV Human Resources, Objective l.3, Line of Activity l.3.1.

Contents

Abstract

The functionalization of conductors and semiconductors using organic molecules is a very important issue in the development of novel organic/inorganic heterostructures suitable as materials in sensors, biosensors, clinical diagnostics, biological sensing and energy storage and conversion. In this context, to obtain a stable, durable bond with the surface and controllable process, the electroreduction of aryldiazonium salts is a promising alternative to conventional techniques (as Self Assembled Monolayer), also to ensure conductivity and homogeneity of the organic coating.
This work, focused on the achievement of innovative materials developed for a wide range of applications that include biosensors, energy storage and metal-free sensors, is divided in four main topics:

1. Polyaniline electropolimerization on gold surface
2. Polyaniline electropolimerization on nanoporous silicon surface
3. DNA immobilization on gold
4. Polyaniline electropolimerization on poly(3,4-ethylenedioxythiophene) polystyrene sulfonate

The common theme about the achievement of these devices is the functionalization of the metal or polymeric electrode base by means diazonium salt (4-nitrobenzenediazonium) electrochemical reduction, prior to further modification with polyaniline or DNA. All these functionalization are realized using electrochemical techniques: organic molecules are grafted on the electrode surface using cyclic voltammetry, as well as aniline electropolimerization. Furthermore, all electrode functionalization step are characterized by

Electrochemical Impedance Spectroscopy (EIS), which can give fast and useful information about the surface state.

In this thesis results of sensor functionalization and performance varying electrochemical parameter and preparation conditions are presented and discussed, giving a well-developed starting point for following applications.

Chapter 1

Overview of the Thesis

A summary of the thesis is given in this chapter, by showing how it is structured in different Chapters.
Furthermore, a list of publications in journals and conference papers and other activities of the author is presented.

1.1. Motivations

It is worth to emphasize that the material functionalization starts with 4-nitrobenezendiazonium salt grafting on the surface for all the studied devices. This allows a controllable surface coating and a stable bond between organic layer and metal or non-metal surface. We studied the development and performance of different devices for a specifically aim, that we are going to discuss in this chapter.

1. Polyaniline electropolimerization on gold surface

The most important characteristic of gold is its high stability over a wide potential range, thanks to which presents suitable properties for all electrochemical techniques. The interest in gold modification is of great relevance; in particular, the covalent bonding of small organic molecules, larger functional biomolecules and conducting polymers allow the development of novel hybridorganic/inorganic materials for bioelectronics, clinical diagnostics and biological sensing.
The main limit of this strategy is the short-term stability of the coating in environmental such water and air.
To solve this issue polymers can be used to introduce interfacial and functional properties to both microscopic and macroscopic objects.
Among different methods to functionalize the surfaces, the electrochemical reduction of aryl diazonium salts is a very versatile alternative to conventional techniques, which was firstly proposed in 1992[1,2]. This approach has been used to promote covalent bonds between aryl groups with different substituents and several substrates (e.g. gold). Another very promising polymer in this context is polyaniline (PANI): it has a potential use in a broad field because of its electronic and optical properties, reversible control of conductivity by charge-transfer doping and protonation, low cost and environmental stability.

2. Polyaniline electropolimerization on nanoporous silicon surface

Based on REN21 report, in 2014 19% of the total energy consumption were satisfied by renewables. Of this percentage, only 2% came from wind, solar, geothermal and biomass: as well known, photovoltaic energy has a large potential of exploitation, and for this reason many research groups are interested to invest and study new materials to reduce the actual high cost and increase the yield of photovoltaic panels. In fact, with the technology available today, big surfaces would be required to have a greater impact in the produced energy.
A promising material that can be used for photovoltaic and as supercapacitor is the Porous Silicon (PSi) coupled with organic molecules, with the aim to maximize the solar radiation adsorbed. In this work, we will investigate the effect in current density of polyaniline layers on Psi. The internal PSi surface is highly reactive and has a short-term stability, but can be stabilized with electrochemical, chemical oxidation or organic nano-coating.

3. DNA immobilization on gold

The development of electrochemical DNA biosensor is a important topic for applications in disease diagnosis, genome sequencing and other biological analyses, due to its cheap, rapid and easy operation if compared with traditional DNA diagnostic methods. Thiol-modified DNA SAMs are widely used for studying and designing DNA sensors; the electrode surface modification by means of the electrochemical reduction of aryl diazonium salts used as a linker could be a valid alternative thanks to its good stability and uniform coverage, as we introduced in the abstract.

In this topic the thesis is focused on the immobilization of different oligonucleotide lengths on the gold surface by means SAM or 4-nitrobenzendiazonium linking, and study if we can differentiate it with easy and fast electrochemical measurement like electrochemical impedance spectroscopy.
This chapter is partially result of my work at Ruhr Universität Bochum, under the supervision of Prof. Wolfgang Schuhmann.

4. Polyaniline electropolimerization on poly(3,4-ethylenedioxythiophene) polystyrene sulfonate

pH sensors are widely used in chemical and biological applications such as environmental monitoring (water quality), blood pH measurements and laboratory measurements. Conducting polymers are ideally suited for sensor applications because they not only exhibit high conductivity and electroactivity but they could also be used as a general matrix and can be further modified with other compounds in order to change selectivity. Furthermore, easy synthetization, lightweight and flexibility are some of the interesting characteristics of the conducting polymers, and they can be used instead of metals to make a metal-free device. In this work, we employed together poly(3,4-ethylenedioxythiophene) prepared using poly(styrenesulfonic acid) (PEDOT:PSS) and polyaniline (PANI) to assemble a new bi-layered all-organic electrode.

1.2. Summary

The Thesis is structured in five main chapters subdivided in paragraphs for each topic, in order to allow the reader to better follow the development of the research project. Electrochemical processes and techniques are reported in the Appendix.

A summary of this Thesis is shown in the following list, where a brief description of each chapter is given.

Chapter 2. A general overview of the electrodeposition of diazonium salts and aniline electropolymerization is given, focusing the attention on the deposited materials properties. This chapter introduces the reader from the basics of electrodeposition and electropolymerization.

Chapter 3. This chapter give an overview about all the procedures to obtain the experimental data used to study and characterize the processes investigated. Also the used devices are shower and discussed.

Chapter 4. Experimental results are presented, divided in the four main topics. Preparation and performance of the device will have wide discussion.

Chapter 5. This final chapter is for the conclusions.

Appendix. Electrochemical processes and electrochemical techniques used in this work.

1.3. Publications in Journal and Conference Papers

Some of the work present in this Thesis has been published in international journal papers, national and international congresses.

International Journal Papers:

A.Vacca, M.Mascia, S.Rizzardini, S.Palmas, L.Mais, *Coating of gold substrates with polyaniline through electrografting of aryl diazonium salts*, Electrochimica Acta (2014) 126:81-89

A.Vacca,, M.Mascia, S.Rizzardini, S.Palmas, S.Lai, C.Napoli, M.Barbaro, *Functionalization of Polycrystalline Gold Through the Electroreduction of Aryldiazonium Salts in Ionic Liquids*, Chemical Engineering Transactions (2014) 41:97-102

A.Vacca, M.Mascia, S.Rizzardini, S.Corgiolu, S.Palmas, M.Demelas, A.Bonfiglio, C.Ricci, *Preparation and characterisation of transparent and flexible PEDOT:PSS/PANI electrodes by ink-jet printing and electropolymerisation*, RSC Advances (2015) DOI: 10.1039/C5RA15295J

National and International Congresses and Conferences:

A.Vacca, M.Mascia, S.Rizzardini, S.Palmas, *Electrochemical preparation of Gold/Polyaniline electrodes through electrografting of diazonium Salts*, ISE 2013, Bochum (Germany), March 2013

S.Rizzardini, A.Vacca, M.Mascia, S.Palmas, M.Barbaro, *Electrochemical functionalization of polyethylene/gold substrates for sensor application*, 9th ECCE, Den Haag (The Netherlands), April 2013

S.Rizzardini, *Electrochemical functionalization of polycristalline gold surface: effect of the solvent*, GEI2013, Pavia (Italy), September 2013

S.Rizzardini, A.Vacca, M.Mascia, S.Palmas, L.Mais, *Electrochemical preparation of gold/polyaniline electrodes through electrografting of diazonium salts*, GEI2013, Pavia (Italy), September 2013

S.Rizzardini, A.Vacca, M.Mascia, S.Lai, D.Jambrec, W.Schuhmann, *Electrochemical characterization of oligonucleotides with different length grafted on gold electrodes*, 65th Annual Meeting of the International Society of Electrochemistry, Lausanne (Switzerland), September 2014

S.Rizzardini, A.Vacca, M.Mascia, S.Palmas, S.Corgliolu, *Electrochemical detection of oligonucleotides linked on gold electrodes by diazonium salts reduction*, XXIII International Symposium on Bioelectrochemistry and Bioenergetics of the Bioelectrochemical Society, Malmö (Sweden), June 2015

S.Rizzardini, A.Vacca, M.Mascia, S.Palmas, S.Corgliolu, *Electrochemical synthesis and pH detection performance of all-organic electrode based on bilayered pedot/pani polymers*, ECCE10, Nice (France), September 2015

Not yet published International Congresses:

G.Mula, M.Tiddia, S.Rizzardini, E.Sechi, S.Corgiolu, M.Mascia, A.Vacca, *pH-Switching Of Photocurrent In Polyaniline/Porous Silicon Hybrids Diffused Heterojunction, Porous Semiconductors,* Science and Technology PSST, March 6-11, 2016 Tarragona (Spain)

In addition to the work presented in this Thesis the author has also participated, during the course of the study, in other research projects:

International Journal Papers:

A. Vacca, M. Mascia, S. Palmas, L. Mais, S. Rizzardini, *On the formation of bromate and chlorate ions during electrolysis with boron doped diamond anode for seawater treatment,* Journal of Chemical Technology and Biotechnology (2013) 88:2244-2251

A. Vacca, M. Mascia, L. Mais, S. Rizzardini, F. Delogu, S. Palmas, *On the Electrodeposition of Niobium from 1-Butyl-1-Methylpyrrolidinium Bis(trifluoromethylsulfonyl)imide at Conductive Diamond Substrates*, Electrocatalysis (2014) 5:16-22

National and International Congresses and Conferences:

S.Palmas, M.Mascia, A.Vacca, S.Rizzardini, L.Mais, I.Nova, R.Matarrese, *PANI/TiO2 NT composite electrodes for possible applications in advanced energy conversion and storage devices*, 64th Annual Meeting of the ISE, Querétaro (Mexico), Sept. 2013

M.Mascia, A.Vacca, L.Mais, S.Palmas, S.Rizzardini, *Electrochemical behaviour of Nb, Ta, Zr, and W in pyrrolidinium based ionic liquid.*, 64th Annual Meeting of the International Society of Electrochemistry, Querétaro (Mexico), September 2013

M. Mascia, A. Vacca, S. Palmas, L. Mais, S. Rizzardini, F. Delogu, *Electrochemical deposition of Cu and Nb in Pyrrolidinium based Ionic Liquid for Multilayers preparation*, Multilayers'13, Madrid (Spain), October 2013

S. Palmas, A. Vacca, M. Mascia, S. Rizzardini, L. Mais, E. Musu, E. Mena and J. Llanos, *Synthesis and characterization of ordered TiO_2 nanostructures*, ELECTROCHEM 2013, Southampton (UK), September 2013

L. Mais, M. Mascia, A. Vacca, S. Palmas, Simone Rizzardini, Francesco Delogu, *On the electroreduction of Tantalum from 1-Butyl-1-Methylpyrrolidinium Bis(trifluoromethylsulfonyl)imide*, XXXV RGERSEQ-$1^{ST}E^3$, Burgos (Spain), July 2014

P.Ampudia, S.Palmas, A.Vacca, M.Mascia, L.Mais, S.Monasterio, S.Rizzardini, E.Musu, *Systematic investigation on the effect of the*

synthesis conditions on the performance of nanotubular structured electrodes, SiO_2 Advanced dielectrics and related devices, X International Symposium, Cagliari (Italy), June 2014

Chapter 2

Introduction

A general overview of the organic materials used to functionalize electrodes is given, focusing the attention on the chemical/physical properties.

2.1. Background

2.1.1 The role of diazonium salt in science

The development of hybrid organic/inorganic structures suitable in bioelectronics, clinical diagnostics and biological sensing requires a stable bond between the organic molecules and the surfaces of the conductors[1]. Among different methods to functionalize the surfaces, the electrochemical reduction of aryl diazonium salts is a very versatile alternative to conventional techniques, which was firstly proposed in 1992[2]. This approach has been used to promote covalent bonds between aryl groups with different substituents and several substrates such as glassy carbon, silicon and gold[3,4]. It is well established that the mechanism of the electrografting involves the electrochemical reduction of a phenyl-diazonium cation to form N_2 and the corresponding phenyl radicals, which react with the electrode surface leading to the attachment of phenyl group[5]. The electrochemistry about diazonium salts grafting will be better discussed in the next subchapter. Different operative mode (cyclic voltammetries, potentiostatic, galvanostatic) and several electrochemical parameters (scan rate, time of reduction) can be selected to control the surface coverage and the density of the resulting film, yielding submonolayer to multilayer films[6,7]. However, the formation of multilayer films was frequently observed due to the difficulties in a fine control of the quantity of material grafted to the surface[8]. Thus, also differents solvents for this reaction have been studied: usually the electrochemical reduction of diazonium salts is proposed in acetonitrile solution as aprotic solvent or in acidic aqueous solution as protic solvent. Recently also different ionic liquids have been tested for the electrochemical reduction of 4-nitrobenzendiazonium salts on glassy carbon[9,10] and graphene sheets[11] (Jin et al. 2009). Fontaine[12] showed that the surface

concentration of grafted 4-nitrophenyl groups decreases with the viscosity of the ionic liquid used in the deposition experiments.
In this work the electrochemical functionalization of polycrystalline gold through the electroreduction of 4-nitrobenzenediazonium salts has been studied using acetonitrile and ionic liquid 1-butyl-1-methylpyrrolidinium bis (trifluoromethylsulfonyl) imide as solvents. The 4-nitrophenyldiazonium was chosen to achieve this study because of the presence of nitro group which could be easily detected electrochemically.

2.1.2 Diazonium salts chemistry and electrochemistry[3]

Diazonium salts can be chemically prepared and grafted on a surface. Since we are working with electrochemistry in this thesis, this subchapter will be focused on the electrochemical grafting of diazonium salts, that is also the common used method in literature.
Aromatic diazonium salts ($ArN_2 + X^-$) are easily synthesized in an acidic aqueous medium (HBF_4) starting from an amine in the presence of $NaNO_2$, and in an aprotic medium (ACN + HBF_4 in ether) in the presence of t-butylnitrite or in ACN + $NOBF_4$[13,14]. As many aromatic amines are available commercially, the preparation of a large number of diazonium salts can be easily carried out. They can be isolated and characterized, but they can be used directly in the solution where they have been prepared[15].
The chemistry of aromatic diazonium salts[13,16,17] is dominated by the electrophilic character of the azo group; they react with aromatic amines and phenols to give azo dyes (C - coupling) that are important coloring materials[18]. Aliphatic diazonium salts are extremely unstable and up to now only a few examples of grafting on carbon black involving the diazonium salt of 2–aminoethanesulfonic acid and 4-bromobenzylamine have been reported[13,19].
As we can see below (Fig.1), when a diazonium reacts with a surface, with a few exceptions, the diazonium group is lost and the radical

reacts with the surface, therefore grafting involves a homolytic dediazonation step; in this respect the dediazonation reactions are important for discussing the grafting mechanism.

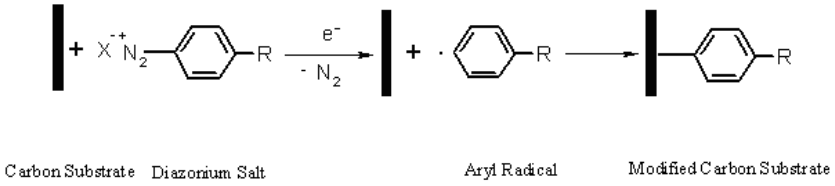

Figure 1 - Example of diazonium salt graftin on conductive surface

This dediazonation can take place heterolytically to give Ar^+ cations, or homolytically to give Ar radicals[20]; these spontaneous reactions can be slowed down by reducing the temperature to below 5°C.
Prior to the discovery of the electrografting reaction, the reduction of diazonium salts $ArN_2 + X^-$ had been investigated in an aqueous medium at mercury electrodes[21]. In an aqueous acidic medium two waves are observed (Fig.2); the first is a one electron wave, while the overall process involves four electrons on the second wave and leads to phenylhydrazine.

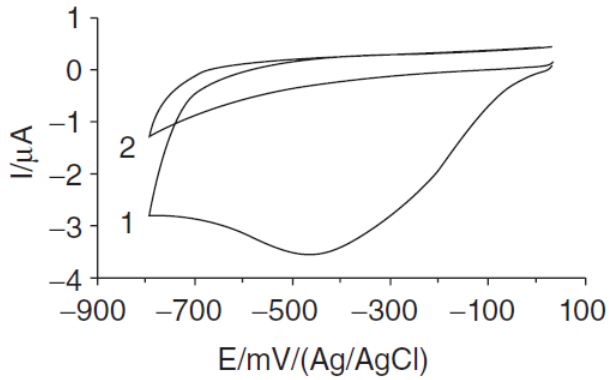

Figure 2 - Diazonium grafting Voltamograms

The involvement of radicals[22] during the electrochemical reduction (on the first wave) of aryldiazonium salts was also observed through the Pschorr synthesis of phenanthrene[23], and also by electron spin resonance (ESR) in ACN in the presence of a spin-trap[24].

Diazonium salt	Reduction potential, V vs SCE
4 - Nitrobenzenediazonium	+ 0.20
4 - Bromobenzenediazonium	+ 0.02
Benzenediazonium	− 0.06
4 - t - Butylbenzenediazonium	− 0.10
4 - Methylbenzenediazonium	− 0.16
4 - Diethylaminobenzenediazonium	− 0.56

Table 1 - Diazonium salts reduction potential

The involved steps in diazonium electrochemical grafting can be summarized in the following reactions a, b and c:

$ArN_2^+ + 1e^- \rightarrow Aryl + N_2$ (a)
$Surf + Aryl \rightarrow Surf\text{-}Aryl$ (b)
$Aryl + 1e^- \rightarrow Aryl^-$ (c)

The aryl radical is responsible for the grafting reaction, its formation and its further evolution are, therefore, important in the context of surface modification. By simulation of the voltammograms the reduction of the benzenediazonium cation is a concerted reaction, which means that, during the electrochemical reduction at the peak potential, there are no intermediates between the diazonium cation and the radical; this also means that the radical is formed directly on the surface, which is a very favourable situation for the grafting reaction[25]. This radical can be reduced, in turn, to an anion that is unfavorable for the grafting reaction. The reduction potential of Aryl has been measured not only by simulation of the voltammetric curves: $E = -0.64$ V vs SCE[25], but also from the number of electrons consumed at different potentials for the reduction of benzenediazonium, diphenyliodonium and triphenylsulfonium salts,

which all provide a phenyl radical upon reduction: E = − 0.95 V vs SCE[26].

The formation of the layer can be easily detected, as shown in Figure 2, through the disappearance of the reduction wave of the diazonium salt; chronoamperometry is also very characteristic, instead of a decrease in the current according to a Cotrell law, a very sharp decrease is observed due to the fast blocking of the surface.

Electrodeposition and other parameter such as scan rate, diazonium salt concentration in solution and solvent can be investigated, and the aim of this work is partially dedicated to study this behaviour.

Aryl diazonium salts were proposed with a wide range of substituent groups useful for surface functionalization, including biotin[27], carboxyl[28], and amine[29]. Among the aryldiazonium derivatives, 4-nitrobenzene diazonium (NBD) salts are probably the most used: since nitrophenyl groups are electroresponsive, their presence can provide a confirm of the success of the grafting reaction. Moreover, by measuring the charge associated with the electrochemical reduction of nitrophenyl groups it is possible to estimate the concentration of the molecules grafted on the surface[30]. The thesis report the results of an experimental study on the electrochemical preparation of PANI films onto polycrystalline gold surfaces through a three steps approach: a gold electrode was functionalized with 4-nitrophenyl groups by electrochemical reduction of 4-nitrobenzenediazonium salts in acetonitrile or ionic liquid media; the nitro groups were then reduced electrochemically to amines[30-32]. The grafting of aminophenyl moieties on gold allowed obtaining a layer similar to aniline, on the top of which the PANI can be electropolymerized. The preparation of electrodes modified with aminophenyl moieties can also be done by one-step procedures involving the direct reduction 4-phenylamino diazonium; due to its instability, the synthesis of diazo groups can be done in situ just before immobilization by a sodium nitrite reaction in acidic media with p-phenylenediamine[33]. Alternatively, several authors use a

multistep protocol to obtain functionalized surfaces in which the first step involves the reduction of 4-nitrobenzenediazonium tetrafluoroborate because it is one of the few diazonium salts that are stable at room temperature[34]. Nevertheless, the grafted layers resulting from the reduction of 4-nitrobenzendiazonium salts are poorly conducting, and once deposited, any electrochemical processes are hardly triggered on these modified surfaces: a second electrochemical step to reduce the nitro to amino groups can provide more conducting and reactive surfaces which can be exploited for the subsequent reactions.

2.1.3 Polyaniline chemistry and proprieties[35]

The electroconducting polymers, from its revolutionary discovery up to today attracts attention of researchers and scientific community, due to their physical-chemical proprieties and conseguently their application potential. Among numerous known electroconducting polymers, polyaniline (PANI) and its derivates are probably the most investigated. The reason of all this popularity, in both theoretical and practical aspects, is a consequence of its unique properties: existence of various oxidation states, electrical and optical activity, low cost monomer (aniline), red/ox reversibility, environmental stability etc.[36-38]. These different and important features seem to be promising in wide area of practical applications as: rechargeable power sources[39-41], sensors[42-46], magnetic shielding, electrochemical capacitors[47], electrochromic devices[48], corrosion protection etc.[49].
PANI is probably the first electroconducting polymer been discovered: in fact it was used for textile coloring one century ago[48-50]. The great interest in research of polyaniline is connected to discovery of its conductivity in the form of emeraldine salt and existence of different oxidation forms, with different characteristics[36].

Polyaniline is commonly obtained by chemical or electrochemical oxidative polymerization of aniline[51,52] although photochemically initiated polymerization[48] and enzyme catalyzed polymerization were also reported[53,54].

In this study, polyanilne is obtained by electrochemical polymerization and deposited on the electrode. Electrochemical polymerization of aniline is routinely carried out in strongly acidic aqueous electrolytes (usually nitric acid or chloridric acid), through generally accepted mechanism which involves formation of anilinium radical cation by aniline oxidation on the electrode[55].

This process is proved to be auto-catalyzed[56], and the experimental conditions, such as: electrode material, electrolyte composition, dopant anions, pH of the electrolyte etc., all have strong influence on the nature of the polymerization process[57-59].

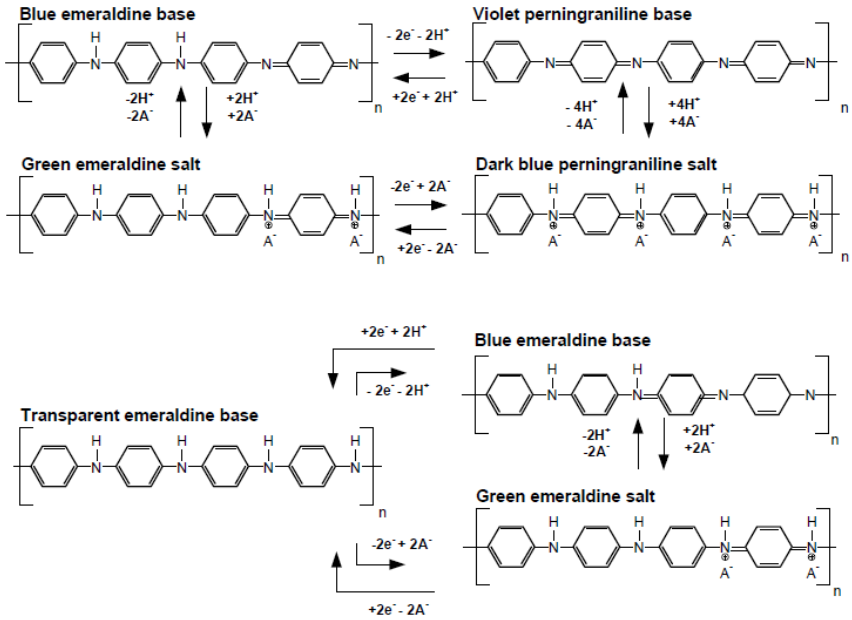

Figure 3: PANI forms and reversibility[35]

The low pH is almost always needed for preparation of the conductive polyaniline in the form of emeraldine salt, since it is

evidenced that at higher pH, the deposited film is consisted of low chain oligomeric material[52]. The doping anion incorporated into polymer usually determines the morphology, conductivity, rate of the polyaniline growth during electrochemical polymerization, and has influence on degradation process[58-60].

The electrochemical polymerization of aniline is practically always carried out in aqueous electrolytes, even if organic solvents as acetonitrile and ionic liquid were investigated although polymerization in organic solvents such is acetonitrile was also

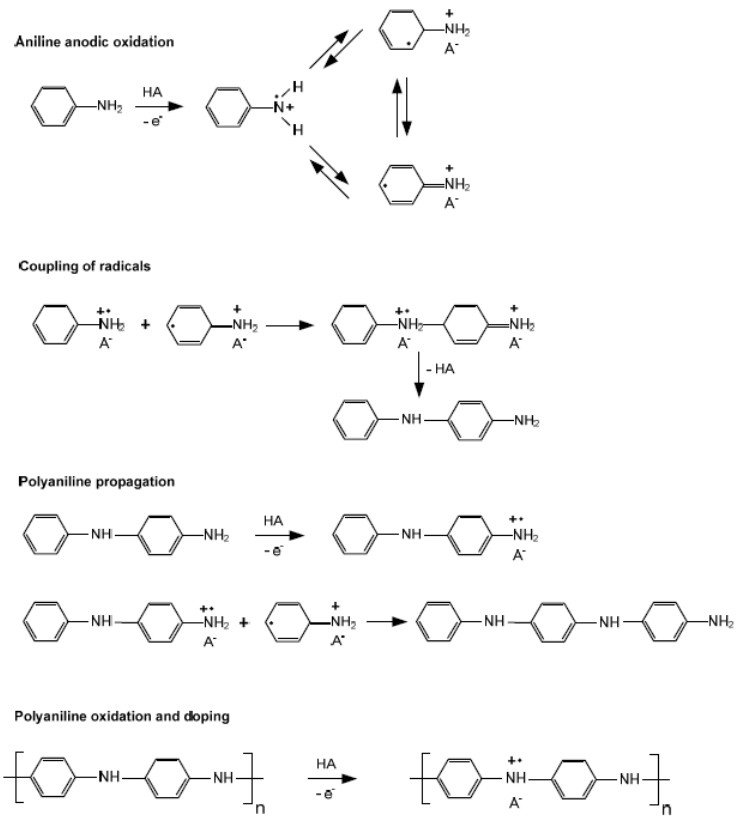

Figure 4: Electrochemical polymerization of aniline mechanism[35].

reported. In this work, e.g., we will need to electropolymerize aniline using acetonitrile to modify porous silicon electrodes: in fact water surface tension is too high to permeate inside the silicon pores.
Finally, electrochemical polymerization and co-polymerization of numerous substituted aniline derivates, resulted in polymer materials with properties different from the parent polymer, were also investigated[61,62].
Unlike other know electroconducting polymers, polyaniline can exist, depending on degree of oxidation, in different forms, known as: leuoemeraldine, emeraldine and perningraniline (Figure 3).
Leucoemeraldine, e.g. leucoemeraldine base, refers to fully reduced form; emeraldine, e.g. emeraldine base, is half-oxidized, while perningraniline, eg. perningraniline base, is completely oxidized form of polyaniline.
The only conducting form of polyaniline is emeraldin salt, obtained by doping or protonation of emeraldine base[63,64].
In Figure 4 we can see the schematic sketch about the steps involved in aniline electrochemical polymerization.
Apart from the changes in oxidation levels, all the transitions among polyaniline forms are manifested by color and conductivity changes[65]. The conducting protonated emeraldine in the form of green emeraldine salt, obtained as a product of electrochemical polymerization of aniline in acidic electrolytes, can be easily transformed by further oxidation to fully oxidized dark blue perningraniline salt (non-conductive form), which can be treated by alkali to form violet perningraniline. Emeraldine salt can also be reduced to transparent leucoemeraldine, or can be transformed by alkali to blue non conducting emeraldine. The two blue forms of polyanilne, perningranilne salt and emeraldine have different shades of blue[65]. Both reduction of emeraldine salt to leucoemeraldine and oxidation to perningraniline states are followed by decrease in conductivity[52].

2.1.4 The Role of PANI in energy topic

Discussing about PANI in the previous subchapter, we said the polymer is suitable also for energy storage device. Over the last few years, hybrid nanocomposite materials were used for improving electrical and optoelectronic properties of several kind of devices, e.g. light emitting devices, solar cells, sensors and biosensors[66]. There is an ongoing intense research[67-69] for cost-effective Si-based light emitting devices, which is hampered by the indirect band gap of silicon. Most often the search for a viable solution has led to hybrid materials whose fabrication and characterization, however, imply complex and costly techniques[70]. A more promising way seems to be to cancel the need of integrating different materials by looking for efficient Si-based light-emitting structures[67-69]. Rare earth doping of Si is a very promising technique to obtain light emission at 1.5 m from silicon[71-73]. However, most research activity in this field has been devoted to the characterization of the doped layers more than to the doping process itself. This is particularly unfortunate when the material to be doped is porous silicon (PSi), because the large internal surface of porous materials makes the doping process quite complex. In this work, we prepared various nanostructured PSi-based heterojunctions by coupling PSi with polyaniline, which is a *p*-type conductive polymer[74]: PSi-PANI interface has already been reported as a rectifying *p-n* junction[75]. Before the impregnation, the inner PSi pores surface was functionalized by the electroreduction of 4-nitrobenzenediazonium salt (NBD).
As we saw in the PANI subchapter, emeraldine salt (protonated form) and emeraldine base (deprotonated form) can be obtained by a doping/dedoping process: in this work we have studied the effects in photocurrent for PANI/PSi when PANI is present in the two forms.

2.1.5 The role of PANI and PEDOT polymers in biosensors/sensors topic

In the field of sensors/biosensors gold surfaces are often used as substrate to functionalize. The reason of this wide use of this precious metal is relational of its suitable properties for all electrochemical techniques due to its high stability over a wide potential range.
The possibility to obtain rods and films as well as to micromachining and photopatterning makes gold one of the most used substrates for transducer in electrochemical biosensors[76]. The interest in gold modification is of great relevance; in particular, the covalent bonding of small organic molecules, larger functional biomolecules and conducting polymers allow the development of novel hybridorganic/inorganic materials for bioelectronics, clinical diagnostics and biological sensing[77]. However, the strategies used to immobilize the biomolecule of interest often lead to short-term stability of the coating in water and air, which can limit the full implementation of these materials. Several methods have been devised and employed to allow surface conjugation including photolithography[76], Self-Assembled Monolayers (SAMs)[78] and electropolymerization[79].
Hence, surface grafting of polymers is an important process to introduce interfacial and functional properties to both microscopic and macroscopic objects[80]. Among various conducting polymers, polyaniline (PANI) has a potential use in a broad field because, as we saw, of its electronic and optical properties, reversible control of conductivity by charge-transfer doping and protonation, low cost and environmental stability[81-83]. In the last two decades the researches have explored the possible applications of PANI in capacitors and supercapacitors, solar cells, ion and gas sensors[56,84].
Moreover, the PANI presents extensive amount of amine groups, which are positively charged in aqueous cell culture medium, thus offering electrostatic anchoring points for cells with negative-

charged surfaces[85]. These properties lead to an extensive field of application in bioelctrochemistry, for preparation of electrochemical biosensors[86,87], cellular adhesion[88] and tissue engineering[89]. Composite scaffolds of PANI with gelatin were fabricated by Li et al. to support the proliferation of H9c2 rat cardiac myoblasts[88].
The electrical stimulation of nerve stem cells on electrospun poly-l-lactide PLLA/PANI scaffolds was also studied[90]. The PANI is a biocompatible conductive, so that polyaniline coating may provide suitable biointerfaces for enhancing cell electrode communication, such as in patterning and recording functionalities of nervous systems[91].
Moreover, the properties of the conductive polymer may be tailored by surface modification and biomolecular immobilization[92,93]. Electropolymerization is a well-known and affordable technique for the synthesis of PANI: the process is initiated by the anodic oxidation of aniline to cation radicals[94]. The electrochemical growth and redox mechanisms of PANI have been widely studied[95,96]: it is well recognized that the redox transitions occur simultaneously with the exchange of ions, compensating the excess charge within the polymer[97]. An important issue when the electropolymerization is intended for coating of surfaces, may be constituted by the weak adhesion between the organic layers and the substrates of different nature: as it was reported in the literature, the lack of strong interfacial bonding may result in the collapse of a PANI/carbon nanotubes structures[98]. The surface modification by grafting organic molecules on the substrates through a stable covalent bond may represent an effective way to improve the interfacial bonding[99].
The electrochemical reduction of diazonium derivatives is an elegant and versatile technique for surface functionalization.
This approach has several advantages including easy surface modification, wide potential window for subsequent electrochemistry and high stability under long term storage in air[26]. Moreover, by tuning the experimental conditions it is possible to

control the surface coverage and the density of the resulting film, yielding submonolayer to multilayer films[1].

The electrodeposition of PANI using an under-layer obtained by electroreduction of aryl diazonium has been proposed by Santos et al.[99], who demonstrated that a thin layer of diphenyl aminegrafted on glassy carbon electrodes prior to PANI electropolymerization allowed to improve the chemical stability of composite under high temperatures and ultrasonication. A similar approach has been adopted by Pilan et al. to obtain PANI/carbon nanotubecomposites using an under-layer of aminophenyl moieties[100]: sample prepared by 10 cycles of electropolymerization showed electrochemical behaviour similar to that of PANI simply electrode-posited on CNTs electrodes, but exhibited significantly improved stability and higher capacitance values. Searching in literature, only in a very recent work the modification of gold by grafting benzendiazonium salt as under-layer has been studied; however the conducting polymer electrodeposited was poly(para-phenylene). PANI film properties, such as resistance and capacitance, depend on the thickness of the film, which in turn depends on the number of electropolymerization cycles.

We made PANI films with different thickness by cycling the potential with different numbers of cycles.

Cyclic voltammetries and electrochemical impedance spectroscopies were used to characterize the electrodes. The morphology of the PANI film was also characterized by Scanning Electron Microscopies. As a comparison, gold electrodes with different thickness of PANI were prepared by direct electropolymerization and were characterized through the same techniques.

Along conducting polymers like PANI, also poly(3,4-ethylenedioxythiophene) (PEDOT) presents very interesting properties including high electrical conductivity, environmental stability, and high transparency[101,102], so that it has been proposed for different electronics applications, such as organic photovoltaic

devices (OPVs)[103] and organic light emitting diodes (OLEDs)[104]. Moreover, PEDOT could be patterned by inkjet printing technique, which is a low-cost, simple, easy method to fabricate flexible devices[105]. Since PEDOT is not soluble in water, aqueous inks are usually prepared using poly(styrenesulfonic acid) (PSS): the formation of the polyelectrolyte complex of PEDOT:PSS enhances the dispersibility of particles in water[106]. The conductivity of the film depends on the ratio of PEDOT to PSS as well as on the size of the PEDOT:PSS particles dispersed in water; however, the pristine films present a very low conductivity (<1 S cm^{-1}) to be used as electrode material[107]. Several authors attribute the low conductivity of the PEDOT:PSS films to the formation of coil structures, in which PEDOT is surrounded by PSS, in a discontinuous granular system with low interconnections between the particles[101,106].

To overcome this drawback, different compounds have been added during the preparation: noticeable increasing in conductivity (up to 2 or 3 orders of magnitude) has been obtained by using surfactants[108], graphene oxide[106,107] or polar solvents[108] which can change the pristine structure. For example, by using ethylene glycol (EG) the de-doping process can partially remove the amorphous and insulating PSS phase improving the conductivity up to 467 S cm^{-1} [109].

Another strategy is the combination of PEDOT:PSS with other conducting polymers, which can allow obtaining hybrid organic systems with tuneable properties: in particular polyaniline (PANI) presents very attractive characteristics including high conductivity and high active surface due to its porous structure. As we discussed, PANI is generally synthesized by chemical or electrochemical oxidative polymerisation of the monomer in acidic aqueous medium: however, the electrochemical polymerisation allows to a better control of the synthesis parameters.

PANI can be easily combined with anionic polymers and polyelectrolytes to form layer-by-layer constructions: the formation of multi-layered complexes of PANI with negatively charged

components can enhance the redox activity of the polymer at higher Ph[110]. Combinations of different conducting polymers can allow obtaining composites which present novel proprieties and unique structures[111]. Composites based on PEDOT:PSS and PANI have been prepared following different strategies allowing to obtain powders or multilayer composites. Zhang and coworkers prepared PEDOT/PANI bilayer nanofibers by subsequent oxidative polymerization of the parent monomers in bulk solution: the obtained nanofibers were used as electrode after a drop-cast onto a glassy carbon[112]. Bilayered nanofilms of PEDOT/PANI have been synthetized by Shi and coworkers by electrochemical polymerization of PANI in a mixed alcohol solution on PEDOT:PSS nanofilm electrode prepared by spin coating of PEDOT:PSS/5% DMSO on glass[113]. Similarly, the same group prepared bylayered PEDOT/PANI electrodes starting form electrodes based on single-walled carbon nanotubes and PEDOT:PSS spin coated on glass[114]. We assembled a flexible and transparent fully organic hybrid electrodes, prepared by ink-jet printing of PEDOT:PSS on Polyethylene Naphtalate (PEN) substrates followed by electrochemical polymerisation of PANI. This approach conjugates the ink-jet printing technique, which is a lowcost and easily scalable method to obtain flexible devices with the electrochemical polymerization which allows a good control and adhesion of the PANI layer on PEDOT:PSS. In the results chapter, we will also discuss the device performance.

2.1.6 Diazonium salts in oligonucleotides chains sensors

A vast number of strategies for nucleic acid determination have emerged[115,116]. Today, DNA sensors and gene chips are capable of high throughput DNA analysis for applications such as sequencing, genetic diagnosis[117], drug phenotyping, computing and gene expression analysis.

A DNA sensor commonly consists of a single-stranded DNA probe grafted at a transducer surface which is used as the recognition layer for hybridization of a complementary DNA target strand. This recognition process caused by the formation of Watson–Crick base pairs through multiple hydrogen bonds is then converted into a measurable signal. Evidently, for these types of DNA sensors the signal transduction process has to be capable of differentiating between single-stranded (ss) and double-stranded (ds) oligonucleotides at the interface. This is commonly achieved by the use of hybridization indicators or through changes in the physico-chemical properties of the sensing layer induced by the complementary binding event. The main challenge, however, is to define the optimum conditions for maximum hybridization efficiency in order to obtain a highly sensitive DNA assay.

Hence, the development of electrochemical DNA biosensor is a very important topic for applications in disease diagnosis, genome sequencing and other biological analyses, due to its cheap, rapid and easy operation if compared with traditional DNA diagnostic methods. Thiol-modified DNA SAMs are widely used for studying and designing DNA sensors; the electrode surface modification by means of the electrochemical reduction of aryl diazonium salts used as a linker could be a valid alternative, again to its good stability and uniform coverage.

In this thesis, the results of the electrochemical preparation of polycrystalline gold electrodes modified with different oligonucleotide chains are discussed. Following the main topic of the presented work, the surface functionalization was done by electroreduction of 4-nitrobenzenediazonium salt (NBD).

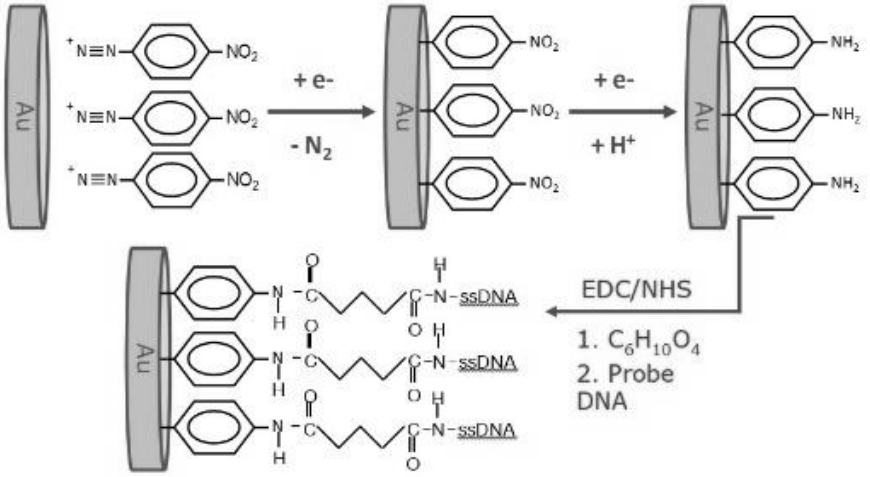

Figure 5: Steps involved in ssDNA immobilization

Afterwards, coupling agents EDC/NHS were used to bind adipic acid to the amino phenyl groups. In the same way, the probe oligonucleotides were immobilized on the modified electrode surface (Figure 5).

Different target oligonucleotide sequences were finally hybridized at the modified electrode and characterized with Electrochemical Impedance Spectroscopy.

Chapter 3

Materials and methods

This chapter is overview of all the procedures to obtain the experimental data and characterize the samples used to study the processes investigated. Along the techniques, also an explanation about the device performance measurements is developed.

3.1. Experimental methods

3.1.1. Materials and Chemicals

Anhydrous acetonitrile (ACN, 99.8%), 1-butyl-1-methylpyrrolidinium bis (trifluoromethylsulfonyl) imide (ionic liquid, [BMP][TFSA]), 4-nitrobenzenediazoniumtetrafluoroborate and tetrabutylammonium hexafluorophosfate ($TBAPF_6$), Hexaammineruthenium(III) chloride ($Ru(NH_3)_6Cl_3$), N-(3-Dimethylaminopropyl)-N′-ethylcarbodiimide (EDC) and N-Hydroxysuccinimide (NHS) were purchased from Sigma–Aldrich®. Nitric acid, sulfuric acid, potassium ferrocyanide ($K_4Fe(CN)_6$), potassium ferri-cyanide ($K_3Fe(CN)_6$), potassium dihydrogenophosphate (KH_2PO_4), di-potassium hydrogenophosphate (K_2HPO_4) and potassium nitrate were supplied by Carlo Erba. Pure ethanol was obtained from VWR. Aniline was freshly distilled and stored in the dark. The aqueous solutions were prepared with double-distilled water (18 MΩ cm).

Probe and target DNA used for oligonucleotides length detection were supplied by Sigma-Adrich and are represented in the picture below (Fig 5):

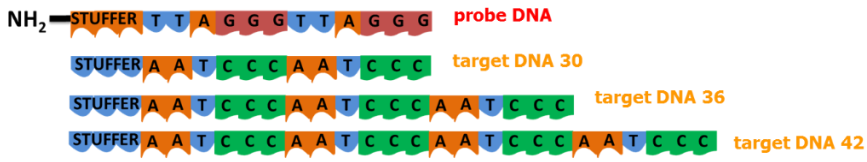

Figure 6 - Probe and target DNAs

Working Electrodes

Gold electrodes used for the studies are 2 mm diameter gold rods (CH instruments). Before every experiment working electrodes were mechanical polished with wet diamond particles (sizes: 3, 1, 0.5 μm)

and colloidal silica gel (particles size: 0.05 μm), each for 5 minutes on polishing cloths and rinsed with triple-distilled water.
Afterwards, 10 voltammetric cycles (-0.45/1.4 V vs SCE, scan rate 100 mV/s) in 0.1M phosphoric buffer were done to additional cleaning and roughtness factor evaluation. The electrodes were then rinsed again with triple-distilled water.

Porous Silicon electrodes (PSi) were prepared by electrochemical etching of highly phosphorous-doped Si wafers from Siltronix[118]. The PSi anodization was carried out in an etching solution composed by HF:H_2O:EtOH in a 15:15:70 proportion, respectively, using a current density of -50 mA/cm^2 [118]. Geometry are circular with 1 cm of diameter.

The PEDOT:PSS electrodes are fabricated on a Poly(ethylene 2,6-naphthalate (PEN) substrate, 125 μm thick. Substrates are cleaned by subsequent 10 min of ultrasonic bath in water and in acetone; they are washed in deionized water, dried under nitrogen flow and then activated by means of a plasma treatment (10 sec at 100 W). The PEDOT:PSS layer is realized by ink-jet printing using the Fujifilm Dimatix Material Printer (DMP) 2800. The ink is prepared by sonicating for 20 minute a solution made of PEDOT:PSS (pH 500 provided from H. C. Starck). Three layers are printed by using three nozzles of a DMC-11601 cartridge (each nozzle generates 1 pL drop of ink) with a drop spacing of 15 μm. During printing, substrates are kept at 45°C to facilitate the solvent evaporation. After printing, samples are annealed in an oven at 130°C for 15 min. After annealing, ethylene glycol is deposited by spin coating and dried in an oven at 130°C for 15 min. These electrodes are denoted as PEDOT:PSS (see figure 1). Active surface is about 0.75 cm^2.

3.1.2. Electrochemical set-up

All electrochemical experiments and characterization were performed at room temperature using an AUTOLAB PGSTAT302N

(Metrohm, Switzerland) potentiostat/galvanostat equipped with a frequency response analyzer controlled with the NOVA software. A conventional three-electrode cell (V = 10 ml) was used in which Saturated Calomel Electrode (SCE) was the reference and Pt wire was used as counter electrode. The working electrodes are described in the previous subchapter.

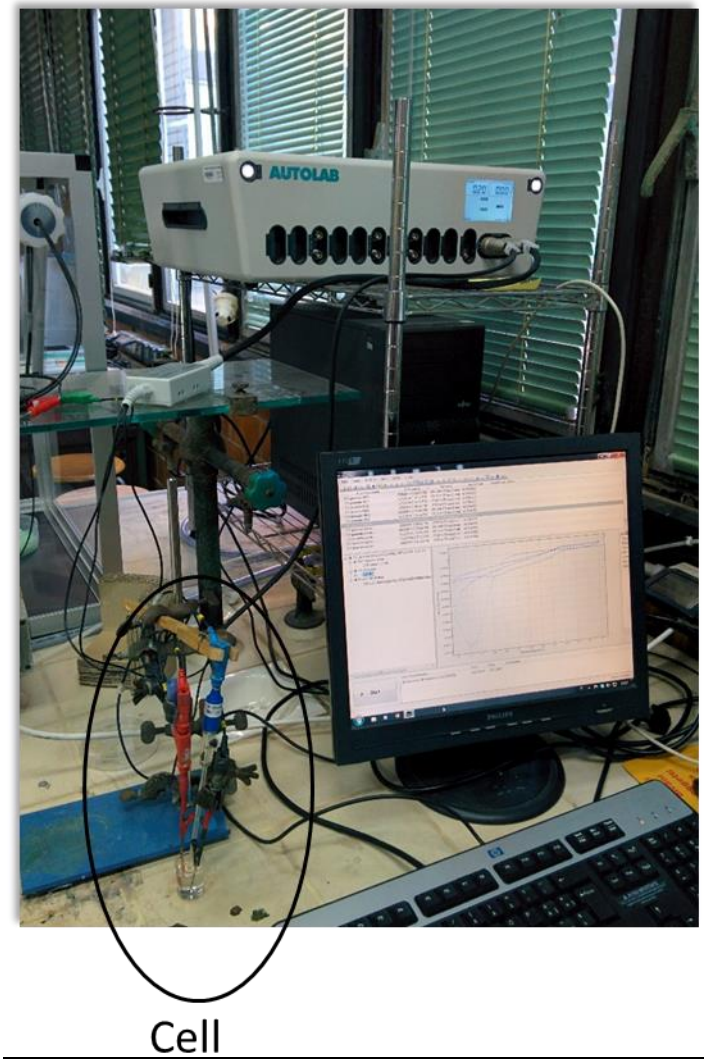

Figure 7: Electrochemical setup

3.2. Electrochemistry

Prior to modification, gold electrodes were manually polished with water and acetone on a cloth polishing pad and then submitted to 70 voltammetric cycles (−0.45/1.4 V, scan rate 100 mV/s) in 0.2 M phosphate buffer at pH 7. The electrodes were then rinsed with double-distilled water. Freshly polished electrodes were modified in ACN + 0.1 M ($TBAPF_6$) solutions containing 1 or 2 mM NBD, by consecutive CV in the potential range 0.6/−0.15 V vs SCE at scan rate of 10-100 mV/s, or between -0.65/0.55 V vs SCE when ionic liquid [BMP][TFSA] is used. Electrochemical reduction of nitro group to amino group was performed by cyclic voltammetry in water/ethanol solutions (90/10%$_V$) containing 0.1 M of KCl; the potential was varied from the open circuit potential to −1.2 V/SCE and back to 0.2 V/SCE. Scan rate was 100 mV/s. The aminophenyl modified electrodes are denoted as Au/NH_2. Polyaniline was electropolymerized on either bare gold or Au/NH_2 electrodes from aqueous solutions of aniline (0.1 M) and HNO_3 (1 M). Electropolymerization was performed by cyclicvoltammetries from 0 to 0.95 V with a scan rate of 100 mV/s. Different numbers of cycles were used to obtain PANI films with different thickness. The electrodes obtained by electropolymerization on bare gold are denoted as Au/PANI, while the electrodes obtained by electropolymerization on aminophenyl modified gold are denoted as Au/NH_2/PANI. After electropolymerization the electrodes were sonicated for 10 min in double-distilled water in order to test the stability of the bonded compounds.

The electrodes were characterized after each step of modification by electrochemical impedance spectroscopy: the frequency was varied from 30 kHz down to 0.1 Hz. Solutions containing $Fe(CN)_6^{3-}$/$Fe(CN)_6^{4-}$ 1 mM in phosphate buffer 0.2 M pH 7 or H_2SO_4 0.1 M were used; the EIS were carried out at 0.23 V or at the open circuit potential (OCP). Scanning electron microscopy (NOVA600,

Nanolab dual beam) was used to characterize the structures of PANI on the electrodes prepared with the different approaches. Focused ion beam (FIB) was also used to very precise cross sections of samples for subsequent imaging via SEM. The nitrophenyl and aminophenyl modified gold electrodes were characterized using an attenuated total reflectance Fourier transform-infrared (ATR/FTIR, NICOLET iN10MX) spectrophotometer, equipped with a micro-ATR germanium tip. Spectra were recorded at room temperature in the range 800–3200 cm^{-1}. The spectra of the bare gold were subtracted from the sample ones.

The PEDOT:PSS electrodes are fabricated on a Poly(ethylene 2,6-naphthalate (PEN) substrate, 125 μm thick. Substrates are cleaned by subsequent 10 min of ultrasonic bath in water and in acetone; they are washed in deionized water, dried under nitrogen flow and then activated by means of a plasma treatment (10 sec at 100 W). The PEDOT:PSS layer is realized by ink-jet printing using the Fujifilm Dimatix Material Printer (DMP) 2800. The ink is prepared by sonicating for 20 minute a solution made of PEDOT:PSS (pH 500 provided from H. C. Starck). Three layers are printed by using three nozzles of a DMC-11601 cartridge (each nozzle generates 1 pL drop of ink) with a drop spacing of 15 μm. During printing, substrates are kept at 45°C to facilitate the solvent evaporation. After printing, samples are annealed in an oven at 130°C for 15 min. After annealing, ethylene glycol is deposited by spin coating and dried in an oven at 130°C for 15 min. These electrodes are denoted as PEDOT:PSS. The electrodes obtained by electropolymerisation on PEDOT:PSS are denoted as PEDOT:PSS/PANI (see figure 1). The electrodes were characterized by cyclic voltammetries (CVs), electrochemical impedance spectroscopies (EIS) and open circuit potential (OCP) measurements in solution with different pH. EIS were performed in solution with different pH.

The impedance spectra were then fitted to an equivalent electrical circuit by using the software ZSimpWin 2.0 (EChem software). Scanning electron microscopy (NOVA 600, Nanolab dual beam) was used to characterize the structures.

Electropolymerization of PANI in PSi electrodes

PANI/PSi hybrid structures were obtained by three electrochemical steps. In the first step PSi electrodes were functionalized by electrochemical reduction of NBD salts (2 mM) in acetonitrile media. The first cycle of deposition of NBD shows a cathodic peak related to the reduction of the diazonium group; in the second the displacement of the cathodic peak, as well as a decrease of the recorded current, are indicative of the progressive covering of the PSi surface. Further potentiostatic reduction of NDB was performed and then the cyclic voltammetries (CV) were repeated until the reduction peak is no more visible: this indicates that all the accessible surface of PSi is functionalized. In the second step, the nitro groups were electrochemically reduced to amino groups in a water/ethanol solution through CV by cycling the potential from the open circuit potential to -1.7 V. Finally, the polymerization of aniline was electrochemically performed by cyclic voltammetry (CV) in a solution containing perchloric acid (0.1 M) and aniline (0.1 M). Since acetonitrile presents a surface tension of 26 mN/m (25°C), comparable to 21.5 mN/m of Ethanol, the electropolymerization has been performed in acetonitrile to ensure an easy penetration of the solution inside pores. The number of CV cycles for the PANI deposition has been determined as the maximum number of cycles before the formation of a clustering of the polymer (visible by the naked eye as a surface roughness) on the external surface of PSi that leads to a decrease of the measured photocurrent value.

Photocurrent measurements

Porous silica sample were submitted to photocurrent measurament to evaluate the device efficiency. Samples were covered with a sputtered semitransparent gold contact, and a tungsten lamp beam were focused on surface. The photocurrent measurements were performed using a series of long-pass filters.
In order to evaluate the reversibility between the two PANI forms, the samples have been dipped first in a basic solution (acetonitrile containing 0.1 M NH3; pH=9) and then in an acid solution (acetonitrile containing 0.1 M $HClO_4$; pH=4). It is important to remember that we are starting from a *p*-type PANI protonated form, since it was polymerized in acid media. After each dipping step, the photocurrent was recorded.

DNA quantification

DNA quantification were done following literature procedures[119-121], starting from the relation:

$$\Gamma_{DNA} = \Gamma_0 \left(\frac{z}{m}\right) N_A$$

Where Γ_{DNA} is the ssDNA surface density in molecules/cm^2, m is the number of bases in ssDNA, z the charge of the redox molecule (3), N_A Avogadro's number and Γ_0 is the amount of redox marker confined near the electrode surface. This last value was measured by means chronocoulometry using ruthenium haxaammine (3+/2+) 100 mM as redox marker, according with the equation:

$$\Gamma_0 = \frac{Q - Q_{dl}}{nFA}$$

Where n is the number of electrons per molecule for reduction, F the Faraday constant, A the effective electrode area, $(Q-Q_{dl})=\Delta Q$ the difference of charge in presence and absence of the redox marker.
The chronocoulometry experiments were performed in phosphoric buffer (PB) and 100 mM ruthenium haxaammine (3+/2+) 100 mM in PB after 30 minutes of argon bubbling to avoid the oxygen presence, both at potential of 0.2 V for 0.5 seconds and then switched at -0.35 V for 0.5 seconds. Results were represented in charge vs square root of time plot in order to calculate Q and Qdl values, extrapolated from curves to determine the intercept at t=0.
ssDNA surface density, as a reference, is compared with values reported in literature[119-121].

3.2.1. Cyclic voltammetry

Electrochemical measurements were carried out using a Metrohm Autolab 302N potentiostat-galvanostat controlled by NOVA software (Metrohm, Switzerland).

Cyclic voltammetries were started from the open circuit potential (OCP) in the negative direction at different potential windows, at different scan rates when specified. In order to avoid ion concentration gradients in the electrolyte, the solution was magnetically stirred prior to each scan.

Figure 8: Autolab 302N potentiostat-galvanostat controlled by NOVA software (Metrohm, Switzerland).

3.3. Surface and structure analysis

Different analytical techniques, such as scanning electron microscopy and Raman Spectroscopy were used to analyse the electrodeposited layers on the substrate.

3.3.1. Scanning electron microscopy

In collaboration with Dr. Elodia Musu and Dr. Simona Podda from Sardegna Ricerche (Pula), a high resolution Scanning Electron Microscopy (SEM) equipped with Energy Dispersive X-Ray (EDX) detector (Zeiss, Germany) was employed to investigate the surface morphology of some modified samples, with focus on the deposited films to obtain information about the deposited layers.

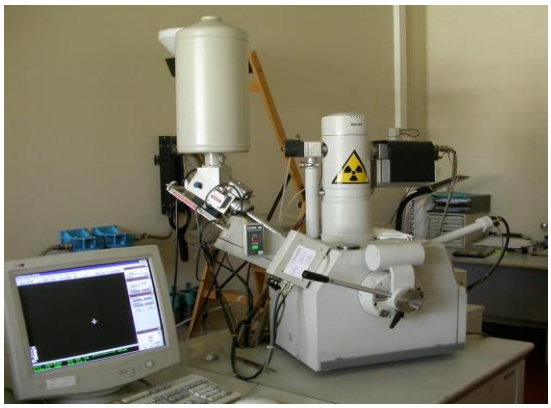

Figure 9: Scanning Electron Microscopy (SEM) equipped with Energy Dispersive X-Ray (EDX) detector (Zeiss, Germany).

Focused ion beam (FIB) was used to very precise cross-sections of a sample for subsequent imaging via SEM, in particular to evaluate the layers thickness.

Focused ion beam (FIB) was also used to very precise cross sections of samples for subsequent imaging via SEM. Raman measurements were performed in air at room temperature with a compact

spectrometer BWTEK i-Raman Ex integrated system, excitation wavelength at 1064 nm (provided by a Nd:YAG laser), in back scattering geometry. The spectra were collected with very low power beam (< 5 mW) focalized in 1 mm2 through a microscope objective Olympus x20 to avoid any heating or photodegradation effect. The threshold to observe the photodegradation of the sample (pure polyaniline) was observed for beam power higher than 15 mW.

Chapter 4

Results and discussion

This Chapter shows all the experimental results obtained for all the hetorogenous materials achieved, focusing the attention on the performance varying the grafting conditions.

4.1. Introduction

Electrochemical conditions of electrodes functionalization are key factors in controlling the grafted organic layers and they will affect the device performance. We will discuss different electrodes preparation and the changes in results we observed.

4.1.1 Diazonium salt grafting: a preliminary study on gold

Figure 10 displays the cyclic voltammetry of gold electrode in the presence of 4-nitrophenyldiazonium tetrafluoroborate in ionic liquid [BMP][TFSA] (figure 1-a) and in acetonitrile (figure 1-b).

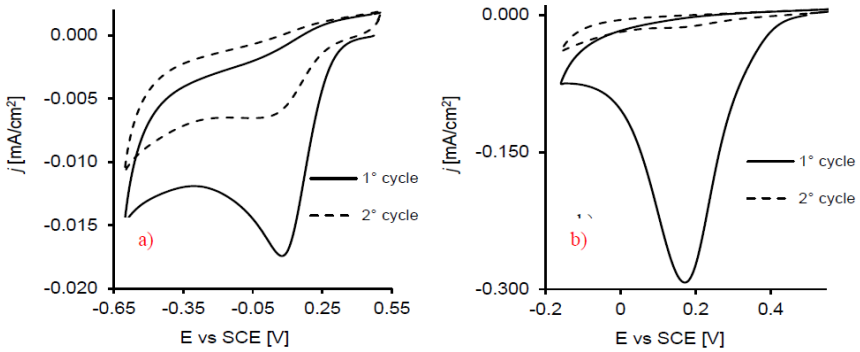

Figure 10: Cyclic voltammograms of gold electrode in 2 mM NBD recorded at 100 mV s^{-1}; a) in [BMP][TFSA]; b) in acetonitrile + 0.1 M ($TBAPF_6$). The first and second potential scans are shown.

As can be seen in ionic liquid the voltammogram presents an irreversible reduction wave at Ep = 0.1 V vs SCE; by analogy with the cyclic voltammogram obtained in acetonitrile, in which the E_p is detected at 0.2 V vs SCE, the reduction wave obtained in [BMP][TFSA] can be attributed to the reduction of the 4-nitrobenzendiazonium leading to the formation of the nitrophenyl radical. Upon the second scan in acetonitrile the cathodic peak is totally suppressed whereas in ionic liquid a decrease of the recorded current can be observed, indicating the progressive blocking of the

electroactive surface due to the formation of the nitrophenyl layer onto gold electrode. It is worth to note that, being the same the scan rate adopted for the electroreduction, the value of the current measured ionic liquid is quite lower than that in acetonitrile.

The amount of NBD reduced can be roughly estimated from the voltammetric charge related to the relevant peak using the Faraday's law $\Gamma=Q/(nFA)$: a value of $7.5x10^{-10}$ [mol cm^{-2}] and $8.9x10^{-9}$ [mol cm^{-2}] were obtained in ionic liquid and acetonitrile respectively. Comparing these values with the theoretical value of $1.2x10^{-9}$ [mol cm^{-2}] calculated for a close-packing layer of nitrobenezene[1] it can be observed that in acetonitrile the molar concentration of nitro-phenyl groups is equivalent to about nine layers whereas in ionic liquid a sub-monolayer can be estimated. However, these values are not a measure of the amount of NBD deposited on the surface because not all the aryl radicals generated graft to the electrode surface, due to the occurrence of reactions with other aryl groups in the solution to give dimers and polymers.

One of the easiest ways to evidence and quantify the presence of nitrophenyl layer attached to the electrode is to reduce the grafted electroactive nitro-groups to amino-groups. To this aim the modified electrodes were removed from the solution and were rinsed with ACN to remove the weakly adsorbed molecule. Following that, the electrodes were immersed in in 1:10 EtOH-H_2O + 0.1 M KCl and cyclic voltammetries were performed at scan rate of 100 mV/s. It is well know that the reduction of nitrophenyl moieties in protic medium occurs through an intermediate reversible step which involves the nitrous/hydroxylamine (NO/NHOH) redox couple, followed by the irreversible amination of the hydroxylamine group. According to this mechanism, data presented in Figure 2 for the electrode modified in [BMP][TFSA], show the anodic peak related to the intermediate process at about -0.35 V vs SCE: just a knee is observable in the direct scan, assessing the corresponding reduction, due to its partial overlapping with the irreversible reduction wave,

which has its maximum at around -0.9 V vs SCE. The presence of this signal indicates that nitro-phenyls are immobilized on the electrode.

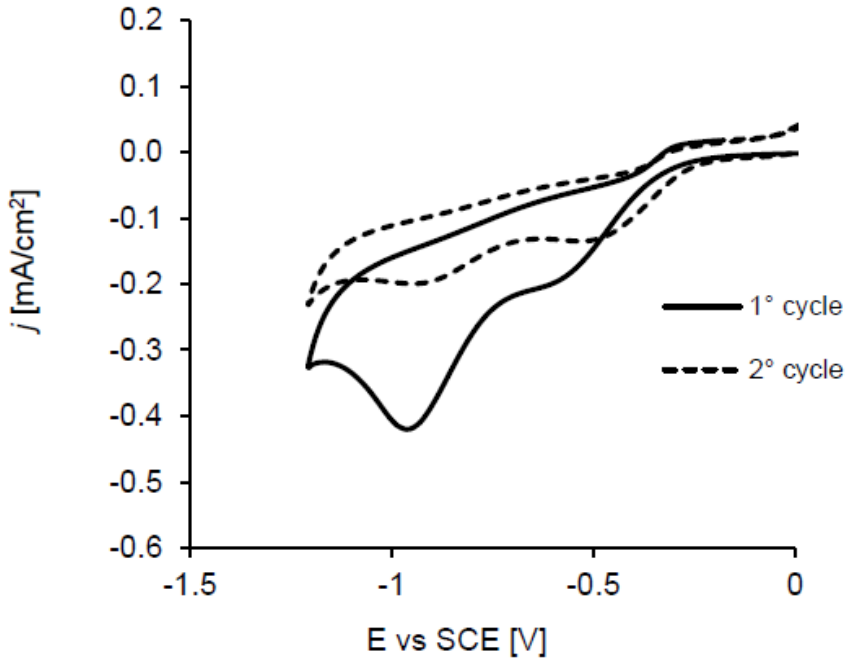

Figure 11: Cyclic voltammetric response of gold electrode modified in [BMP][TFSA] and 2 mM NBD recoded in water/ethanol solutions (90/10%$_V$) containing 0.1 M KCl at 100 mV s^{-1}.

The nitro-phenyl surface concentration can be evaluated taking into account that the reduction of nitro-groups exchange 4 or 6 electrons, corresponding to the formation of NHOH or NH_2 (Figure 11), respectively by the following equation (derivates by Faraday's law):

$$\Gamma_{NO_2}= \frac{Q(NO_2 \rightarrow NH_2)}{6FA} + \frac{Q(NO_2 \rightarrow NHOH)}{4FA}$$

Where Q corresponds to the charge measured by integration of the two electrochemical signals, reduction wave at -0.9 V and oxidation

wave at -0.35 V vs SCE, F is the faraday constant, and A represents the area of the electrode.

Values of $5.42x10^{-10}$ [mol cm^{-2}] and $1.3x10^{-9}$ [mol cm^{-2}] were obtained in ionic liquid and acetonitrile respectively. These values are lower than those estimated form the deposition of NBD, since only electroactive nitro groups are reduced and furthermore not all groups are transformed to NH_2.

It is possible that there are nitrophenyl groups relatively far from the surface for which electron tunnelling is very inefficient leading to groups that are electro-inactive and not detected voltammetrically[6]. In acetonitrile, where a multilayer structure has been obtained, the molar concentration calculated with the equation is about one order of magnitude lower than that obtained from deposition of NBD indicating that many nitro-groups are inaccessible to the electrons due to the thickness of the layer. In the case of ionic liquid the molar concentration obtained with the equation is quite similar to that evaluated from deposition voltammogram which is in agreement with a higher electrochemical accessibility of nitro-groups due to less dense sub-monolayer.

However, the surface molar concentration do not allow to determine the degree of coverage of the surface, i.e. how the layer is distributed on the gold electrodes. Thus, this evaluation have been performed determining the blocking properties of the film for the electron transfer reactions of the ferri/ferrocyanide redox probe by faradaic impedance spectroscopy. Figure 12 shows the Nyquist plots of the bare gold (Figure 12-a), the modified electrodes in [BMP][TFSA] (Figure 12-b) and in acetonitrile (Figure 12-c). The Nyquist plot of gold shows the typical shape of a faradaic impedance spectrum for conductive electrodes, with a very small semicircle at high frequencies correlated to a very low electron transfer resistance followed by a 45° straight line which is typical of a diffusion limited electron-transfer process.

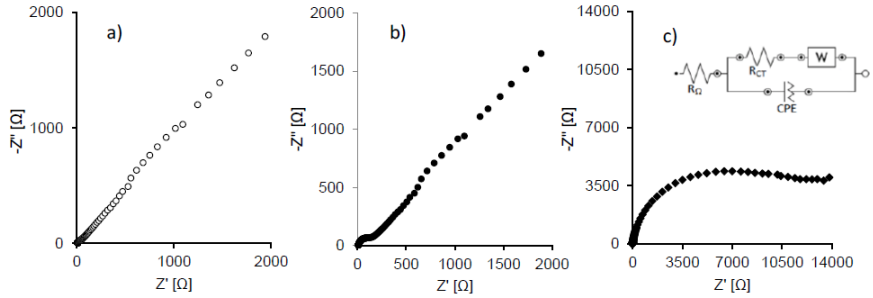

Figure 12: Nyquist plots for the Faradaic impedance measurements in 1 mM $[Fe(CN)_6]^{3-/4-}$ + 0.1 M KNO_3 (buffered solution pH=7) of a) bare gold; b) electrode modified in [BMP][TFSA] and 2 mM NBD c) electrode modified in acetonitrile + 0.1 M ($TBAPF_6$) and 2 mM NBD. The inset shows the electrical equivalent circuits used to model the impedance spectra.

The impedance plots for the NBD modified electrodes significantly differ from that of bare gold: the diameter of the semicircle is increased indicating that the surface is partially ([BMP][TFSA]) or totally (acetonitrile) blocked to the electron transfer. The electron-transfer kinetics and the diffusional characteristics have been obtained by modelling the EIS spectra with a simple equivalent electrical circuit (see inset in Figure 12), which comprises the solution resistance R_Ω, the charge-transfer resistance R_{ct}, the Warburg impedance W and a constant phase element (CPE) for model the pseudo-capacitance of the surface. The apparent electrode coverage (θ) can be calculated by equation 2, assuming that all the current is passed via bare spots on the electrode, and R^0_{ct} and R_{ct} represent the charge-transfer resistances measured on bare and modified gold electrodes, respectively:

Equation 2

$$\theta = 1 - \frac{R^0_{ct}}{R_{ct}}$$

Table 2 reports the values of charge transfer resistance of the modified electrodes along with the corresponding values for the bare electrodes obtained from the equivalent circuit model. Also the

apparent electrode coverage (θ) calculated by equation 2 are reported for each data set. As can be observed, a fractional coverage close to 100 % was obtained working with acetonitrile solution indicating that the nitrophenyl film covers the whole surface. When ([BMP][TFSA]) is used as solvent, the fractional coverage is about 80%: this data is in agreement with the voltammetric evaluation confirming the formation of a less dense organic layer.

Table 2: Values of charge transfer resistances obtained by the impedance analysis with the corresponding apparent fractional coverage (θ).

Scan rate ($mV\ s^{-1}$)	Solvent	R^0_{ct} (Ω)	R_{ct} (Ω)	θ %
2	[BMP][TFSA]	12	775	98.45
10	[BMP][TFSA]	14	495	97.17
100	Acetonitrile	28	11490	99.75
100	[BMP][TFSA]	21	101	79.25
500	[BMP][TFSA]	15	36	58.33
1000	[BMP][TFSA]	15	32	53.12

The low surface coverage obtained in [BMP][TFSA] agrees with data in the literature, in which less dense layer were obtained on carbon electrodes using ionic liquids as solvents: this behaviour has been explained considering the high viscosity of the ionic liquids with respect to acetonitrile and a correlation between viscosity and surface concentration has been also proposed.

To better clarify this point, depositions of NBD in ionic liquid have been performed at different scan rate and each modified electrode has been characterized by EIS. Figure 13-a shows the current peaks (j_p) related to the deposition process as a function of the square roots of the scan rates. A linear trend can be observed, which may be indicative of a diffusion controlled process even if the peak potentials slightly shift towards more positive potentials as the scan rate decreases (data not shown).

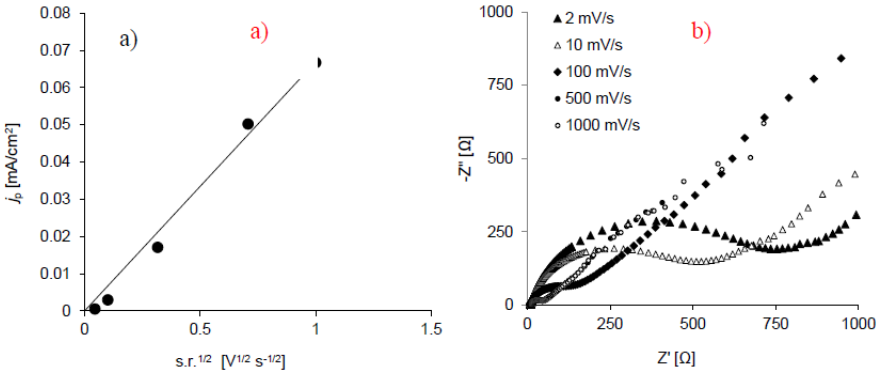

Figure 13: Results obtained for gold electrode modified with NBD at different scan rates: a) Values of current densities measured at the deposition peak as a function of the square roots of the scan rate (s.r.); b) Nyquist plots for the Faradaic impedance measurements in 1 mM $[Fe(CN)6]^{3-/4-}$ + 0.1 M KNO_3 (buffered solution pH=7).

In Figure 13-b are reported the impedance spectra of the electrode modified in ionic liquid and 2 mM NBD at different scan rates; the corresponding values of charge transfer resistance are presented in Table 2.

The decrease of scan rate during the deposition allows to obtain more covered surface; at 2 mV/s the nitrophenyl film covers the whole surface also when ionic liquid is used as solvent.

4.1.2 Aniline electropolymerization

As we saw in the previous chapter, acetonitrile or ionic liquid as solvent affects the surface concentration as well as surface coverage. Even if we could have more process control with ionic liquid, we decided to proceed with acetonitrile in order to have a complete coverage of the electrode's surface with diazonium salt organic layer. Figure 14 reports the cyclic voltammograms recorded during the electrodeposition of NBD on bare gold electrode in acetonitrile containing 2 mM NBD and 0.1 M ($TBAPF_6$) as supporting

electrolyte. As the number of cycles increases the reduction peak become less evident and it completely disappears in the third scan.

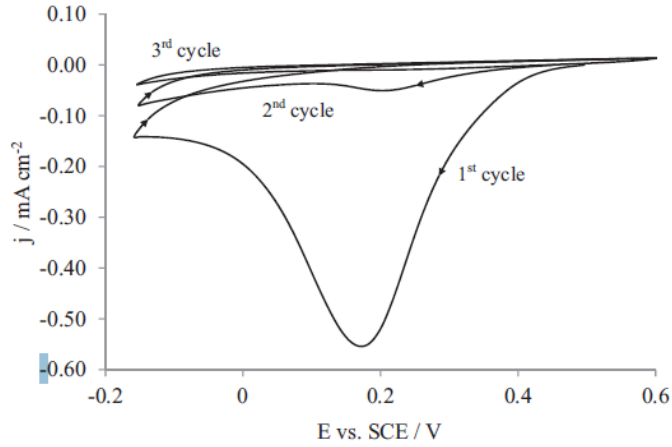

Figure 14: Cyclic voltammograms of gold electrode in 2 mM NBD + 0.1 M (TBAPF6) in acetonitrile solution recorded at 100 mV/s. The first, second and third potential scans are shown.

For our study we obtained a diazonium salt surface concentration in the range of 5.64-8.9×10^{-9} [mol cm^{-2}], which is 6-9 times the teorethical monolayer.

The multilayer formation has been attributed to a polymerization-type reaction between the grafted layer and the free radicals in the solution, as well as to conductance switching and electrochemically catalyzed aromatic homolytic substitution, which can lead to non-uniform deposition of the layer. To evaluate the surface coverage of the NBD modified electrodes we use the equation 2.

Figure 15 shows the Nyquist plots of the bare Au (inset) and of the electrodes modified with 1 mM or 2 mM NBD. The Nyquist plot of bare gold shows the typical shape of a Faradaic impedance spectrum for conductive

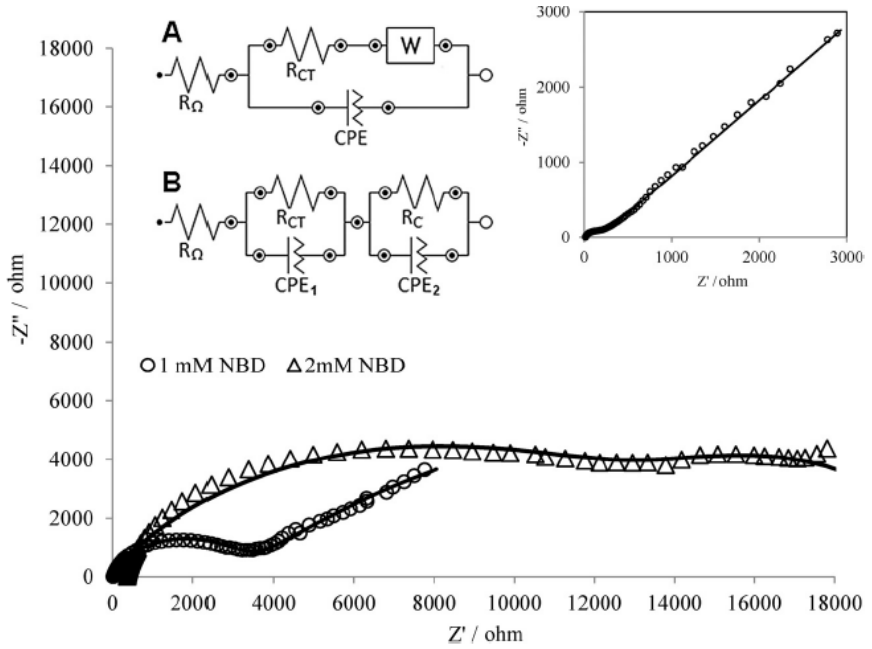

Figure 15: Nyquist plots for the Faradaic impedance measurements of the modified electrodes in 1 mM $[Fe(CN)_6]^{3-/4-}$ + 0.1 M KNO_3 (buffered solution pH = 7). The inset showsthe Nyquist plot of the bare gold. Fitting curves have been calculated by the electrical equivalent circuits in figure: bare gold (A) modified electrodes (B).

electrodes, with a very small semi-circle at the high frequencies correlated to a very low electron transfer resistance, followed by a 45° straight line which is typical of a diffusion limited electron-transfer process. The impedance plots of the modified electrodes significantly differ from that of the bare gold: at the high frequencies the responses of both the electrodes show a semicircle with high diameter, due to the increasing of the charge transfer resistance. At the low frequencies, the straight line cannot be observed, and a

second not completely resolved semicircle seem to appear, with a response similar to that observed in modified gold electrodes.

The electron-transfer kinetics were obtained by modelling the EIS spectra with the equivalent electrical circuits shown in the inset of Figure 15 (the first one is the well known "Randles circuit", introduced in the previous subchapter). Data related to the bare gold were fitted with the circuit A in Figure 15. The circuit elements are the ohmic resistance of the electrolyte solution (R_Ω), the Warburg impedance, resulting from the diffusion of ions from the bulk to the electrode interface (W), and the electron-transfer resistance of the ferro/ferrycyanide redoxprobe (R_{ct}). Instead of capacitance, a constant phase element (CPE) was used which takes into account for deviations from the ideal capacitance behaviour $1/ZCPE= Y_0(j\omega)^n$, where Y_0 and n are the admittance and the exponent of CPE respectively. As the response of the modified electrodes is concerned, the circuit A may be used to obtain the parameters related to the high frequencies, without regard to the fit at low frequencies. Otherwise the circuit has to be modified, with other elements and other parameters: the curves in Figure 15 were obtained by the fitting of the data with the circuit B, already used by Khoshroo and Rostami[122], which considers the resistance (RC) and capacitance (CPE_2) of the coated layer. In any case, the values of R_{ct} calculated from the high frequency data with both the circuits (or with a simple parallel R/CPE) differ by less than 5%.

Table 3 summarizes the parameters obtained by fitting the EIS spectra, along with the corresponding errors. The data in the table clearly show that the charge-transfer resistance increases with the modification of the gold surface from avalue of 193 Ω for the bare electrode to 15.1 × 103 Ω after electrochemical modification with 2 mM of NBD in the solution.

	R_{ct} / Ω	Y_0 / µS s^n	n	θ%
Au	193 (1.8%)	22.7 (0.35%)	0.79 (0.04%)	-
AuNBD (1mM)	3’260 (4.8%)	6.47 (1.1%)	0.83 (0.16%)	94.0
AuNBD (2mM)	15’100 (4.9%)	5.53 (2.2%)	0.72 (0.5%)	98.7

Table 3 - Values of circuital parameters obtained by the impedance analysis with the corresponding errors in brackets.

A value of fractional coverage θ close to 100% was obtained working with 2 mM NBD solution, indicating that the nitrophenyl film coversthe whole surface although, considering the voltammetric charge passed during the NBD reduction, a non-uniform thickness may be expected. The further modifications were carried out using electrodes with the highest fractional coverage. The reduction of the nitrophenyl moieties to aminophenyl hasbeen performed by cyclic voltammetry in 1:9 EtOH–H_2O + 0.1 M KCl.

Data presented in Fig. 16 show the presence of an irreversible reduction wave around -1.0 V/SCE in the first scan, while in the reverse scan an anodic wave at Ep = −0.25 V/SCE was observed. As we discussed, in the second scan only a pair of reversible redox peaks can be observed, with a redox potential E = −0.4 V/SCE.

The reduction of nitrophenyl moieties in protic medium occurs through the formation of hydroxylamine (NHOH) group which belongs to the reversible nitroso/hydroxylamine (NO/NHOH) redox couple. The further reduction results in the amination of the hydroxylamine groups:

$$Au - Ar - NO_2 \xrightarrow{+4e^- +4H^+} Au - Ar - NHOH + H_2O$$

$$\xrightarrow{+2e^- +2H^+} Au - Ar - NH_2 + H_2O$$

$$Au - Ar - NHOH \underset{+2H^+ +2e^-}{\overset{-2H^+ -2e^-}{\longleftrightarrow}} Au - Ar - NO$$

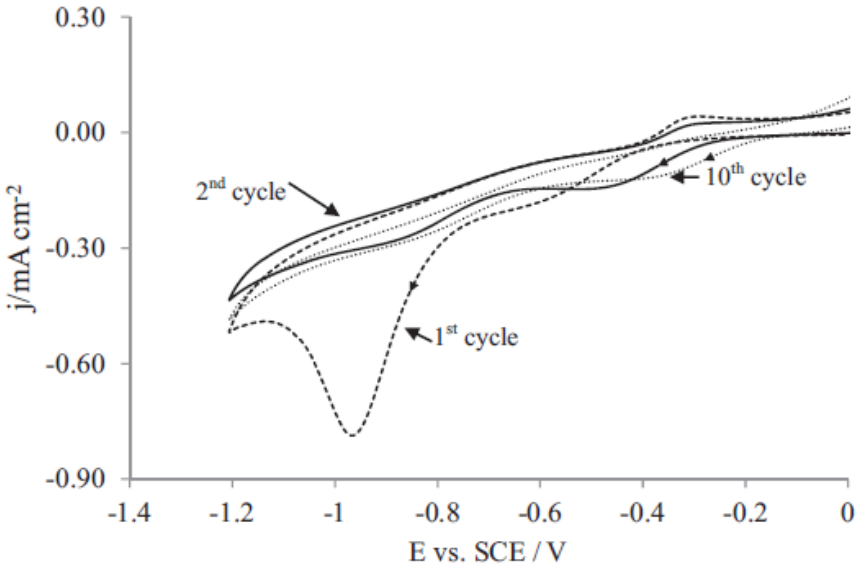

Figure 16: Cyclic voltammetric response of an Au/NBD electrode in water/ethanol solutions (90/10%$_V$) containing 0.1 M KCl at 100 mV/s.

As can be seen from Fig. 16, during the second scan, the extent of the reduction peak is drastically diminished, indicating that nearly all the electroactive NO_2 groups are reduced in the first scan. In the second cycle the redox couple associated with reaction is well visible indicating that the reduction of nitro to amino group is incomplete. The oxidation peak decreases with the number of cycles and it tends to disappear after ten cycles. This may indicate that all the electroactive grafted groups are virtually reduced, although the decrease in the nitroso/hydroxylamine voltammetric signal has been also attributed to the coupling reactions between 4-nitrophenyl group and 4-aminophenyl group, to form azo or azoxy compounds, which in turn lead to the inactivation of the grafted film and a gradual loss of the voltammetric signals. The modification of the surface sites after the two electrochemical steps has been also analyzed by ATR-FTIR spectrophotometry: the relevant spectra are shown in Figure 17. The curve (a) in Fig. 17 is related to a sample after grafting with

NBD, and two peaks can be observed at 1534 cm^{-1} and 1351 cm^{-1}, which are characteristic of the asymmetric and symmetric stretch modes, respectively, of the nitro group. Moreover in the region of 2000–2300 cm^{-1} no evidence of the diazonium group is present, indicating that the nitrophenyl groups are generated by the electrochemically produced nitrobenzene radicals and not by physic adsorption of the NBD. After reduction of the nitrophenyl modified electrode, the ATR FTIR spectra showed (curve b) a decrease of the response of the nitro group and the appearance of three band: at about 1650 cm^{-1} attributed to the deformation band of N–H in NH_2, at 1400 cm^{-1} which is related to the N–H bending in plane and at 950 cm^{-1} attributed to N–H bending out of plane. The density of aminophenyl groups available for the subsequent reaction can be estimated as we saw:

$$\Gamma_{NH_2} = \frac{Q_1 - Q_2}{6F}$$

where Q_1 is the voltammetric charge associated to the reduction peak at −1 V, which takes into account both for the $6e^-$ reaction of nitrophenyl to aminophenyl groups and for the partial reduction (4 electrons) of nitrophenyl to hydroxylamine; Q_2 is the charge related to the oxidation of hydroxylamine which can be evaluated from the oxidation peak in the reverse scan of the first voltammetric cycle (third reaction); 6 is the number of electrons involved in the aminophenyl formation and F is the Faraday constant. A value of NH_2= 7.3 × 10 mol cm^{-2} has been obtained; this value is about one order of magnitude lower than the total concentration of NO_2 groups estimated from the deposition curves of NBD, since only electroactive nitro groups can be reduced and accordingly not all groups are transformed to NH_2.

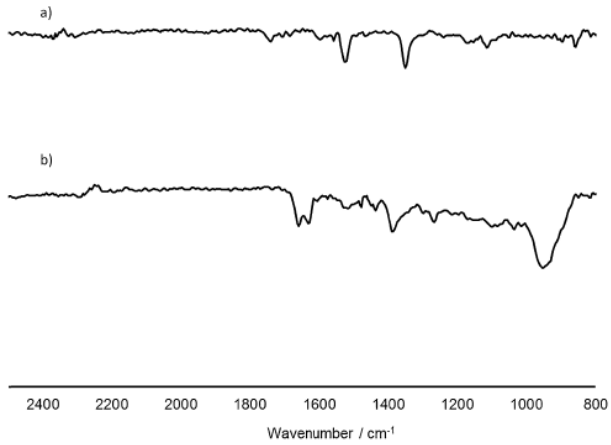

Figure 17: ATR FTIR spectra of (a) nitrophenyl modified gold electrode and (b) aminophenyl modified gold electrode.

Figure 18 presents the CVs obtained during the electropolymerization of the Au/PANI and $AuNH_2$/PANI films, respectively. The CVs have been performed in the potential range of 0.0–0.95 V/SCE at a scan rate of 0.1 V/s. Both the electrodes show the characteristic oxidation/reduction peaks for the formation of polyaniline (see Figure 18c and d): the peak A_1 corresponds to the first oxidation step, which leads to the formation of cation–radicals. The peak A_3 corresponds to the formation of the dication–diradical: since the current peak A_3 also contains the superimposed current of oxidation of the aniline monomer, the propagation of the polymerization reaction occurs at potential values higher than that of the peak A_3[123]. Several works on the PANI electropolymerization have highlighted the presence of one or two waves between the leucoemeraldine/emeraldine (0.15 V/SCE) and emeraldine/pergraniline (0.7 V/SCE) transitions. These peaks (denoted as A_2) are usually attributed to the presence of by-products adsorbed in the polymer matrix, such as ortho-coupled polymers or by-products like benzoquinone orhydroquinone[123]. The oxidation/reduction peaks at gold and Au/NH_2 were found at the same potential, and the current densities of these characteristic peaks

increase with the number of cycles, indicating that also at modified electrode the polymerization process occurs regularly. As it can be seen from the comparison between Figure 18a and b (first two cycles of deposition) in the first scan the anodic peak at 0.8 V/SCE is present only for $AuNH_2$ electrode which is indicative for the presence of NH_2 termination in the surface. Similar behavior has been reported for aminophenyl modified carbon electrodes: the electrochemical response examined in the positive potential region (0.0–1.2 V/SCE) in 0.25 M H_2SO_4 showed a redox couples centred between 0.3 and 0.6 V followed by a broad irreversible oxidation at 0.9 V assigned to the oxidation of aminophenyl groups[30].

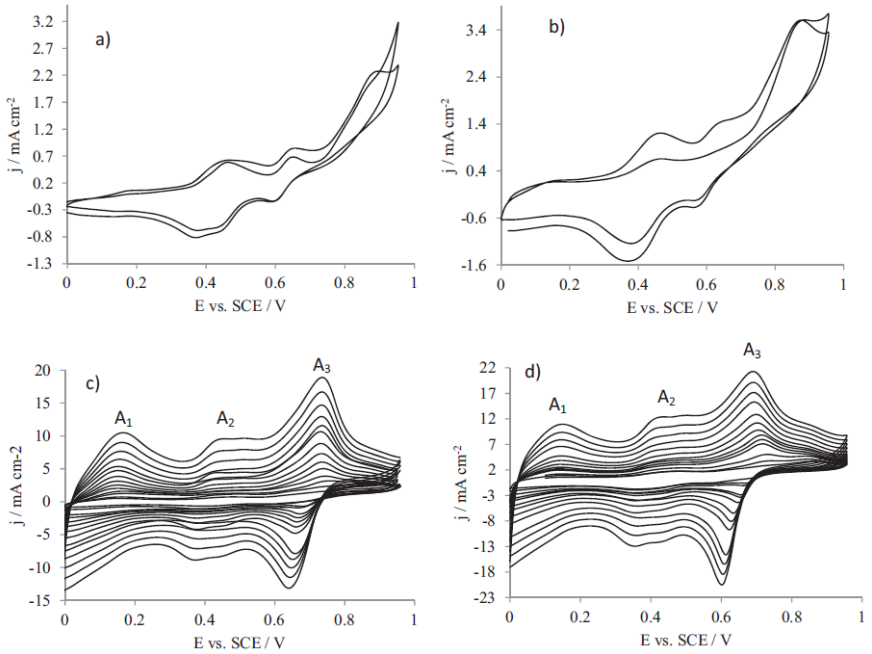

Figure 18: Cyclic voltammograms recorded during the PANI electropolymerization in 0.1 M aniline + 1 M HNO_3 aqueous solution on bare gold (a–c) and Au/NH_2(b–d) electrodes. Panels a and b refer to the first two cycles of CVs; panels c and d refer to different cycles of CVs up to the 35th cycle.

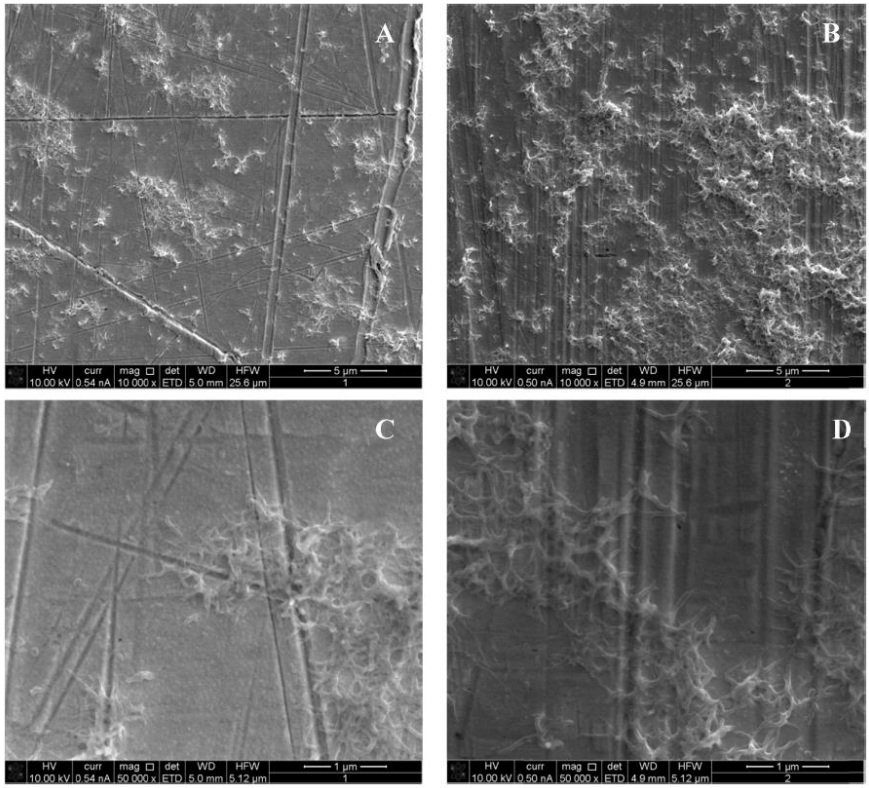

Figure 19: SEM images of Au/PANI (A and C) and $AuNH_2$/PANI (B and D) prepared by three cycles of CV, scan rate 100 mV/s.

Moreover, the current densities associated to oxidation/reduction peaks are higher for $AuNH_2$ electrode, the number of voltammetric cycles being the same. This behaviour may indicate that at aminophenyl modified electrode the polymerization process is more effective: as pointed out by Budnikov et al.[110], the polymerization of PANI is a self-catalytic head-to-tail process, thus the aminophenyl layers may offer several starting points of propagation of the oxidative radicalic polymerization. Figure 19 shows the SEM images of Au/PANI and $AuNH_2$/PANI recorded at the early stage of polymerization (3 cycles of CVs). The presence of PANI can be observed in both the electrodes, moreover, at the highest

magnification, both electrodes show nanofibrous structures which are slightly thicker for $AuNH_2$/PANI electrode. In order to characterize the electrodes EIS analyses have been performed in acidic aqueous solution at OCP. The analyses were performed after different number of cycles of polymerization on both types of electrodes. Figure 20a and b reports the Nyquist plots obtained after 15 and 35 cycles for Au/PANI and $AuNH_2$/PANI. In the low frequency region, a line almost vertical to the real axis was observed which can be attributed to the pseudo-capacitance of the PANI electrode. The imaginary impedance values of the Nyquist spectra decrease with the number of polymerization cycles (i.e. with the thickness of the PANI layer) indicating an increase of the PANI pseudo-capacitance. The capacitances of the electrode materials were calculated, according to the equation: $C=-1/(2\pi fZ'')$ (f=frequency; Z"=imaginary impedance) from the slope of the linear trend Z" vs. $1/(2\pi f)$, at low frequencies[100]. The values of the parameters obtained with the Au/PANI and $AuNH_2$/PANI electrodes are summarized in Table 4 along with the corresponding regression coefficients, for different numbers of deposition cycles. As can be seen, as the number of cycles increases the capacitive behaviour ofthe layers increases: as suggested by Zic, this could be related to an enlargement of the PANI/electrolyte surface[124]. Also the values of the real impedance at the low frequencies, which takes into account for the resistance of the electrolyte and the film, including both electronic and ionic contributions, have been reported in Table 4 at the fixed values of 0.01 Hz[100]. The resistive behaviour of both layers decreases with the number of cycles of CV, this can be attributed to an increase in the counter-ion flux due to a less dense PANI structure of the layers with higher thickness[124]. Moreover, the $AuNH_2$/PANI exhibits higher capacitive behaviour and resistance with respect to the Au/PANI electrode, the difference being higher as the number of polymerization cycles increases. It is worth to observe that parameters such as resistance and capacitance depend on the

thickness of the PANI layer[124] as well as on its uniformity. Fig. 21 shows SEM and the FIB cross section of Au/PANI and $AuNH_2$/PANI, obtained after 35 voltammetric cycles of polymerization. The $AuNH_2$/PANI shows a more uniform polymeric layer with a regular structure, small pores and almost constant thickness of about 7.5 μm, while Au/PANI shows a very irregular structure and a thickness ranging from 3.0 to 7.2 μm. The stability of these two samples was checked by repeating the EIS measurements after the samples were submitted to sonication for 10 min: as can be seen in Table 4, lower values of capacitance have been obtained for both samples with a higher decrease of thecapacitance for Au/PANI electrode. Moreover, a visible peeling-off was observed only for the Au/PANI. A similar result has been found by Santos et al.[99] for PANI electropolymerized using an under-layer of 4-aminodiphenylamine.

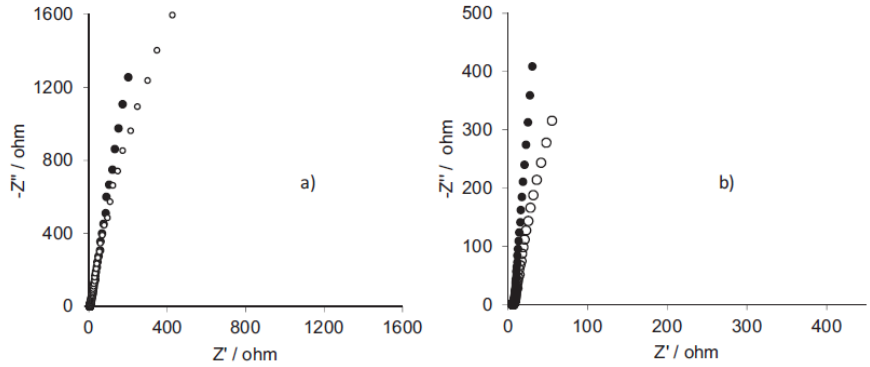

Figure 20: Nyquist diagrams (Z_{im} vs. Z_{re}) for the impedance measurements in acidic solution at the OCP for Au/PANI (full symbols) and $AuNH_2$/PANI (empty symbols) obtainedafter 15 cycles of CVs (a) and 35 cycles of CVs (b).

N° cycles of CVs	Au/PANI			$AuNH_2$/PANI		
	C (mF cm^{-2})	Z' (0.01 Hz) (Ω)	R^2	C (mF cm^{-2})	Z' (0.01 Hz) (Ω)	R^2
5	8.29	737.1	0.9975			
10	9.01	650.7	0.9983	10.86	1117.0	0.9884
15	25.16	202.0	0.9985	19.85	427.2	0.9958
20				32.70	204.8	0.9990
25	42.81	72.5	0.9999	50.20	160.4	0.9995
35	78.88	31.0	0.9998	101.08	55.6	0.9993
35[a]	18.55	178.2	0.9992	43.5	140.0	0.9984

[a] Data obtained after 10 min of sonication.

Table 4: Values of capacitance and Z'' at 0.01 Hz obtained by the impedance analysis. Regression coefficients of the linearization used to obtain C are reported as R^2.

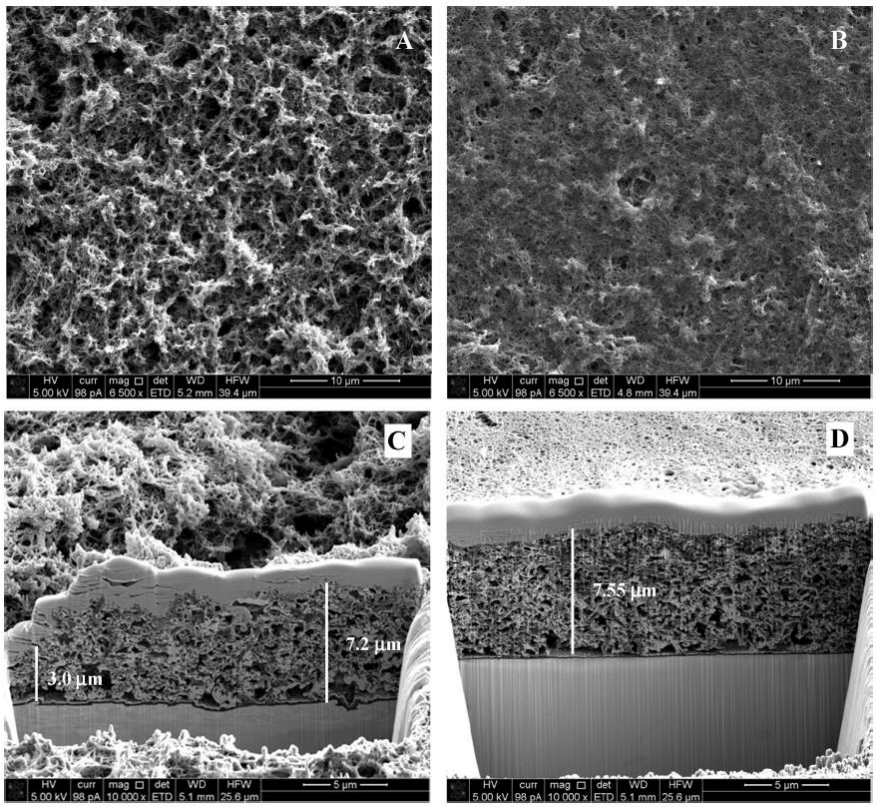

Figure 21: SEM micrograph of surfaces (A and B) and of the focused ion beam (FIB) cross sections (C and D) of polyaniline samples obtained after 35 voltammetric cycles: Au/PANI(A and C); $AuNH_2$/PANI (B and D).

4.1.3 A metal-free sensor: pedot:pss-pani coupling

After the electropolymerization on functionalized gold electrode work we tried to assemble a metal-free sensor. In particular two conductive polymers were used, polyaniline andand in this subchapter we will discuss its preparation and performance.

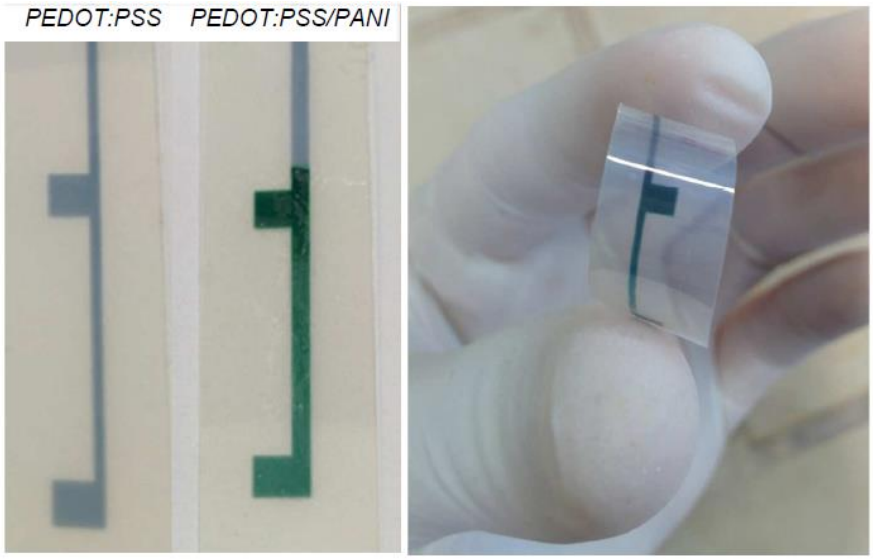

Figure 22: Pictures of the ink-jet printed PEDOT:PSS and PEDOT:PSS/PANI electrodes.

Figure 23 shows the cyclic voltammogram of aniline swept at 100 mV s^{-1} during 10 scans in aqueous solution containing 0.1 M aniline and 1.0 M HNO_3 at Poly(3,4-ethylenedioxythiophene): poly(styrenesulfonic acid) complex (PEDOT:PSS) working electrode (Figure 22). We discussed the electropolymerisation process of PANI on gold electrodes, that usually exhibits well-defined redox peaks corresponding to a series of redox transitions, which are related to the polymerisation processes. In the present case, two oxidation waves and one reduction wave can be identified (see inset of figure 23), although with difficult due to the low conductivity

of the PEDOT electrode. Anyway, both oxidation and reduction currents progressively increase with the scans, thus evidencing the growing of a conductive film on the electrode surface.

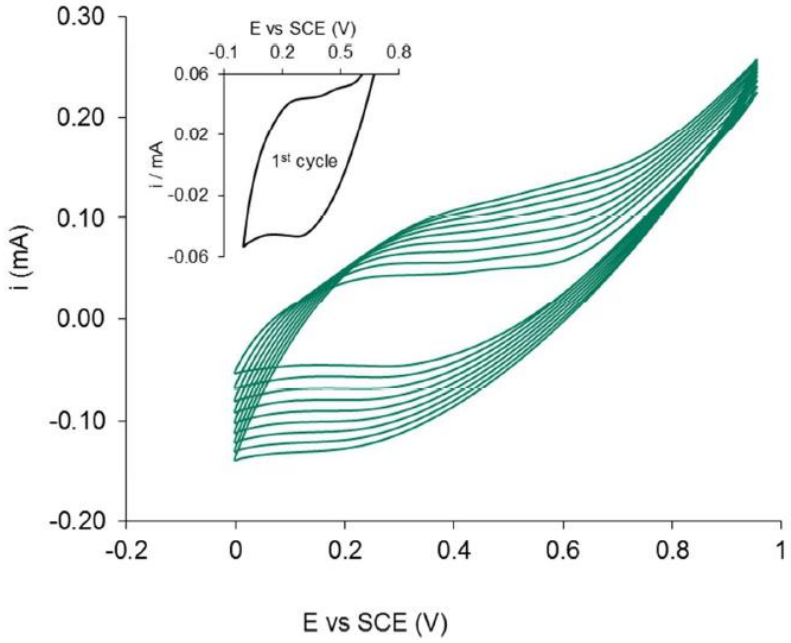

Figure 23: Cyclic voltammograms recorded during PANI electropolymerisation in 0.1 M aniline + 1 M HNO3 aqueous solution on PEDOT:PSS electrodes. Inset shows the first voltammetric cycle of polymerisation.

The thickness of the deposited layer of PANI can be estimated from the voltammetric charge associated to the oxidation of the monomer (Q_a) by assuming a current yield of 1, as follows[125]:

$$h = \frac{Q_a M_w}{zFdA}$$

Where M_w is the molecular weight of aniline (93 g mol^{-1}), z = 0.5 (number of electrons/aniline), A is the area of the electrode, d is the specific density of aniline, and F is Faraday's constant. After ten cycles, the estimated thickness of the PANI coating is about 305 nm and a green layer is visible on the grey surface of PEDOT:PSS. The surface morphology of the electrodes has been observed by SEM: Figure 24 shows the micrographs of ink-jet PEDOT:PSS and PEDOT:PSS/PANI films. As it can be seen, the PEDOT:PSS layer is uniform and relatively smooth; after the electropolymerisation of PANI a porous layer with a fibrous nanometric structure is visible, which covers the under-layer of PEDOT:PSS. The FIB cross section shows that the PEDOT:PSS layer is about 930 nm, while after the PANI electropolymerisation the overall thickness of the layer is 1300 nm with non-uniform profile.

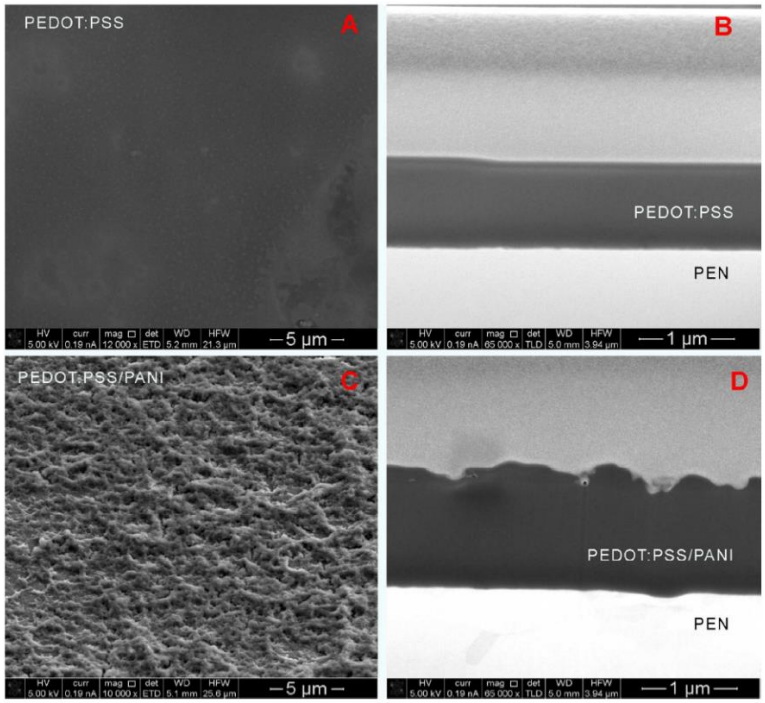

Figure 24: SEM micrograph of surfaces (A and C) and of the focused ion beam (FIB) cross sections (B and D) of PEDOT:PSS (A and B) and PEDOT:PSS/PANI (C and D) on PEN substrate.

Figure 25 reports the Raman spectra collected on PEDOT:PSS/PANI sample, and, for comparison, the spectrum of pure polyaniline and from PEDOT.PSS. As can be observed the Raman spectrum of the PEDOT:PSS/PANI film presents all the main vibrations of polyaniline: at 1170 cm^{-1} (C–H bending vibration of the quinoid/benzenoid ring), the $C\text{-}N^{+}$ vibration at 1327 cm^{-1}, the vibration due to delocalized polaron in the extended polymeric conformation at 1365 cm^{-1}, the band to the NH vibration at about 1500 cm^{-1} and, finally the band at 1595 cm^{-1}, related to the stretching vibration of C-C in the benzenoid ring[126]. Moreover, the band related to the PEDOT:PSS at about 1250 cm^{-1} and at 1422 cm^{-1} are still visible. Actually, the IR laser beam at 1064 nm is not totally absorbed from the polyaniline thin film, being able to reach and stimulate the organic substrate. On the other hand, the low energy laser beam avoid any luminescence effect from polyaniline.

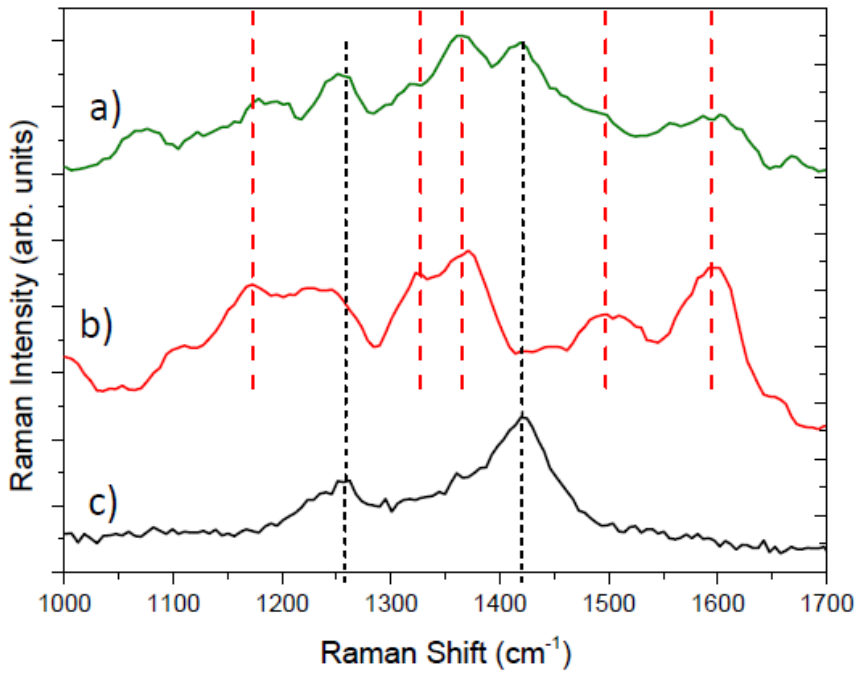

Figure 25: Raman spectra of PEDOT:PSS/PANI (a), PANI (b) and PEDOT:PSS (c).

The presence of electroactive PANI layer on the PEDOT:PSS substrate can be evidenced by cyclic voltammetries in monomer-free solutions. Figure 26 shows the voltammograms of PEDOT:PSS and PEDOT:PSS/PANI electrodes in 1M HNO_3. The CV at PEDOT:PSS electrode shows a nearly rectangular shape, and only two redox shoulders are present at 0.6 and 0.26 V, indicating low faradic activity and highly capacitive behaviour. Similar results have been already observed for PEDOT inkjet printed on flexible material without metal current collector, which are similar to those used in the present work[127]. In the CV of PANI modified electrode, the typical

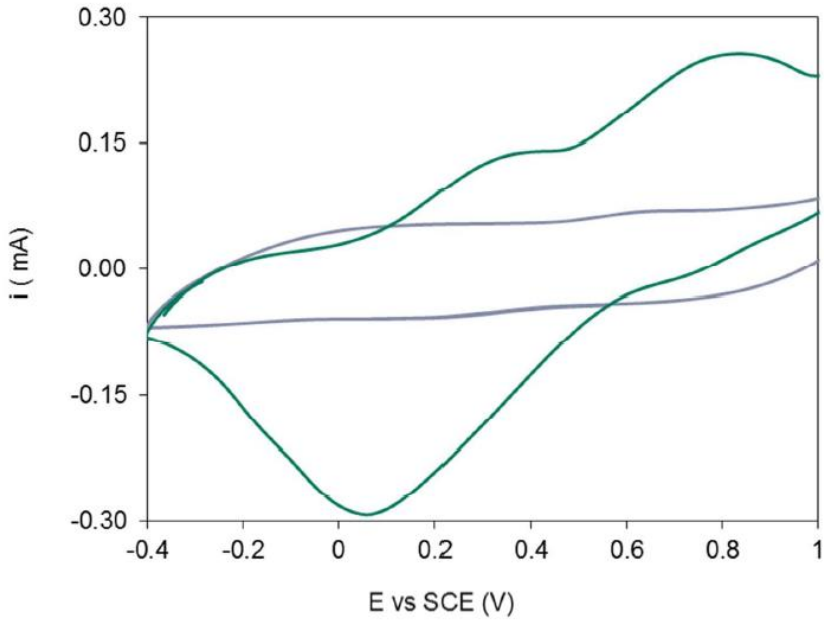

Figure 26: Cyclic voltammetries of PEDOT:PSS (grey line) and PEDOT:PSS/PANI (green line) electrodes performed in monomer-free solutions containing 1 M HNO_3. Scan rate 100 mV/s.

peaks related to doping and undoping of protons and anions in the polymeric film, as well as to the transformation between different forms of PANI, are well visible. The oxidation peak around +250 mV

is attributed to the conversion from leucoemeraldine into emeraldine form, while the second peak appearing around +800 mV is due to emeraldine/pernigraniline transformation[81]. Moreover, comparing the CVs of PEDOT:PSS and PEDOT:PSS/PANI it can be observed that the capacitance in presence of PANI is considerably larger than in case of PEDOT:PSS, thus indicating that PEDOT:PSS/PANI has higher electrochemical active area.

The electrochemical proprieties of the polymeric electrodes have been investigated by electrochemical impedance spectroscopy in aqueous solutions at different pH. Figure 27 shows the Nyquist plots of PEDOT:PSS and PEDOT:PSS/PANI, recorded in acidic solution at the OCP: as can be seen for PEDOT the impedance plot presents a 90° capacitive line in the low frequencies range, while at higher frequencies two deviations can be observed (see magnification of Nyquist plot in the inset of figure 27).

The high-frequency intercept of the semicircle with the real axis can be used to evaluate the internal resistance, which includes the resistance of the electrolyte solution, the intrinsic resistance of the active material, and the contact resistance at the electroactive material/current collector interface[128]. PEDOT:PSS and PEDOT:PSS/PANI show similar impedance spectra, but the second one is shifted to the left, indicating a less resistive behaviour. In order to investigate the effect of the presence of PANI over the PEDOT, some electrodes with an higher PANI load have been prepared by 20 cycles of voltammetric polymerisation (PEDOT:PSS/PANI20): the EIS spectrum of one of them is compared with the previous one in figure 27. As can be seen, the reduction of the resistivity due to PANI layer is emphasised in samples with higher PANI load.

In order to obtain the characteristic parameters of the electrodes, the impedance spectra have been modelled with the equivalent circuit proposed by Danielsson et al.[129] for PEDOT electrodes (see inset of figure 27). The following elements have been inserted in the circuit: the uncompensated resistance (R_Ω), the charge transfer resistance

(R_{ct}), the double layer capacitance (C_{dl}), the electronic contribution to the capacitance (C_d) and the finite-length Warburg element (Z_D) which represents the diffusion within a thin layer of electrolyte. Z_D includes a diffusion capacitance (C_D), a diffusional time constant (τ_D) and a diffusion resistance ($R_D=\tau_D/C_D$)[130]:

$$Z_D = \frac{(\tau_D/C_D)\coth(j\omega\tau_D)^{1/2}}{(j\omega\tau_D)^{1/2}}$$

where ω is the angular frequency ($2\pi f$) and $j=(-1)^{1/2}$.
All the impedance spectra obtained for PEDOT:PSS, PEDOT:PSS/PANI and PEDOT:PSS/PANI20 have been modelled with this equivalent circuit obtaining a very good fit of the impedance spectra ($\chi^2 < 6x10^{-5}$). The fitting curves of the Nyquist plots can be seen in figure 27, while Table 5 reports the values of the circuit parameters. As can be seen in table 5, the uncompensated resistance for PEDOT:PSS is 1180 Ω, indicating high intrinsic resistance of this electrode. After the electropolymerisation of PANI on PEDOT:PSS, R_u decreases: values of 900 and 733 Ω are obtained for PEDOT:PSS/PANI and PEDOT:PSS/PANI20 respectively. Similarly, the charge transfer resistance decreases after the PANI deposition and the lowest values correspond to the higher PANI load. As the capacitance is concerned, the total interfacial capacitance Ctot of the polymers can be evaluated combining in series the electronic contribution to the bulk capacitance Cd and the ionic contribution to the bulk capacitance C_D as follow[130]:

$$C_{tot} = \frac{1}{1/C_d + 1/C_D}$$

As can be seen for PEDOT:PSS C_d << CD meaning that the total interfacial capacitance is dominated by the electronic contribution: similar behaviour has been found by other authors for PEDOT:PSS electrodes[130]. For PEDOT:PSS modified with PANI, the ionic

contribution becomes more important due to the porous structure of PANI: as the PANI load increases the diffusional time constant increases indicating a slower access of the counter ions into the pores of polymer.

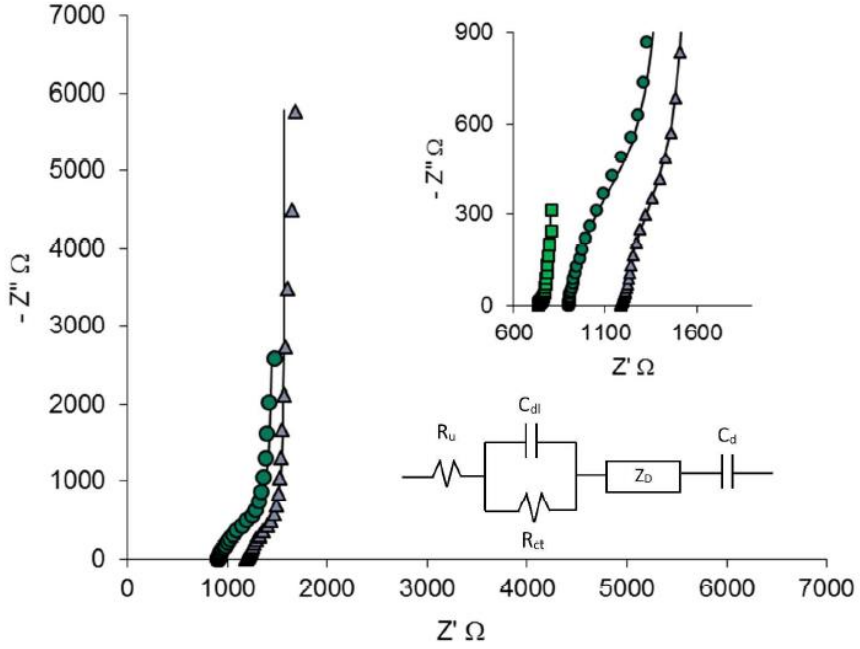

Figure 27: Nyquist plots of PEDOT:PSS (triangles), PEDOT:PSS/PANI (circles) and PEDOT:PSS/PANI20 (squares) recorded in solution at pH = 2.8.

	PEDOT:PSS	PEDOT:PSS/PANI	PEDOT:PSS/PANI20
Ru (ohm)	1183	900	734.2
Cdl (mF)	0.33	0.40	0.66
Rct (ohm)	171.8	66	13.2
Cd (mF)	0.31	0.72	6.37
τ_D (s)	1.44	3.92	7.21
C_D (mF)	2.26	4.81	34.77

Table 5: Values of the elements calculated from model of the equivalent circuit fitted to impedance spectroscopy data at pH 2.8.

The electrochemical activity of the organic bilayer has been tested via measurements of pH vs. OCP. Figure 28 shows the behaviour of PEDOT:PSS/PANI electrode at different pH: the potential equilibrium response shows a linear trend with pH in the range from 2 to 13.5, with a slope of 58.9 mV/pH unit which indicates a near-Nerstian behaviour of the organic bilayer. In order to investigate the reversibility of the response to pH, PEDOT:PSS/PANI electrode was tested with increasing and decreasing pH. As can be seen from figure 6 the potentiometric responses did not show significant dependence on the direction of pH changes indicating a very low hysteresis. Different results were obtained for PEDOT:PSS/PANI20: the trend of OCP vs. pH showed two slopes of 51.1 mV/pH unit and 8.9 mV/pH unit in acidic and neutral-alkaline pH, respectively.

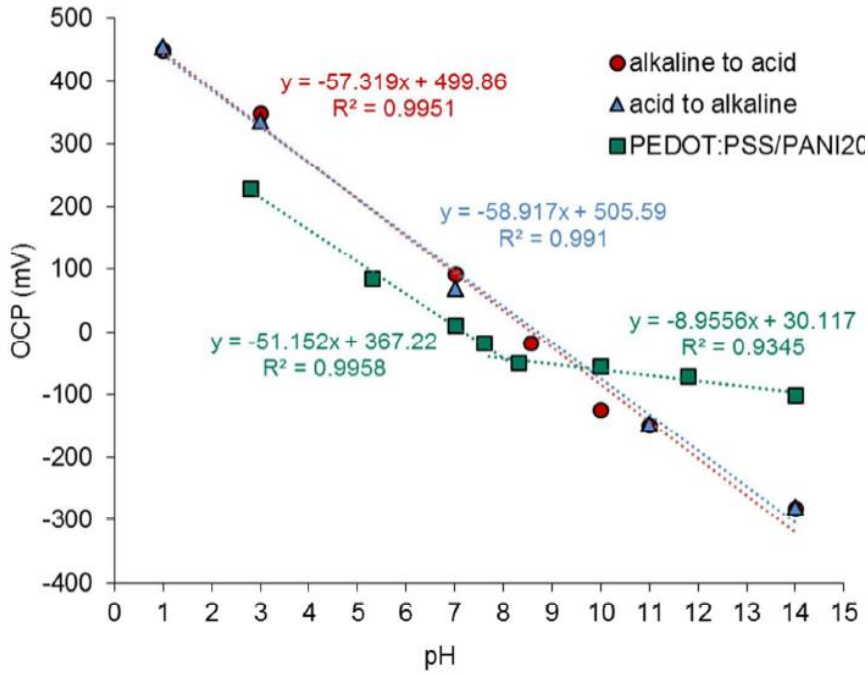

Figure 28: Trends of open circuit potentials (OCP) versus pH for PEDOT:PSS/PANI electrode (measurements performed from alkaline to acidic or from acidic to alkaline) and PEDOT:PSS/PANI20 electrode (measurements performed from acidic to alkaline).

Moreover, measurements of OCP vs. pH have been performed using electrodes of either PANI or PEDOT:PSS onto plastic substrates, without metallic current collector. PEDOT layers have been obtained by ink-jet printing, and PANI was dip-coated. As can be seen in figure 29, PEDOT shows a linear trend of the potential equilibrium response as a function of pH with a slope of 10.5 mV/pH unit indicating a very low sensitivity toward pH variations, which can be attributed to the low conductivity of the ink-jet printed film. As highlighted in the literature, appreciable increasing in conductivity has been obtained only when PEDOT:PSS was modified with ethylene glycol[131], graphene oxide[132] and dimethyl sulfoxide[101]. As highlighted by different authors, the pristine PEDOT:PSS presents a coil structure were PEDOT grains are surrounded by a PSS insulating shield which prevents the interactions between the hydrophobic PEDOT and water[101,132]. Thus, the low pH responses may be attributed both to the low conductivity and to the inactivity of the SO_3^- groups of the PSS.

The dip-coated PANI shows a linear trend for pH between 2 and 7 with a slope of 50.7 mV/pH unit, while at higher values of pH the slope of OCP vs. pH decreases down to 7.7 mV/pH unit indicating a considerable loss of sensitivity at neutral-alkaline pH. It is well known that PANI is a conducting polymer that shows a very high sensitivity toward pH: a linear dependence of OCP from pH in acidic solutions has been found for PANI electropolymerized on different substrates[133]. At neutral or basic pH the sensitivity significantly decreased and, depending on the preparation conditions and on the substrates, the detection of pH is limited below[132], while in the acidic range of pH PANI usually presents a near-Nerstian or a sub-Nerstian behaviour[134]. At higher values of pH, the sensitivity decreases and a reduction of the slope in pH vs. OPC curve has been often observed. In alkaline solution, the PANI becomes deprotonated and the conductivity of the films undergoes a dramatic decrease in magnitude.

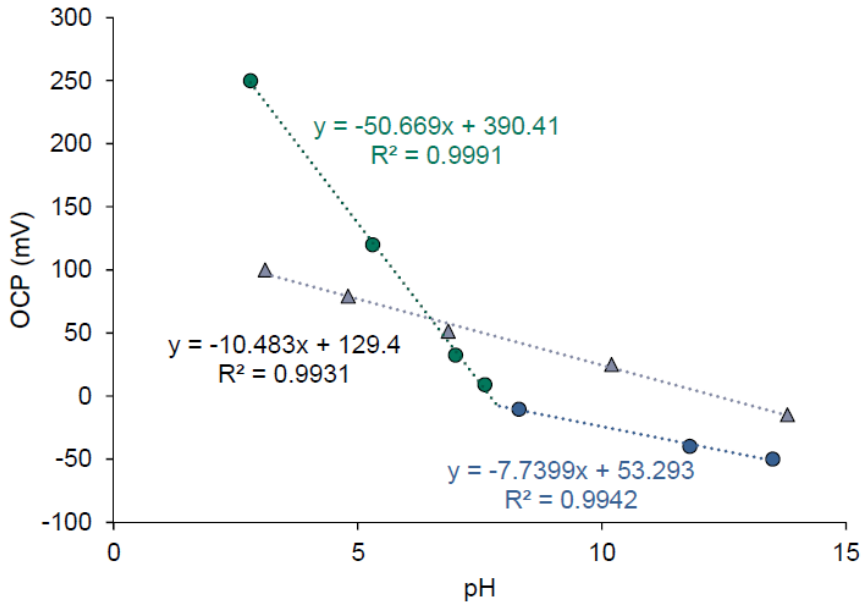

Figura 29: Trends of open circuit potentials (OCP) versus pH for PEDOT:PSS (grey triangles) and PANI (green and blue circles) electrodes.

Based on the above considerations, the high sensitivity of PEDOT:PSS/PANI in a wide range of pH, can be really attributed to a synergistic effect. In the low pH range the response is due to protonation/deprotonation of amino groups of conducting PANI. At neutral and alkaline pH the sensitivity of PEDOT/PANI can be explained considering that the ink-jet printed PEDOT:PSS contains large amounts of amorphous PSS as insulators which is added to dissolve PEDOT in water. When the PANI is electropolymerized on PEDOT:PSS, the positive charge in the PANI backbone may weaken the coulumbic attraction between PEDOT and PSS creating conductive pathways which allows an increase of the conductivity of the pristine PEDOT:PSS structure (see scheme in figure 30), similarly to the results obtained with PEDOT:PSS treated with DMSO[101], graphene oxide[132] and ethylene glycol. Thus, when PANI in the organic bilayer is in its insulating form at alkaline pH, the extended-coil conformation of PEDOT:PSS can guarantee higher

conductivity while the negative charged groups SO_3^- can contribute to the responses at neutral and alkaline pH of the solution. It is worth observing that, when the PANI load increases, the behavior of the bilayered film is similar to that of dip-coated PANI indicating that an excessive PANI load hinders the interactions between the negative charged groups SO_3^- and the solution.

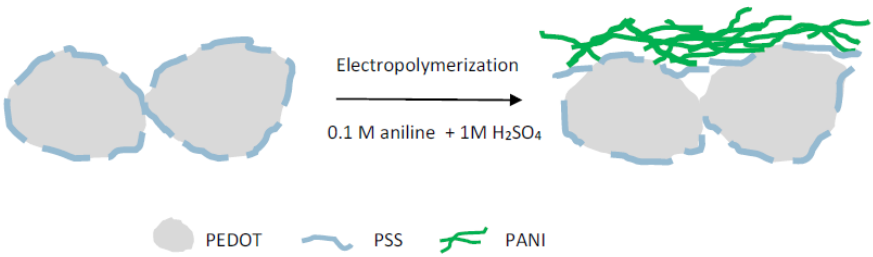

Figure 30: Sketch of the modifications of the conformation of pristine PEDOT:PSS after the electropolymerization of PANI. The grey grain and the light blue lines stand for PEDOT and PSS respectively. The green fibers stand for PANI.

4.1.4 PANI functionalized porous silicon

PANI/PSi hybrid structures were obtained by the electrochemical steps we used for the gold and PEDOT electrodes. In the first step PSi electrodes were functionalized by electrochemical reduction of NBD salts (2 mM) in acetonitrile media (Figure 31 a). The first cycle of deposition of NBD shows a cathodic peak related to the reduction of the diazonium group; in the second the displacement of the cathodic peak, as well as a decrease of the recorded current, are indicative of the progressive covering of the PSi surface. Further potentiostatic reduction of NDB was performed and then the cyclic voltammetries were repeated until the reduction peak is no more visible: this indicates that all the accessible surface of PSi is functionalized.

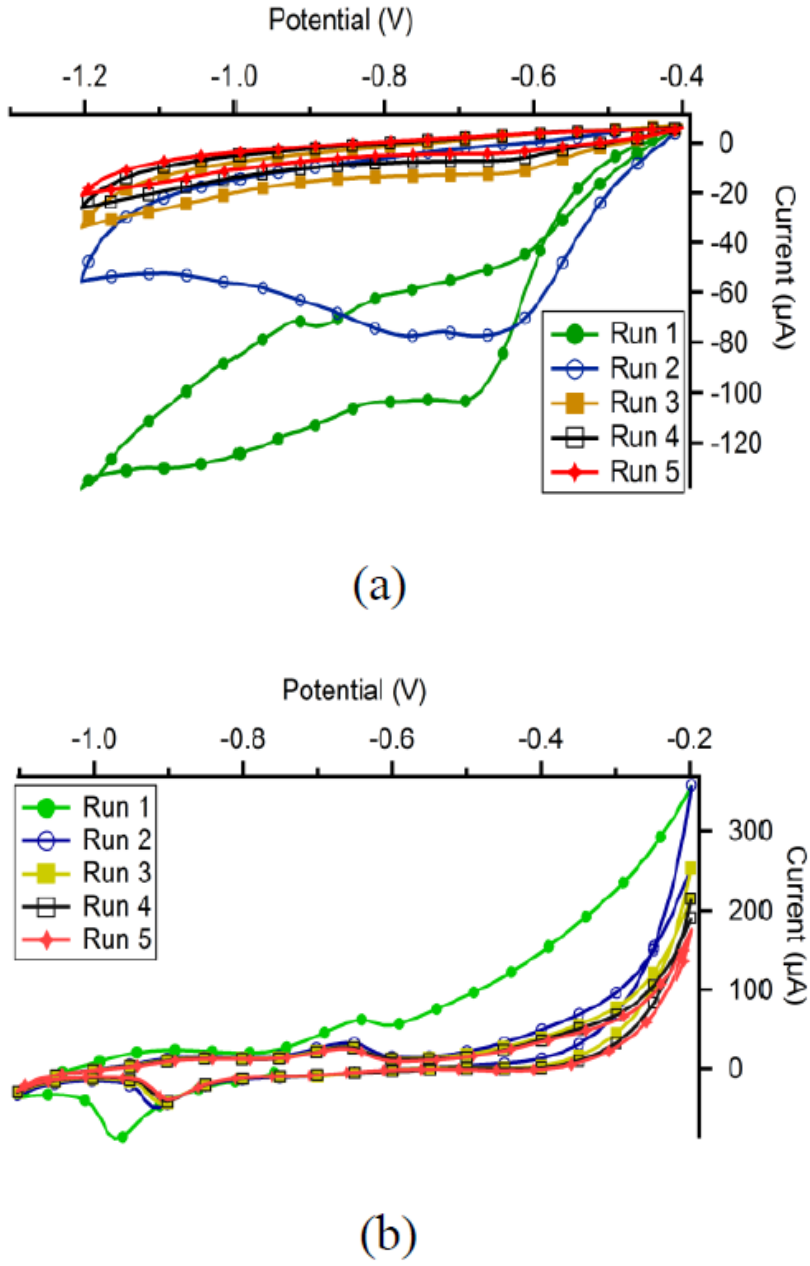

Figure 31: Cyclic voltammetries measured for the electrochemical reduction of NBD (a) and aniline polymerization (b)

In the second step, the nitro groups were electrochemically reduced to amino groups in a water/ethanol solution through CV by cycling potential from the open circuit potential to -1.7 V. Finally, the polymerization of aniline was electrochemically performed by cyclic voltammetry (CV) in a solution containing perchloric acid (0.1 M) and aniline (0.1 M) (Figure 31 b). Since acetonitrile presents a surface tension of 26 mN/m (25°C), comparable to 21.5 mN/m of Ethanol, the electropolymerization has been performed in acetonitrile to ensure an easy penetration of the solution inside pores. The number of CV cycles for the PANI deposition has been determined as the maximum number of cycles before the formation of a clustering of the polymer (visible as a surface roughness) on the external surface of PSi that leads to a decrease of the measured photocurrent value.

All samples were covered with a sputtered semitransparent gold contact and illuminated with a tungsten lamp in order to obtain photocurrent measurements, that were performed using a series of long-pass filters and using a normalization procedure as described in literature[135]. The results are shown in Figure 32.

We observe that the *p-n* junction between PANI and PSi improves the light absorption in the visible range compared to the empty porous silicon (Figure 32 a). The absolute white-light photocurrent was also higher for the hybrid junction.

In order to evaluate the reversibility between the two PANI forms, the samples have been dipped first in a basic solution (acetonitrile containing 0.1 M NH3; pH=9) and then in an acid solution (acetonitrile containing 0.1 M HClO4; pH=4).

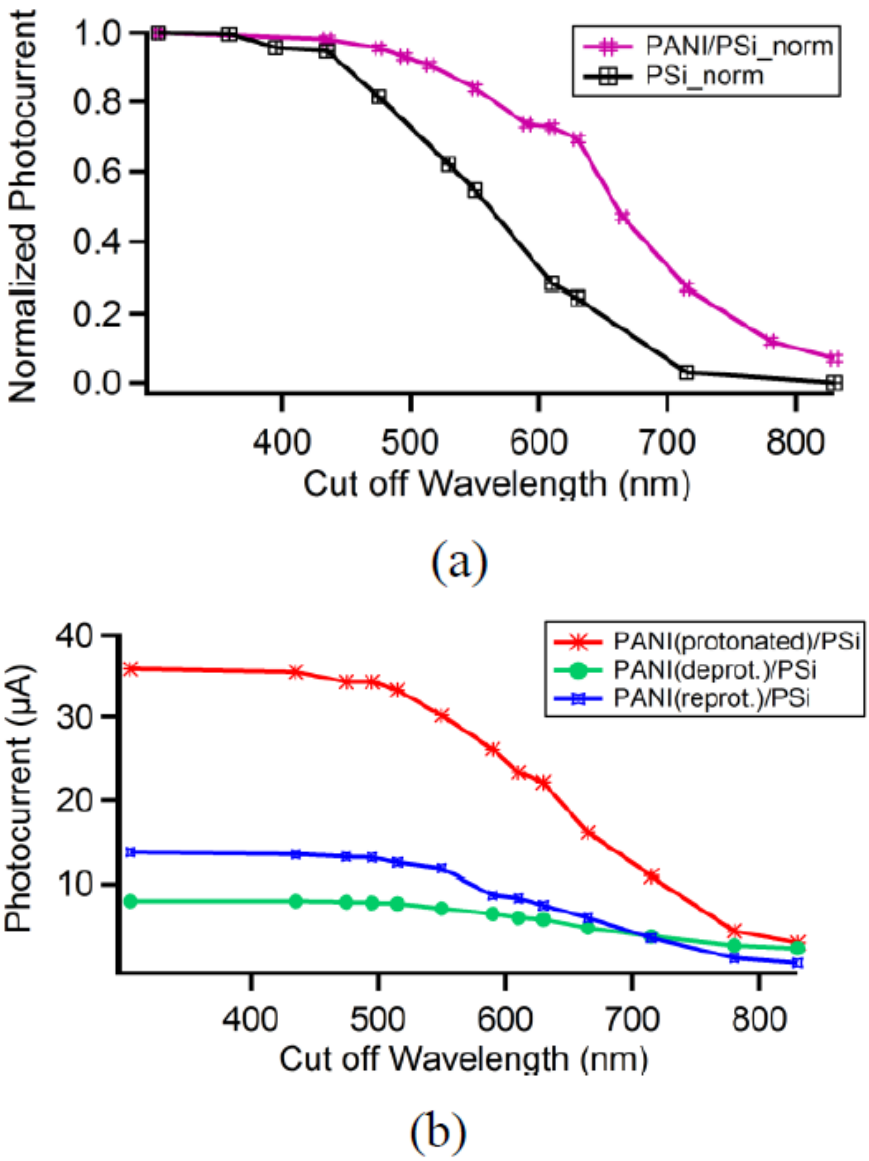

Figure 32: (a) Normalized photocurrent of PSi and PANI/PSi heterojunction. (b) Photocurrent of a PANI/PSi heterojunction before and after immersion in basic and acid solutions.

It is important to remember that we are starting from a *p*-type PANI protonated form, since it was polymerized in acid media. After each dipping step, the photocurrent was recorded. As can be seen from the Figure 32 (b), the photocurrent decreases after the dipping in basic solution. A possibile explanation of this behavior could be the transformation of *p*-type protonated PANI form at least partially in *p*-type deprotonated form, decreasing then the efficiency of the *p*-*n* junction. After the second dipping in acid media PANI partially acquires again its starting *p*-type proto-nated form as it is suggested from the photocurrent results (Figure 32 b).

4.1.5 Electrochemical detection of oligonucleotide sequences linked on gold eletrodes by diazonium salts reduction

In the field of electrochemical DNA biosensors, in literature is well studied the Self Assembled Monolayer (SAM) as oligonucleotides immobilization technique[136-138]. This procedure takes advantages of the affinity between the thiol groups and the gold surface of the electrode. This bond, however, is weaker compared with the gold-nitrophenyl group, which has also other advantages such as controllable surface concentration and stability over time (Figure 33). As the previous electrodes we discussed, functionalization is realized by the 4-nitrobenzendiazonium electroreduction.
Fig. 33 compares the functionalization of the electrode using SAM and electrografting techniques: in the second case we have 2 electrochemical steps, with a first NBD grafing and the electrochemical reduction from nitro to amino groups, and 2 chemical step, with the binding of a linker molecule (adipic acid) and finally the ssDNA immobilization on the surface, by means EDC/NHS activators, that promote the $–NH_2$ / -COOH bond (Figure 34).

The aim of the study is to investigate the influence of NBD surface concentration on the ssDNA detected.

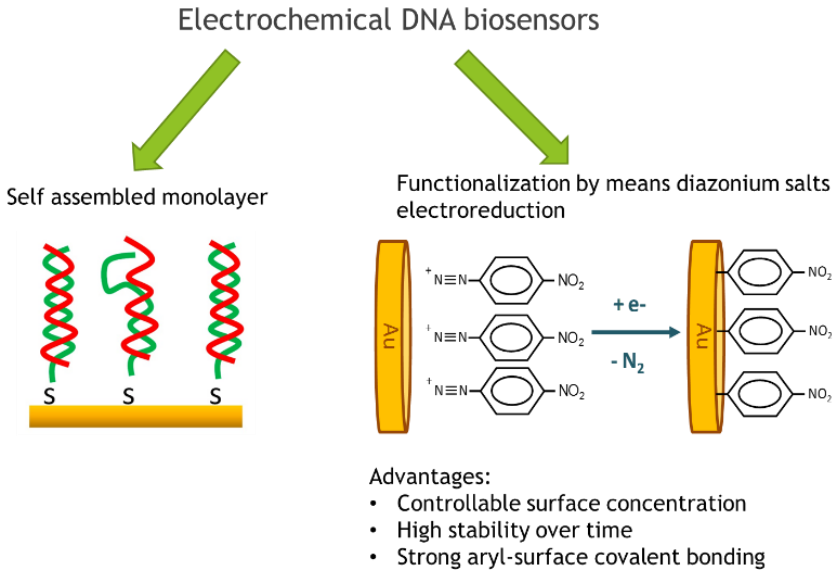

Figure 33: Comparison between Self Assembled Monolayer and electrochemical electrode functionalization.

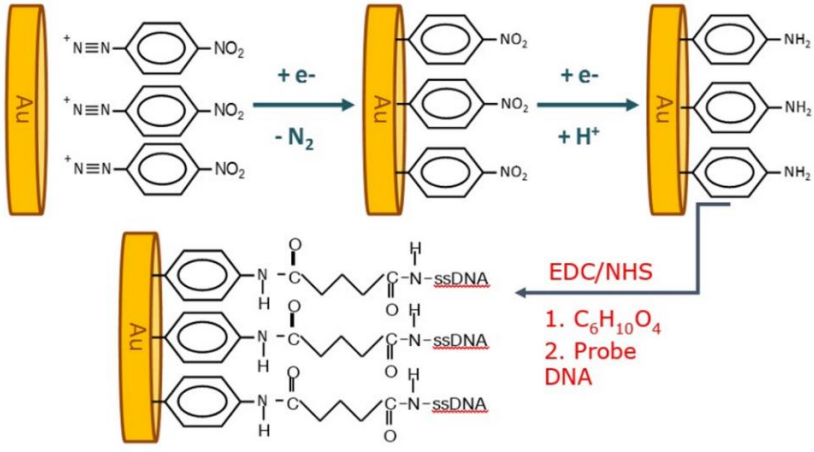

Figure 34: Steps involved in oligonucleotides chain immobilization on gold electrode.

In Figure 35 we can see the oligonucleotide chains we used for the study, that are probe 30, directly immobilized on the electrode, and fully complementary 30, 36 and 42 target DNA. These target oligonucleotides have 0, 6 and 12 overhang respectively to simulate different oligonucleotides lenght.
Also for this study the electrodes were characterized after every step with electrochemical impedance spectroscopy in presence of ferro/ferricyanide redox couple, and, to evaluate the surface concentration of ssDNA ad dsDNA, chronocoulometry with ruthenium hexamine.

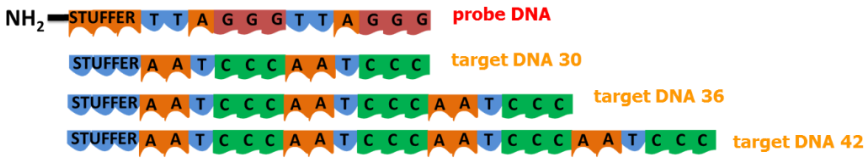

Figure 35: Probe and target DNAs

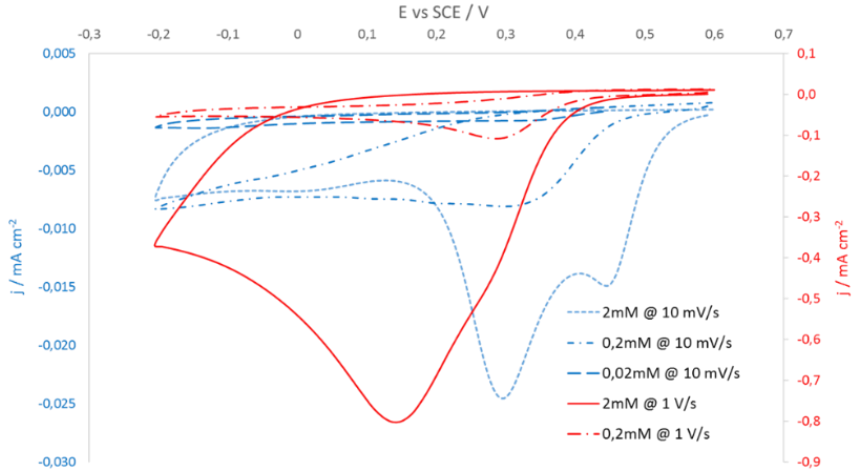

Figure 36: CV NBD grafting on gold in different scan rate and NDB solution concentration

Following the common line in this Thesis, the first electrochemical step is the NBD grafting on the gold surface. The electrodes were submitted to cyclic voltammetry varying the NDB concentration in solution (bulk concentration) from 0.02 mM up to 2 mM and the scan rate, that was 10 or 1000 mV/s.
As we can see from the Figure 36, in all the cases the reduction peak decreases with the decreasing of NBD concentration. We can observe that varying the scan rate also a peak voltage shifting is present, probably due to the different speed of surface coverage.
Figure 37 shows the different surface concentration of NBD calculated for all the scan rate/NBD bulk concentration. When bulk concentration 2mM and the scan rate 10 mM this value is about 4 times the theoretical monolayer. This value decreases along the decreasing of NBD concentration (down to 0.02 mM) and increases if we increase the scan rate.

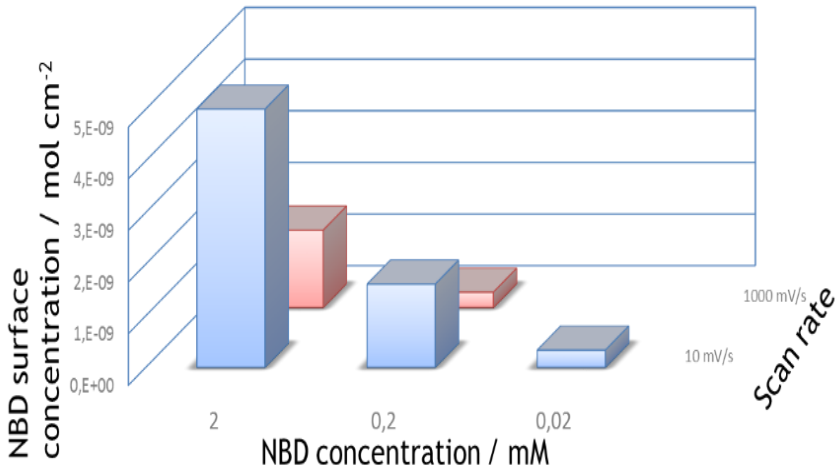

Figure 37:7 NBD surface concentration on gold at different scan rate and bulk concentrations

What is also important is how this organic layer is distributed on the surface. Using impedance spectroscopy (Fig. 38) and modeling spectra with the Randles circuit, we calculated the charge transfer

resistance before and after NBD grafting to estimate the apparent electrode coverage. From the Table 7 is it possible to see that when we use high NBD bulk concentration and low scan rate the surface coverage is almost 100%. In the other cases we have a non neglectable percentage of surface that remains bare.
As following step we did a cyclic voltammetries in presence of ethanol to reduce the nitro groups to amino groups (Figure 39).
With the aim of DNA immobilization on the surface, we decided to do not proceed with the study in the cases where the coverage was very low (about 50%).

Scan rate / mV s^{-1}	NBD conc. / mM	Surface C_{NH_2}/C_{NO_2}	Apparent electrode coverage θ
10	2	13%	99.2%
10	0.2	39%	97.9%
10	0.02	99%	53.8%
1000	2	47%	79.3%
1000	0.2	99%	57%

Tabella 7 - Apparent electrode coverage related to the different conditions of NBD grating

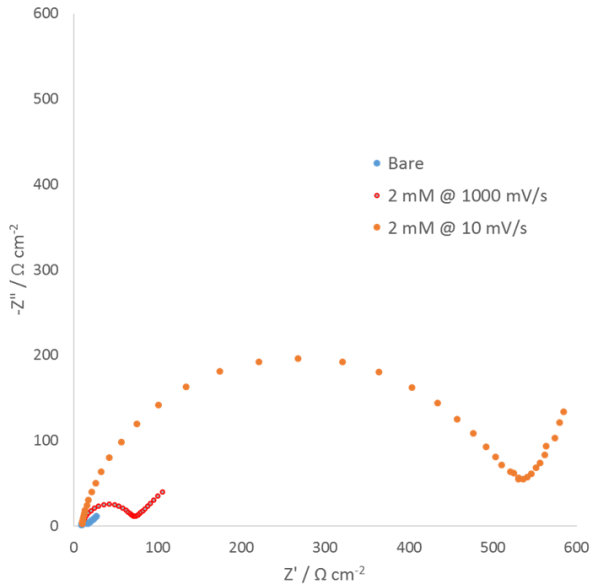

Figure 38: NBD functionalized eletrode EIS analysis

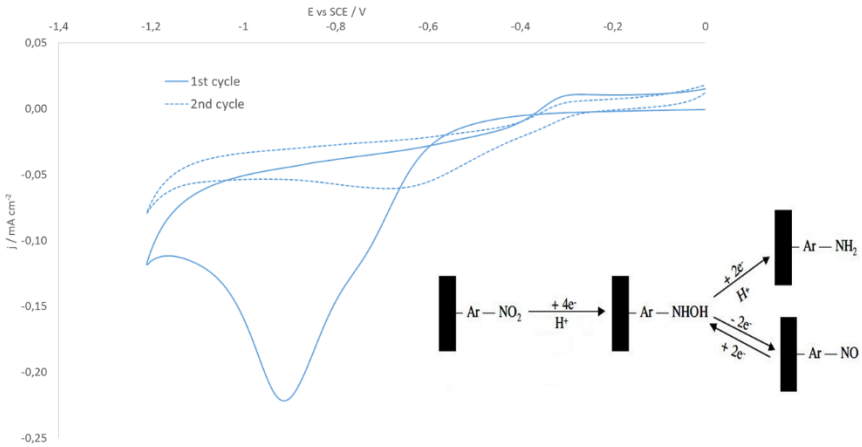

Figure 39: Nitrophenyl reduction to aminophenyl

Again using Faraday' Law, calculation of amino groups surface concentration was done (Figure 40). When extreme condition were analized, low values were obtained, while in all the other conditions this value is almost constant. What is changing is the ratio between amino and nitro groups concentrations: when scan rate is low and NBD concentration is high this ratio is near 10%, and increases in the other conditions (Table 7). The reason of this behavior was deeply discussed in the previews chapters.

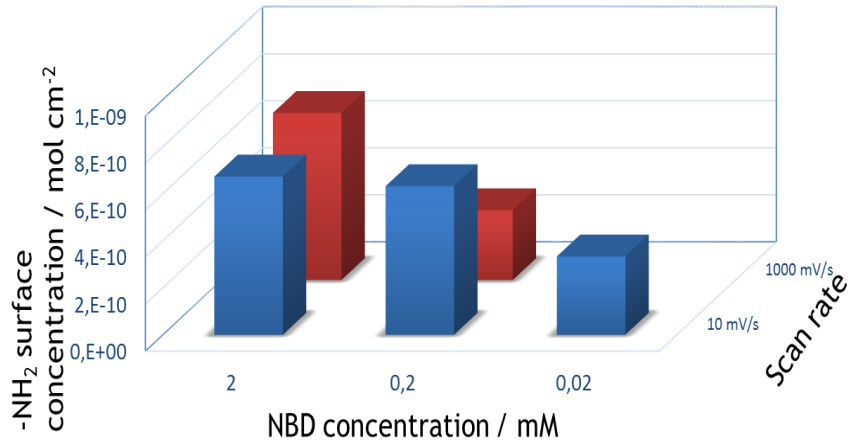

Figure 40: NH_2 groups surface concentration

Using EDC/NHC activators, first adipic acid and then ssDNA where linked on the electrode following the procedure described by Piro et al.[139], before hybridize the 3 different targets DNA (30, 36 and 42). To evaluate the surface concentration of ssDNA and dsDNA we did a chronocoulometry in presence of ruthenium hexamine to obtain the charge passed and so calculate the value by means of Cottrel' equation with the diffusion term neglected (Table 8)[120,121].
Is interesting to observe that the ssDNA concentration changes with the conditions of NBD grafted, and in particular we have the lowest value if the NBD concentration in solution is high and the scan rate is low. Looking at the hybridization efficiency, it appears independent of C_{ssDNA} when the target DNA is fully complementary, while this efficiency decreases with the increasing of C_{ssDNA} and overhang. In this context the best experimental condition in terms of DNA concentration is the first showed in the table.

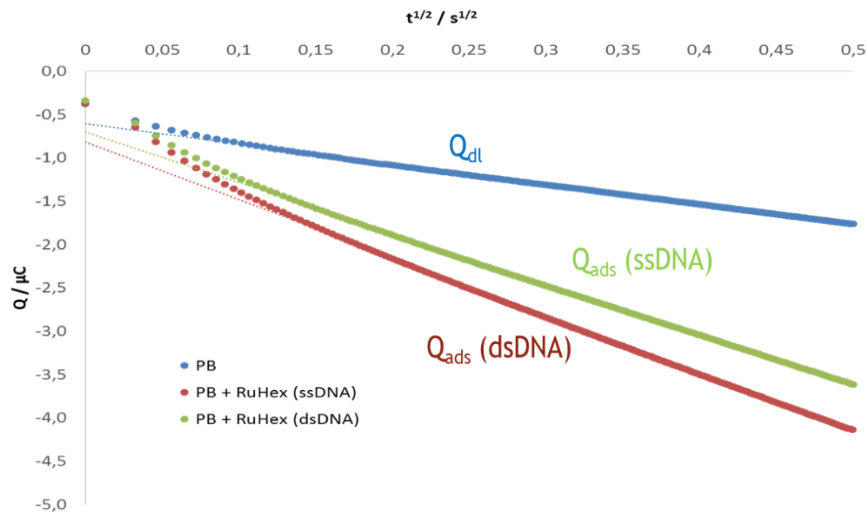

Figure 41: Chronocoulometry to evaluate the DNA surface concentration

Electrochemical impedance spectroscopy was measured before and after hybridization in order to see differences in terms of changing surface charge transfer resistance.

Nyquist plots (Figure 42) show a R_{CT} value that increases in all the cases, but if we observe the relative increasing reported in the Table 8 is different with different target DNAs. We have to consider that these values do not consider the hybridization efficiency.

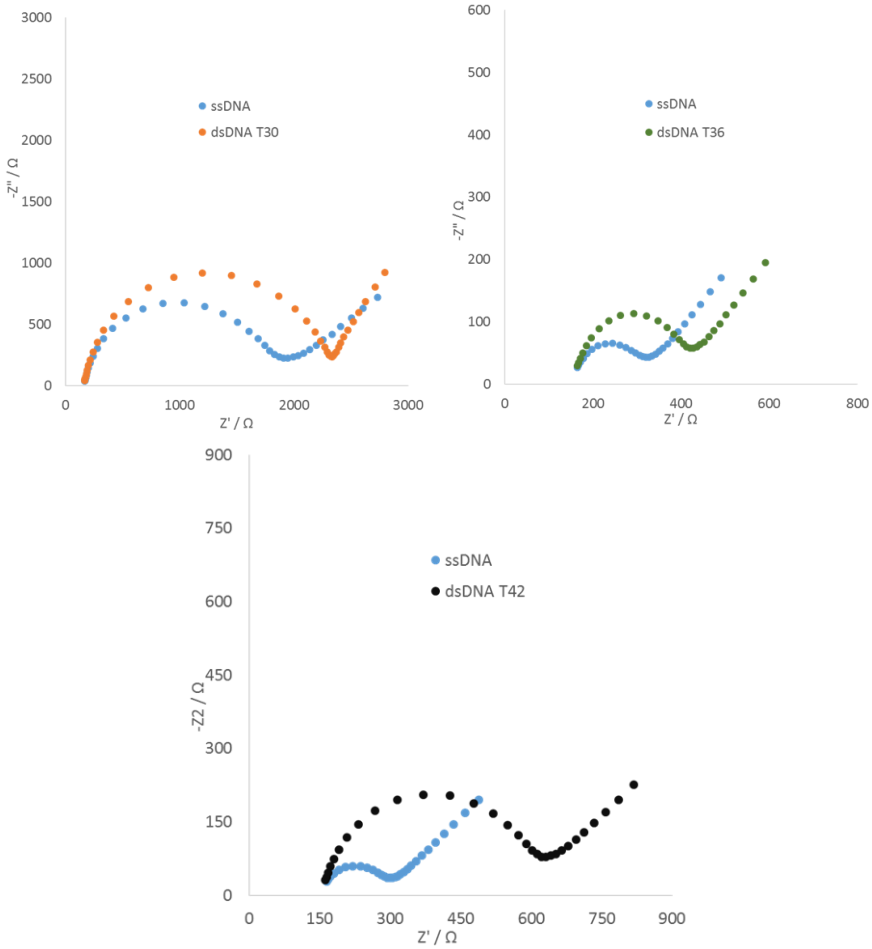

Figure 42: EIS analysis with the 3 target DNAs after and before hybridization

	dsDNA T30	dsDNA T36	dsDNA T42
$\frac{R_{CT}(ssDNA) - R_{CT}(dsDNA)}{R_{CT}(ssDNA)}$	22%	42%	215%

Table 8: Relative charge transfer resistance after hybridization

Chapter 5

Conclusions

In this Chapter conclusions are given.

Based on the objectives introduced at the beginning of this thesis, several conclusions can be drawn from this study. For a better understanding, the different topics will be analysed separately.

Diazonium salt grafting: a preliminary study on gold

The results presented indicate that nitro-phenyl groups have been successfully deposited on gold electrodes using [BMP][TFSA] as solvent for the electrochemical reduction. The amount of nitrophenyl grafted on gold and the surface coverage can be controlled by changing the scan rate during the reduction of NBD in ionic liquid. Moreover, the use of a high viscosity ionic liquid instead of acetonitrile as solvent allows to obtain low amount of the attached molecules and less dense layer.

Aniline electropolymerization

The results of the experimental study demonstrated the effec-tiveness of the approach proposed for the preparation of compositefilms of PANI onto polycrystalline gold surfaces. Through elec-trografting of nitrobenzendiazonium salt, PANI layers are moreregular and present small pores. Moreover, EIS allowed to calcu-late the higher capacitance of AuNH2/PANI with respect to thesamples prepared by simple electropolymerization. The effect ofthe under-layer on the capacitance and resistance of AuNH2/PANIis still visible also at very high number of electropolymerizationcycles. The samples obtained by the proposed approach showeda better stability if compared with analogous procedure in whichelectrografting of NBD was not used.

A metal-free sensor: pedot:pss-pani coupling

Hybrid polymeric electrodes were obtained by inkjet printing of PEDOT:PSS combined with electropolymerisation of aniline. With this approach we obtained a bilayer electrode in which PEDOT:PSS

was both active material and current collector, since metallic components were not used.

A thin film of PANI onto PEDOT:PSS was evidenced by SEM and Raman analyses. The electrodes were characterised by electrochemical impedance spectroscopy, which evidenced a large increase in the specific surface and a reduction of resistivity after coating of PEDOT:PSS substrates with PANI. The electrodes were tested as pH sensors: the results show that the hybrid structures have linear response in pH window larger than those of either PEDOT:PSS or PANI electrodes, as well as higher sensitivity.

PANI functionalized porous silicon

The results presented demonstrates that PANI/PSi heterojunctions show an increased light absorption in the visible range compared with PSi and generate higher photocurrents. We also demonstrated the possibility to modify the PANI/PSi photocurrent efficiency by a doping/de-doping process controlled by the pH. This can be used, for in-stance, to build a photovoltaic pH sensor.

Electrochemical detection of oligonucleotide sequences linked on gold eletrodes by diazonium salts reduction

In this work we have shown that we can control the surface concentration of ssDNA changing the condition of NBD grating; a complete hybridization occurs when fully complementary oligonucleotide is used and we can differentiate targets dsDNA with electrochemical impendance spectroscopy.
A possible evolution of this work could be done using different linker molecules instead of adipic acid and different diazonium salts or mixtures of diazonium salts, to change the first organic layer nature.

Appendix

Electrochemical background and techniques

This chapter is focused on the electrochemical processes taking place at electrode surface and electrochemical techniques used to investigate the electrochemical behaviour of electrode materials[140].

A.1. Electrochemical processes

Electrochemical reactions are heterogeneous chemical processes which involve the transfer of charge in a ionic conductor (electrolyte) to or from a surface (electrode), generally a metal or a semiconductor. Charge is transported through the electrode by the movement of electrons. In the electrolyte phase, charge is provided by the movement of ions. Electrochemical cells are defined most generally as two electrodes (anode and cathode) separated by at least one electrolyte phase.

The electrochemical reaction taking place in a cell is the result of two independent half-reactions, which describe the real chemical changes at the two electrodes. The reaction that take place at the electrode of interest (working electrode) can be studied by using a second electrode (counter electrode). The potential of the working electrode can be controlled with respect to the reference electrode; since reference electrode has a fixed potential it is possible to relate any changes in the cell to the working electrode.

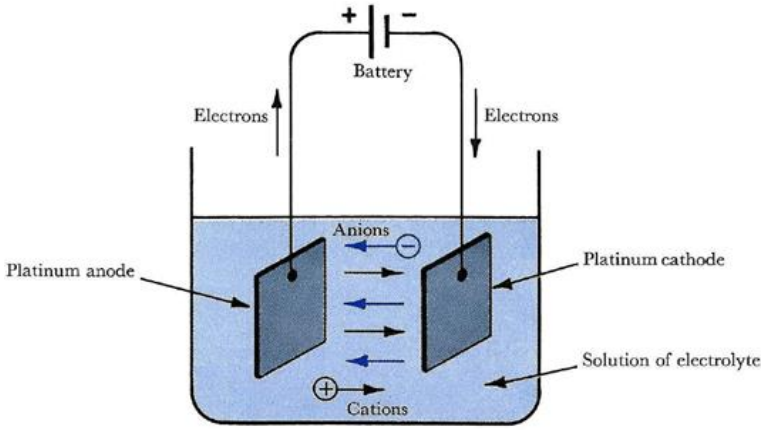

Figure 1: *Schematic diagram of an electrochemical cell.*

In a typical electrochemical experiment were a working and a reference electrode are immersed in a solution, the variation of the potential, E, by means of an external power supply, can produce a current flow in the external circuit because, as reactions occur, electrons cross the electrode/solution interfaces.
Moreover, when electrolysis occurs, in addition to electron transfer at the anode and cathode surfaces, ions must pass through the solution between the electrodes and electrons though the wires externally interconnecting the two electrodes (in order to maintain electrical neutrality at all points in the system).
Hence the current through the external circuit, *I*, given by

$$I = A\, i$$

(when *A* is the electrode area and *i* the current density), is a convenient measure of the rate of the cell reaction.
The number of electrons that cross an interface is measured in terms of the total charge, *Q*, passed in the circuit. Moreover, the current through the external circuit is a measure of the rate of the cell reaction.
The relationship between charge and amount of product formed is given by Faraday's law.

$$Q = \int_0^t I\, dt = mnF$$

where *Q* is the charge, passed during a period *t*, required to convert *m* moles of starting material to product in an electrode reaction involving the transfer of *n* electrons/molecule; *F* is 96485.4 C.
Two types of processes occur at electrodes: one kind involves processes in which charges are transferred across the electrode-solution interface. Since such reactions are governed by Faraday's law they are called faradaic processes. Electrodes at which faradaic

processes occur are sometimes called charge transfer electrodes. Under some conditions, a given electrode-solution interface will show a range of potentials where no charge-transfer reactions occur because such reactions are thermodynamically or kinetically unfavourable. However, processes such as adsorption and desorption can occur, and the structure of the electrode-solution interface can change with changing potential or solution composition. These processes are called nonfaradaic processes. Although charge does not cross the interface, external currents can flow (at least transiently) when the potential, electrode area, or solution composition change. Both faradaic and nonfaradaic processes occur when electrode reactions take place. Although the faradaic processes are usually of primary interest in the investigation of an electrode reaction, the effects of the nonfaradaic processes must be taken into account in using electrochemical data to obtain information about the charge transfer and associated reactions.

A.1.1. Nonfaradaic processes

An electrode at which no charge transfer can occur across the metal-solution interface, is called an ideal polarized electrode (IPE). While no real electrode can behave as an IPE over the whole potential range available in a solution, some electrode-solution systems can approach ideal polarizability over limited potential ranges.

At any interface between two phases and particularly between an electrode and an electrolyte solution, there exists a segregation of positive and negative charge in a direction normal to the phase boundary. These charges may be associated in the form of dipolar molecules or polarised atoms, or they may be free as holes, electrons, or ions. The charge segregation may occur through the preferential adsorption of either positive or negative ions at the interface, through the transfer of charge across the interface, or through the deformation of polarisable molecules by the asymmetrical force field at the interface. The theory of the electrical double layer is concerned with

the charge distribution and electrical potentials that arise as a consequence of this charge separation.

The study of the electrical double layer is intimately concerned with the concept of the ideally polarisable electrode; since, at ideally polarisable electrode, charge does not cross the interface during potential changes, the interface behaves like a capacitor. For a given applied potential, charge is stored in equal measure on the electrode and in the solution. In the case of a metallic electrode, the excess or deficiency of electrons is limited to a very thin surface layer, while the charge in solution is distributed in the proximity of the electrode surface. This charge distribution at the interface is called double layer with which a double-layer capacitance (C_{dl}) is associated.

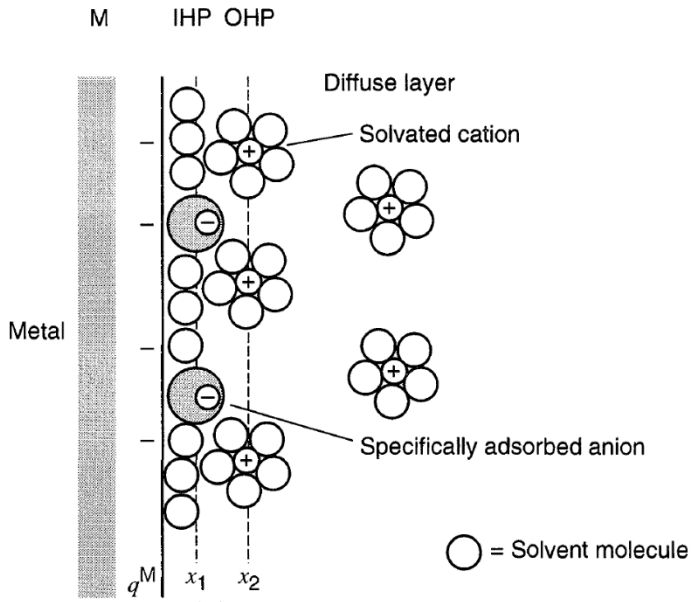

Figure 2: *Proposed model of the double-layer region under conditions where anions are specifically adsorbed.*

The solution side of the double layer is constituted of several "layers". That closest to the electrode, the inner layer, called also the Helmholtz layer, contains solvent molecules and sometimes other

species (ions or molecules). The locus of the electrical centres of the specifically adsorbed ions is called the inner Helmholtz plane (IHP), which is at a distance x_1. Solvated ions can approach the metal only to a distance x_2; the locus of centres of these nearest solvated ions is called the outer Helmholtz plane (OHP). The interaction of the solvated ions with the charged metal involves only long-range electrostatic forces, so that their interaction is essentially independent of the chemical properties of the ions. These ions are said to be nonspecifically adsorbed. Because of thermal agitation in the solution, the nonspecifically adsorbed ions are distributed in a three dimensional region called the diffuse layer, which extends from the OHP into the bulk of the solution. The structure of the double layer can affect the rates of electrode processes.

A.1.2. Faradaic processes

Electrochemical cells in which faradaic currents are flowing are classified as either galvanic or electrolytic cells. A galvanic cell is one in which reactions occur spontaneously at the electrodes when they are connected externally by a conductor.
Considering a general electrode reaction such as $O + ne^- \leftrightarrow R$, it is possible to consider that the current (or electrode reaction rate) is governed by the rates of processes such as:

- Mass transfer to the electrode surface and vice versa
- Electron transfer at the electrode surface
- Homogeneous or heterogeneous chemical reactions on the electrode surface
- Other surface reactions, such as adsorption, desorption, or crystallization (electrodeposition).

The rate constants for some of these processes depend on the potential. The simplest reaction only involves mass transfer and electron transfer steps, however, chemical reactions and adsorption/desorption processes are taking place in some reactions.

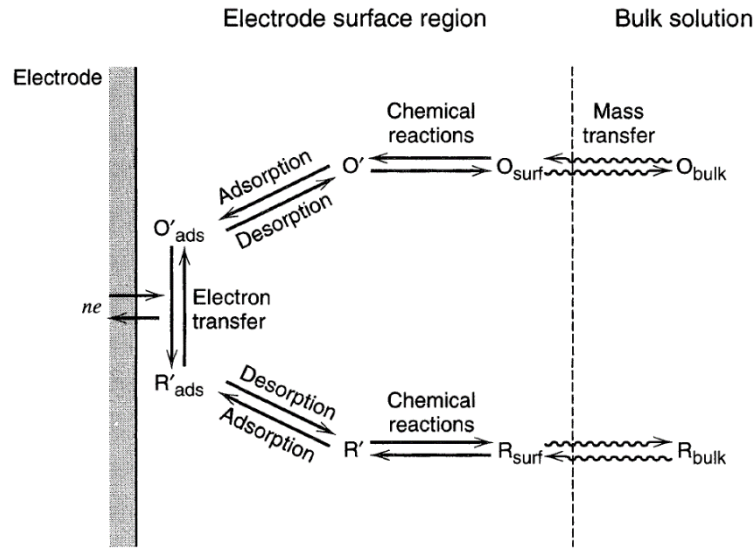

Figure 3: *Pathway of a general electrode reaction.*

The response of the electrode to the current flow corresponds to an overpotential that is the sum of different terms associated with the reaction steps occurring with a finite rate in the electrochemical cell: η_{mt} (the mass-transfer overpotential), η_{ct} (the charge-transfer overpotential), η_{rxn} (the overpotential associated with a preceding reaction), etc. The electrode reaction can then be represented by a resistance, R, composed of a series of resistances (or more exactly, impedances) representing the various steps: R_m, R_{ct}, etc.

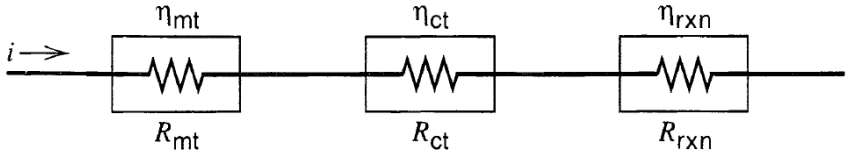

Figure 4: *Processes in an electrode reaction represented as resistances.*

A fast reaction step is characterized by a small resistance (or impedance), while a slow step is represented by a high resistance.

The kinetic of a system is strongly influenced by the applied potential, the nature and the structure of the reacting species, the solvent, the electrode material and adsorbed layers on the electrode.

A.1.3. The Butler-Volmer equation [52]

As reported above the potential of an electrode strongly affects the kinetics of reactions occurring on its surface. The phenomenological model of Butler-Volmer is able to relate the reaction rate (current density) with the applied electrode potential.
The simplest electrode process can be represented as one electron process:

$$O + e^- \leftrightarrow R$$

It is necessary to consider the thermodynamics and the kinetics of the electron transfer process. If the kinetics of electron transfer are rapid, the concentrations of *O* and *R* at the electrode surface can be assumed to be at equilibrium with the electrode potential, as governed by the Nernst equation:

$$E_{eq} = E^0 + \frac{RT}{nF}\ln\left(\frac{c_O^\sigma}{c_R^\sigma}\right)$$

where the equilibrium potential is related to the standard potential of the couple *O/R*, E^0, and the surface concentration of *O* and *R*. The standard potential clearly represents the particular equilibrium potential when the surface concentrations of *O* and *R* are equal. If no current passes through the cell no chemical change can occur; the surface concentrations must therefore be equal to the bulk concentrations c_O^∞ and c_R^∞. While no net current is flowing and there is no overall chemical change in the cell, there must be a dynamic equilibrium at the working electrode surface, for example the reduction of *O* and the oxidation of *R* are both occurring, but the processes are of equal rate:

$$i_0 = -\vec{\imath} = \overleftarrow{\imath}$$

where I_0 is the exchange current density, and $\vec{I}$ and $\overleftarrow{I}$ are the partial current densities for the forward and backward reactions.
The magnitude of the current flowing at any potential depends on the kinetics of electron transfer. At any potential the measured current density in given by

$$i = \vec{\imath} + \overleftarrow{\imath}$$

(where $\vec{\imath}$ is negative); the current density is dependent on a rate constant and the concentration of the electroactive species at the site of the electron transfer, the electrode surface, i.e.

$$\vec{\imath} = -nF\vec{k}c_O^{\sigma} \qquad and \qquad \overleftarrow{\imath} = -nF\overleftarrow{k}c_R^{\sigma}$$

The rate constant vary with the applied electron potential according to the equations of the form

$$\overrightarrow{k_c} = \overrightarrow{k_0}\exp\left(-\frac{\alpha_c n\,F}{R\,T}E\right) \qquad and \qquad \overleftarrow{k_a} = \overleftarrow{k_0}\exp\left(\frac{\alpha_a n\,F}{R\,T}E\right)$$

where α_a e α_c are constants (between 0 e 1 and generally approximately 0.5) known as the transfer coefficients for the anodic and cathodic reactions, respectively. For a simple electron transfer reaction $\alpha_a + \alpha_c = 1$, so that one transfer coefficient may be eliminated from any equation; $\overrightarrow{k_c}$ and $\overleftarrow{k_a}$ represent the heterogeneous rate constant of the reduction and oxidation reaction, respectively.

At equilibrium ($E=E_{eq}$) the net current density is zero and the potential of the working electrode is given by the Nernst equation.

Taking these information into account it is possible define the overpotential as the deviation of the potential from the equilibrium value:

$$\eta = E - E_{eq}$$

Taking into account the definition of the exchange current density, $i_0 = -\vec{\imath} = \overleftarrow{\imath}$ at $\eta=0$ it is possible to obtain the Butler-Volmer equation:

$$i = i_0 \left[\exp\left(\frac{\alpha_a nF}{RT}\eta\right) - exp\left(\frac{\alpha_c nF}{RT}\eta\right)\right]$$

It is possible to observe how current density varies with exchange current density, overpotential, and the transfer coefficients.
Depending on the overpotential value, three cases can be distinguished: the first two applying an high overpotential value, while the third applying a very low overpotential:

- $|\overleftarrow{\imath}| \gg |\vec{\imath}|$
  $logi = logi_0 + \frac{\alpha_a nF}{2.3\ RT}\eta$

- $|\vec{\imath}| \gg |\overleftarrow{\imath}|$
  $log - i = logi_0 - \frac{\alpha_c nF}{2.3\ RT}\eta$

- $\eta \ll RT/\alpha_c nF$ and $\eta \ll RT/\alpha_a nF$
  $i = i_0 \frac{nF}{RT}\eta$

The first two cases are known as the Tafel equations and are the basis of a simple method of determining the exchange current density and a transfer coefficient.

As shown in Figure 5, both linear segments extrapolate to an intercept of $logi_0$. The plots deviate sharply from linear behaviour as η

approaches zero, because the back reactions can no longer be regarded as negligible.

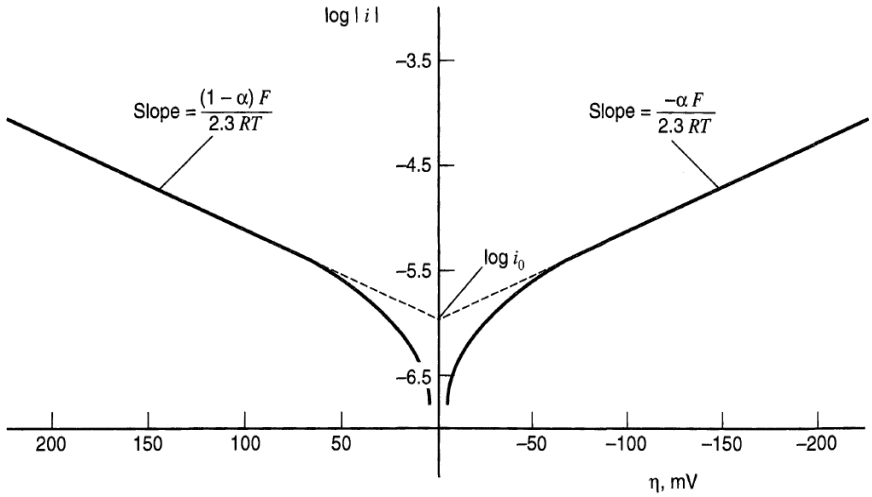

Figure 5: *Tafel plots for anodic and cathodic branches of the current-overpotential curve for O + e *= R with a = 0.5, T = 298 K.*

A.2. Electrochemical techniques

A.2.1. Potential sweep techniques and cyclic voltammetry

The electrochemical behaviour of a system can be obtained through a series of steps to different potentials with recording of the current-time curves. Potential sweep techniques, such as cyclic voltammetry, are widely used to determine the kinetic parameters for a large variety of mechanisms. This technique permits to obtain the potentials at which processes occur and to identify the presence of coupled homogeneous reactions. Although better techniques probably exist for the determination of precise kinetic data, cyclic voltammetry is the technique of choice when studying a system for the first time.

Figure 6 shows the potential-time waveforms used for sweep measurements.

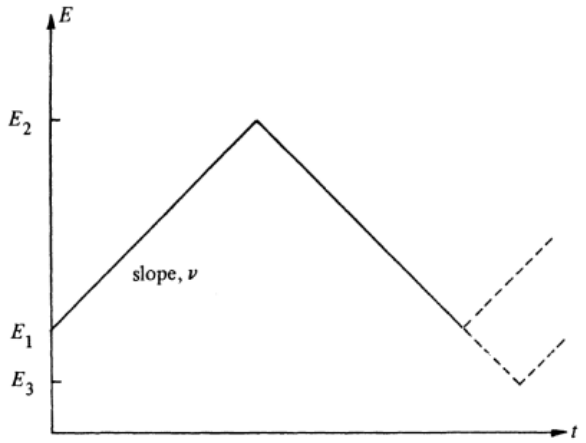

Figure 6: *Potential-time profiles for sweep-voltammetry.*

Cyclic voltammetry (CV) involves sweeping the electrode potential between limits E_1 and E_2 at a known sweep rate, v; on reaching the potential E_2 the sweep is reversed. On again reaching the initial potential, E_1, there are several possibilities. The potential sweep may be halted, again reversed, or alternatively continued further to a value E_3. The linear sweep voltammetry (LSV) involves sweeping the electrode potential between limits E_1 and E_2 at a known sweep rate, v. In both CV and LSV experiments the cell current is recorded as a function of the applied potential. Cyclic voltammetry techniques are used to study a system for the first time: it is usual to start by carrying out qualitative experiments before proceeding to semi-quantitative and finally quantitative ones from which kinetic parameters may be calculated.

Voltammograms are recorded over a wide range of sweep rates and for various values of E_1, E_2 and E_3; observing how peaks appear and disappear as the potential limits and sweep rate are varied it is possible to determine how the processes represented by the peaks are related. At the same time, from the sweep rate dependence of the peak

amplitudes the role of adsorption, diffusion, and coupled homogeneous chemical reactions may be identified.

A.2.2. Reversible reactions

For a simple reversible reaction where only O is initially present in solution

$$O + e^- \leftrightarrow R$$

it is possible to record a voltammogram that appear like a steady-state *I* vs *E* curve when a very slow linear potential sweep is applied to such a system. Figure 7 shows a typical cyclic voltammogram where it is possible observe that the charge associated with the anodic process is low compared to the forward reduction process.

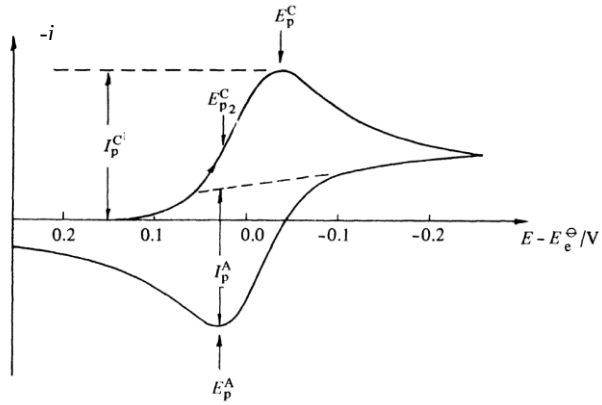

Figure 7: *Cyclic voltammogram for a reversible process; Initially only O is present in solution.*

This is because throughout most of the experiment, there is a concentration difference driving *R* away from the electrode; most of the product, *R*, therefore diffuses into the bulk solution and cannot be reoxidised on the timescale of a cyclic voltammetric experiment.

The peak current density has been found to be proportional to the concentration of electroactive species and to the square roots of the sweep rate and diffusion coefficient for a planar diffusion:

$$i_p = -0.4463\, nF \left(\frac{nF}{RT}\right)^{1/2} c_O^{\infty} D^{1/2} \nu^{1/2}$$

This is called the Randles-Sevčik equation and at 25°C this reduces to the form

$$i_p = -(2.69 \times 10^5) n^{3/2} c_O^{\infty} D^{1/2} \nu^{1/2}$$

where i_p, the peak current density is in A cm^{-2}, D is in cm^2 s^{-1}, v is in V s^{-1}, and c_O^{∞} is in mol cm^{-3}.

The reversibility of the system can be tested checking whether a plot of i_p as a function of $v^{1/2}$ is both linear and passes through the origin (or alternatively whether $i_p/v^{1/2}$ is a constant). If this is found to be true further diagnostic tests can be applied, all of which should be satisfied by a reversible system.

The test of reversibility has to be applied over a wide range of sweep rates or false conclusions may be reached. A reversible cyclic voltammogram can only be observed if both *O* and *R* are stable and the kinetics of the electron transfer process are fast so that at all potentials and potential scan rates the electron transfer process on the surface is in equilibrium so that surface concentrations follow the Nernst equation.

The following experimental parameter values can be useful to characterize the cyclic voltammogram of a reversible process at 25°C:

- $\Delta E_p = E_p^A - E_p^C = {}^{59}/_{n}\ mV$
- $\left|E_p - E_{p/2}\right| = {}^{59}/_{n}\ mV$
- $\left|i_p^A / i_p^C\right| = 1$
- $i_p \propto \nu^{1/2}$

- E_p is independent of ν
- At potentials beyond E_p, $i^{-2} \propto t$

A.2.3. Irreversible systems

In the case of the reversible system discussed above, the electron transfer rates at all potentials are significantly greater than the rate of mass transport, and therefore Nernstian equilibrium is always maintained at the electrode surface. When the rate of electron transfer is insufficient to maintain this surface equilibrium then the shape of the cyclic voltammogram changes. For such a system at low potential scan rates the rate of electron transfer is greater than that of mass transfer, and a reversible cyclic voltammogram can be recorded; however, the rate of mass transport increases with increasing scan rates and becomes comparable to the rate of electron transfer leading to increase the peak separation. Furthermore the peak height is slightly reduced from that for a reversible system.

For irreversible systems the peak current density can be calculated by:

$$i_p = -(2.99 \times 10^5) n (\alpha_C n_\alpha)^{1/2} c_O^\infty D_O^{1/2} \nu^{1/2}$$

where n_α is the number of electrons transferred up to, and including, the rate determining step. The peak current density is proportional not only to the concentration and to the square root of the sweep rate, as in the case of reversible system, but also to the square root of the transfer coefficient. For an irreversible system, $E_p{}^c$ is found to vary with the sweep rate as shown below:

$$E_p^C = K - \frac{2.3\ RT}{2\alpha_C n_\alpha F} log\nu$$

where

$$K = E^0 - \frac{RT}{\alpha_C n_\alpha F}\left[0.78 - \frac{2.3}{2} log\left(\frac{\alpha_C n_\alpha F D}{k_0^2 RT}\right)\right]$$

The shape factor $\left|E_p - E_{p/2}\right|$ is different for the irreversible case and is given by

$$\left|E_p - E_{p/2}\right| = \frac{48}{\alpha_C n_\alpha}\, mV\ at\ 25°C$$

From this equation it is possible to estimate the factor $\alpha_C n_\alpha$ required for the estimation of *D* and k^0.

The following experimental parameter values can be useful to characterize the cyclic voltammogram of an irreversible process at 25°C:

- No reverse peak
- $i_p^C \propto \nu^{1/2}$
- E_p^C shifts $-30/\alpha_C n_\alpha mV$ for each decade increase in ν
- $\left|E_p - E_{p/2}\right| = 48/\alpha_C n_\alpha\ mV$

A.2.4. Quasi reversible systems

It is quite common for a process that is reversible at low sweep rates to become irreversible at higher ones after having passed through a region known as quasi-reversible at intermediate values. This transition from reversibility occurs when the relative rate of the electron transfer with respect to that of mass transport is insufficient to maintain Nernstian equilibrium at the electrode surface. This

change from reversible, to quasi-reversible and finally irreversible behaviour can readily be seen from a plot of i_p as a function of $v^{1/2}$ as shown in Figure 8.

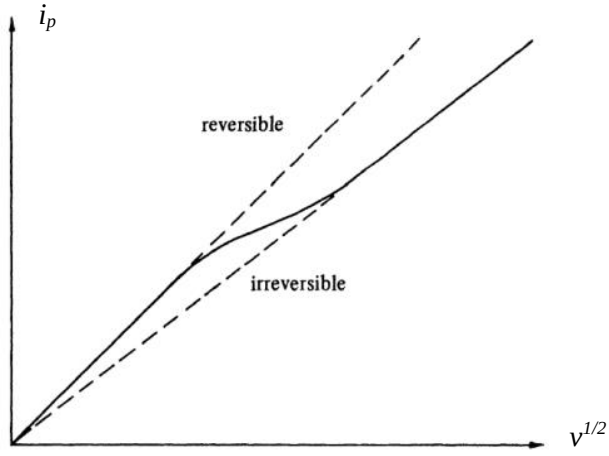

Figure 8: *Plot of the dependence of the peak current density on the square root of the potential sweep rate, showing the transition from reversible to irreversible behaviour with increasing sweep rate* α_c*= 0.5.*

The following experimental parameter values can be useful to characterize the cyclic voltammogram of a quasi-reversible process:

- $|i_p|$ increases with $v^{1/2}$ but is not proportional to it
- $|i_p^A/i_p^C| = 1$ provided $\alpha_A = \alpha_C = 0.5$
- ΔE_p is greater than $59/n$ mV and increases with increasing v
- E_p^C shifts negatively with increasing v

A.3. Potential step techniques

A complete analysis of any electrochemical process requires the identification of all the individual steps and, where possible, their quantification. Such a description requires at least the determination

of the standard rate constant, k_0, and the transfer coefficients, α_A and α_C, for the electron transfer step, the determination of the number of electrons involved and of the diffusion coefficients of the oxidised and reduced species (if they are soluble in either the solution or the electrode).
For an electrode reaction where only *O* is initially present in the solution

$$O + e^- \leftrightarrow R$$

the potential-time profile (Figure 9) can be obtained choosing a potential E_1 such that no reduction of *O*, or indeed any other electrode reaction, occurs.

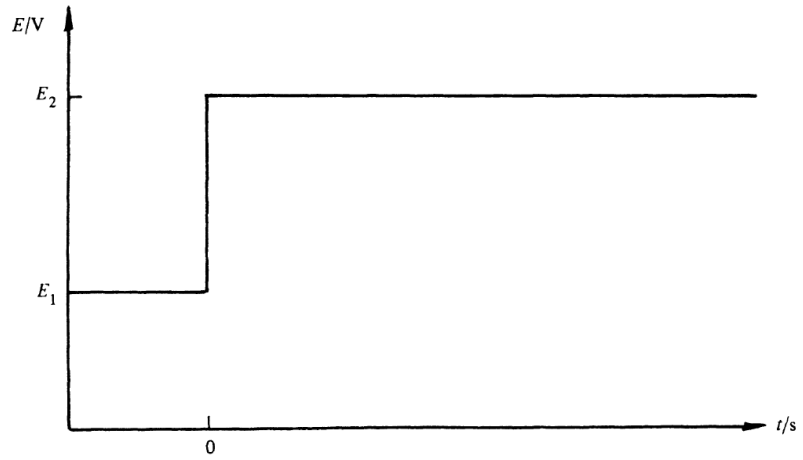

Figure 9: *The potential-time profile for a single potential step chronoamperometric experiment.*

Then at time $t = 0$ the potential is instantaneously changed to a new value E_2, where the reduction of *O* occurs at a diffusion controlled rate. Solving the Fick's 2nd Law with the appropriate boundary conditions for a planar electrode it is possible to obtain the Cottrell equation:

$$|i| = \frac{nFD^{1/2}c_O^{\infty}}{\pi^{1/2}t^{1/2}}$$

It is possible to observe in Figure 10 (curve a) that the current falls as $t^{-1/2}$. A plot of i vs $t^{-1/2}$ should therefore be linear and should pass through the origin, and the diffusion coefficient of species *O* can be found from the gradient of the straight line.

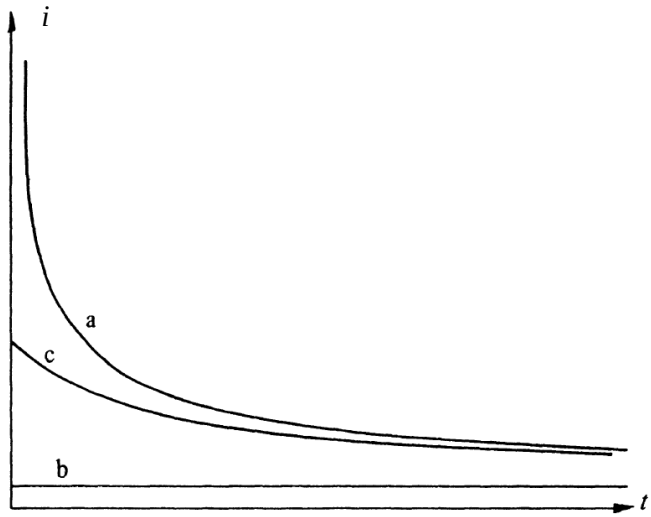

Figure 10: *I-t responses for a potential step experiment. The potential E_2 is chosen so that a: the reaction is diffusion controlled, b: the reaction is kinetically controlled, and c: there is mixed control.*

If the standard rate constant for the reaction described above is very small (or E_2 corresponds to a low overpotential for the reaction), a current time transient of the type shown by curve *b* of Figure 10 will be observed. This is because the surface concentration of *O* does not change significantly (<1%) due to the imposition of the pulse, and therefore diffusion does not play a significant role in determining the rate. The measurement is essentially a steady state one. For the intermediate situation, where the rates of diffusion and electron transfer are comparable, the *i* vs *t* transient has the form shown by curve *c* of Figure 10; the current falls with time but less steeply than

for the diffusion controlled case. Under these conditions the system is said to exhibit mixed control.

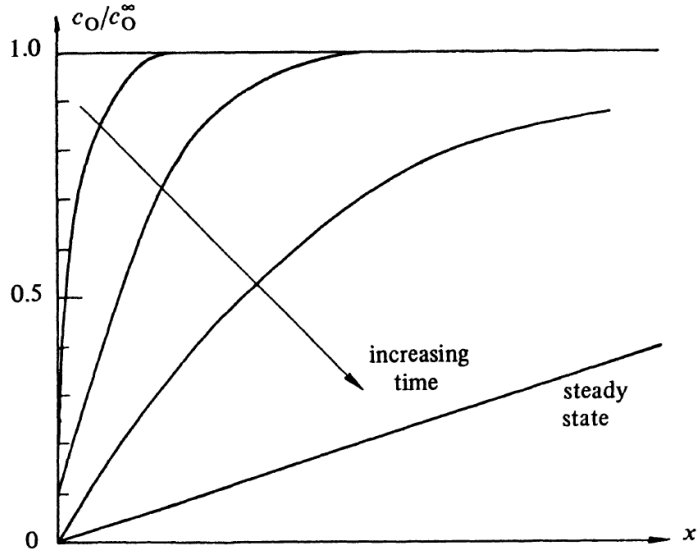

Figure 11: *A schematic diagram of the time evolution of the concentration profiles for a species O undergoing reduction under conditions of mixed control.*

The time evolution of the concentration profile for species *O* under mixed control is shown in Figure 11. The flux of *O* at the surface is simply given by Fick 's 1st Law:

$$J = -D(\partial c_O/\partial x)_{x=0}$$

From Figure 11 it can be seen that this flux is greatest at short times. Indeed at time *t=0*, i.e. immediately after the potential step is applied, the flux would be infinite and therefore the current density at time *t=0* ($i_{t=0}$) would be kinetically controlled, and from its value the rate constant for the electrode reaction could be found. Unfortunately, for a number of reasons, the value of $i_{t=0}$ cannot be directly measured.
Since $i_{t=0}$ cannot be measured directly it is necessary to resort to an extrapolation procedure to obtain its value, and whilst direct extrapolation of an *i* vs *t* transient is occasionally possible, a linear

extrapolation is always preferable. In order to see how this should be done we must first solve Fick's 2nd Law for a potential step experiment under the conditions of mixed control. The differential equations to be solved are

$$\frac{\partial c_O}{\partial t} = D_O \frac{\partial^2 c_O}{\partial x^2}$$
$$\frac{\partial c_R}{\partial t} = D_R \frac{\partial^2 c_R}{\partial x^2}$$

and for the case where both *O* and *R* are present in the solution prepared for the experiment, and the potential is stepped to negative overpotentials, these must be solved subject to specific initial and boundary conditions appropriate to mixed control. It has been found that at short times a plot of i vs $t^{1/2}$ should be a straight line of intercept $i_{t=0}$ given by

$$i_{t=0} = -nF\vec{k}c_O^{\infty}$$

from which the potential dependent rate constant k can be obtained.

An analysis of experimental transient data can be made in the following manner: $it^{1/2}$ is first plotted as a function of $t^{1/2}$ as shown in Figure 12.
The horizontal region at large values of $t^{1/2}$ corresponds to the diffusion controlled region, whereas the short time data are affected by kinetics.
With all determinations of reaction kinetics it is usual to perform experiments over a range of potentials, thus obtaining a range of potential dependent rate constants.

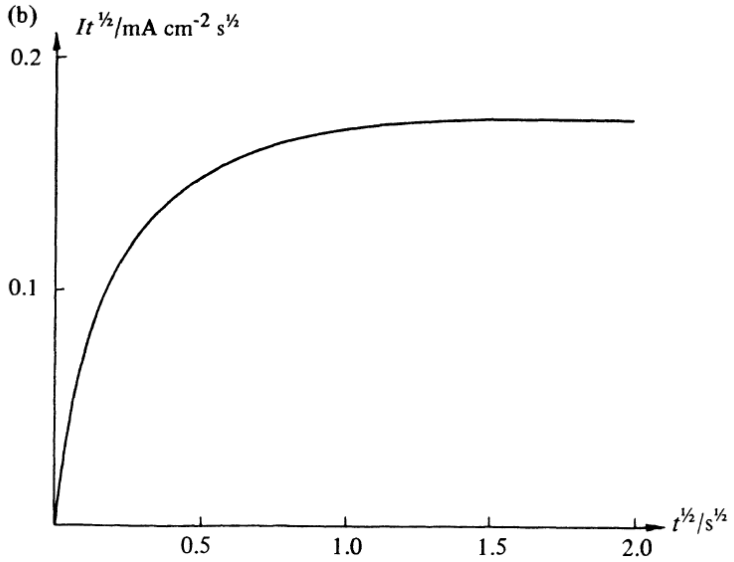

Figure 12: *Analysis of i-t data from a chronoamperometric experiment corresponding to* $\vec{k}$ *= 10^{-2} cm s^{-1}, D = 10^{-5} cm^2 s^{-1}, and* c_O^{∞}*=10^{-6} molcm^{-3}; it$^{1/2}$ plotted as a function of t$^{1/2}$*

$$\vec{k} = k^0 exp\left(-\frac{\alpha_C nF\left(E - E_{eq}^0\right)}{RT}\right)$$

$$\overleftarrow{k} = k^0 exp\left(-\frac{\alpha_A nF\left(E - E_{eq}^0\right)}{RT}\right)$$

Plots of $log\vec{k}$ or $log\overleftarrow{k}$ as a function of *E* should therefore be linear, and from the gradient of these straight lines the values of the transfer coefficient α_A and α_B may be obtained. If $log\vec{k}$ (or $log\overleftarrow{k}$) is not a linear function of *E* it is probable that the reaction mechanism is more complex than had been assumed.

Bibliography

1. Pinson J., Podvorica F., «Attachment of organic layers to conductive or semiconductive surfaces by reduction of diazonium salts.» Chem Soc Rev. 2005 May;34(5):429-39. Epub 2005 Feb 23.

2. C. Bourdillon, M. Delamar, C. Demaille, R. Hitmi, J. Moiroux, J. Pinson, «Immobilization of glucose oxidase on a carbon surface derivatized by electrochemical reduction of diazonium salts» Journal of Electroanalytical Chemistry, Volume 336, Issues 1–2, 30 September 1992, Pages 113-123

3. M. M. Chehimi, J. Pinson, «Attachment of Organic Layers to Materials Surfaces by Reduction of Diazonium Salts» DOI: 10.1002/9783527650446.ch1

4. A.Vacca, M.Mascia, S.Rizzardini, S.Palmas, L.Mais, «Coating of gold substrates with polyaniline through electrografting of aryl diazonium salts» Electrochimica Acta (2014) 126:81-89

5. P. Allongue, C.Henry de Villeneuvea, J. Pinson, F. Ozanam, J.N. Chazalviel, X. Wallart, «Organic monolayers on Si(111) by electrochemical method» Electrochimica Acta Volume 43, Issues 19–20, 16 June 1998, Pages 2791–2798

6. M. Ceccato, A. Bousquet, M. Hinge, S. Uttrup Pedersen, K. Daasbjerg, «Using a Mediating Effect in the Electroreduction of Aryldiazonium Salts To Prepare Conducting Organic Films of High Thickness» Chem. Mater. 23 1551- 1557

7. Combellas C., Kanoufi F., Pinson J., Podvorica F., «Time-of-flight secondary ion mass spectroscopy characterization of the covalent bonding between a carbon surface and aryl groups», 2005 Langmuir 21, 280-286.

8. Kariuki J.K., McDermott M.T., «Formation of multilayers on glassy carbon electrodes via the reduction of diazonium salts» 2001 Langmuir 17, 5947-5951.

9. Actis P, Caulliez G., Shul G., Opallo M., Mermoux M., Marcus B., Boukherroub R., Szunerits S., «Functionalization of glassy carbon with diazonium salts in ionic liquids» 2008 Langmuir 24, 6327- 6333.

10. Ghilane J., Martin P., Fontaine O., Lacroix, J.C., Randriamahazaka H., «Modification of carbon electrode in ionic liquid through the reduction of phenyl diazonium salt. Electrochemical evidence in ionic liquid» 2008 Electrochem. Commun. 10, 1060-1063.

11. Jin Z., Lomeda J.R., Price B.K., Lu W., Zhu Y., Tour J.M., «Mechanically assisted exfoliation and functionalization of thermally converted grapheme sheets» 2009 Chem.Mater. 21, 3045-3047.

12. Fontaine O., Ghilane J., Martin P. Lacroix J.C., Randriamahazaka H., «Ionic liquid viscosity effects on the functionalization of electrode material through the electroreduction of diazonium» 2010 Langmuir 26, 18542- 18549

13. Smith M.B., March J., «March's Advanced Organic Chemistry 5th edn» John Wiley & Sons, Inc. , New York , p. 448 2001.

14. Vogel A.I. , Tatchell A.R. , Furnis B.S. ,Hannaford A.J. , Smith P.W.G., «Vogel's Textbook of Practical Organic Chemistry» 5th edn , Pearson Education Limited , Harlow, England , p. 920 1989

15. Baranton S. ,Bélanger D., «Electrochemical Derivatization of Carbon Surface by Reduction of in Situ Generated Diazonium Cations» 2005, J.Phys. Chem. B , 109 , 24401.

16. Zollinger H., «Diazo Chemistry» 2004, John Wiley & Sons, Inc. , New York.

17. Hegarty A.F., «Kinetics and Mechanisms of Reactions Involving Diazonium and Diazo Groups, in The Chemistry of Diazonium and Diazo Groups» 1978, John Wiley & Sons, Inc. , New York , pp. 511 – 591.

18. Acevedo D.F., Rivarola C.R., Miras M.C., Barbero C.A., 2011 Electrochim. Acta ,56 , 3468.

19. Belmont J.A. ,Amici R.M., Galloway C.P., 2001 US Patent 7294185 (to Cabot Corporation).

20. Galli C., 1988, Chem. Rev. , 88 , 765

21. Elofson R.M., 1958, Can. J. Chem. , 36 ,1207.

22. Koval'chuk E.P., Kozlovs'ka Z.E., Jackowska K., Roshal A. ,Wroblewska A., Reshetnyak O.V., Blazejowski J., 2004, Pol. J. Chem. , 78 , 139.

23. Elofson R.M., Gadallah F.F., 1971, J. Org. Chem. , 36 , 1769.

24. Bard A.J., Gilbert J.C., Goodin R.D., 1974, J. Am. Chem. Soc. , 96 , 620.

25. Andrieux C.P., Pinson J., 2003, J. Am. Chem. Soc. , 125 , 14801.

26. Vase K., «Novel Approaches for Electrochemically assisted Covalent Modifi cation of Carbon Surfaces» 2007, PhD Thesis, University of Aarhus, DK.

27. M. Dequaire, C. Degrand, B.J. Limoges, «Biotinylation of screen-printed carbonelectrodes through the electrochemical reduction of the diazonium salt of p-aminobenzoyl biocytin» J. Am. Chem. Soc. 121 (1999) 6946

28. B.P. Corgier, C.A. Marquette, L.J.J. Blum, «Diazonium-protein adducts for graphiteelectrode microarrays modification: direct and addressed electrochemicalimmobilization» J. Am. Chem. Soc. 127 (2005) 18328.

29. A. Shabani, A.W.H. Mak, I. Gerges, L.A. Cuccia, M.F. Lawrence, «DNA immobiliza-tion onto electrochemically functionalized Si(1 0 0) surfaces» Talanta 70 (2006) 615

30. S.S.C. Yu, E.S.Q. Tan, R.T. Jane, A.J. Downard, «An electrochemical and XPS studyof reduction of nitrophenyl films covalently grafted to planar carbon surfaces» Langmuir 23 (2007) 11074

31. Z. Nazemi, E. Shams, M.K. Amini, «Covalent modification of glassy carbonelectrode by Nile blue: preparation, electrochemistry and electrocatalysis» Electrochim. Acta 55 (2010) 7246

32. Y.C. Liu, R.L. McCreery, «Reactions of organic monolayers on carbon surfacesobserved with unenhanced raman spectroscopy» J. Am. Chem. Soc. 117 (1995)11254

33. J. Lyskawa, D. Bélanger, «Direct modification of a gold electrode withaminophenyl groups by electrochemical reduction of in situ generatedaminophenyl monodiazonium cations» Chem. Mater. 18 (2006) 4755

34. O.I. Covaci, B. Bucur, M.P. Bucur, G.L. Radu, «Optimization of acetylcholinesteraseimmobilization on microelectrodes based on nitrophenyl diazonium for sensitive organophosphate insecticides detection» Microchim. Acta 169 (2010) 335.

35. M. M. Gvozdenović, B. Z. Jugović, J. S. Stevanović, T. Lj. Trišović, B. N. Grgur, «Electrochemical Polymerization of Aniline» DOI: 10.5772/28293

36. Inzelt G., «Conducting Polymers – A New Era in Electrochemistry» 2008, Springer-Verlag, ISBN 978-3-540-75929-4, Berlin, Heidelberg

37. Horvat-Radošević V., Kvastek K., «Role of Pt-probe pseudo-reference electrode in impedance measurements of Pt and polyaniline (PANI) modified Pt electrodes» 2006, Journal of Electroanalytical Chemistry, Vol. 591, No. 2, pp. 217-222, ISSN1572-6657

38. Gospodinova N., Terlemezyan L., «Conducting polymers prepared by oxidative polymerization: polyaniline» Progress in Polymer Science, Vol. 23, No. 8, (December 1998), pp. 1443-1484, ISSN0079-6700

39. Gvozdenović M., Jugović B., Trišović T., Stevanović J., Grgur B. «Electrochemical characterization of polyaniline electrode in ammonium citrate containing electrolyte» Materials Chemistry and Physics, Vol. 125, No. 3, (February 2011), pp. 601-605, ISSN0254-0584

40. Jugović B., Trišović T., Stevanović J., Maksimović M., Grgur B., «Novel electrolyte for zinc–polyaniline batteries» Journal of Power Sources Vol. 160, No. 2, (October 2006), pp. 1447-1450 ISSN0378-7753

41. Jugović B., Gvozdenović M., Stevanović J., Trišović T., Grgur B., «Characterization of electrochemically synthesized PANI on graphite electrode for potential use in electrochemical power sources» Materials Chemistry and Physics, Vol. 114, No. 2-3, (April 2009), pp. 939-942, ISSN0254-0584

42. BezbradicaD., Jugović B., Gvozdenović M., Jakovetić S., Knežević-Jugović Z., «Electrochemically synthesized polyaniline as support for lipase immobilization» Journal of Molecular Catalysis B: Enzymatic, Vol. 70, No. 1-2, (June 2011), pp. 55-60, ISSN1381-1177

43. Dhaoui W., Bouzitoun M., Zarrouk H., Ouada H., Pron A., «Electrochemical sensor for nitrite determination based on thin films of sulfamic acid doped polyaniline deposited on Si/SiO2structures in electrolyte/insulator/semiconductor (E.I.S.) configuration» Synthetic Metals, Vol. 158, No.17-18, (October 2008), pp. 722-726, ISSN0379-6779

44. Grummt U., Pron A., Zagorska M., Lefrant S., «Polyaniline based optical pH sensor» Analytica Chimica Acta, Vol. 357, No. 3, (December 1997), pp. 253-259, ISSN0003-2670

45. Gvozdenović M., Jugović B., Bezbradica D., Antov M. Knežević-Jugović Z., Grgur B. «Electrochemical determination of glucose using polyaniline electrode modified by glucose oxidase» Food Chemistry, Vol. 124, No.1, (January 2011), pp.396-400, ISSN0308-8146

46. Mu S., Xue H., «film. Sensors and Actuators», B: Chemical, Vol. 31, No. 3, (March 1996), pp.155-160 ISSN0925-4005

47. Xu G., Wang W., Qu X., Yin Y., Chu L., He B., Wu H., Fang L., Bao Y., Liang L. «Electrochemical properties of polyaniline in p-toluene sulfonic acid solution» European Polymer Journal, Vol. 45, No. 9, (September 2009), pp. 2701-2707, ISSN0014-3057

48. Wallace G., Spinks G., Kane-Maguire L., Teasdale P., «Conductive Electroactive Polymers» CRC Press, Taylor & Francis Group, ISBN 978-1-4200-6709-5, Boca Raton

49. Biallozor S., Kupniewska A., «Conducting polymers electrodeposited on active metals» Synthetic Metals, Vol. 155, No. 3, (December 2005), pp. 443-449, ISSN0379-6779

50. Syed A., Dinesan M., «Polyaniline—A novel polymeric material» Talanta, Vol. 38, No. 8, (August 1991), pp. 815-837 ISSN0039-9140

51. Elkais A., Gvozdenović M., Jugović B., Stevanović J., Nikolić N., Grgur B. «Electrochemical synthesis and characterization of polyaniline thin film and polyaniline powder» Progress in Organic Coatings, Vol. 71, No. 1, (May 2011) pp. 32-35, ISSN0300-9440

52. Stejskal J., Sapurina I., Trchová M. «Polyaniline nanostructures and the role of aniline oligomers in their formation» Progress in Polymer Science, Vol. 35, No. 12, (December 2010), pp. 1420-1481, ISSN0079-6700

53. Bhadra S., Khastgir D., Singha N., Lee J., «Progress in preparation, processing and applications of polyaniline» Progress in Polymer Science, Vol. 34, No. 8, (August 2009), pp. 783-810, ISSN0079-6700

54. Nagarajan R., Tripathy S; Kumar J., Bruno F. & Samuelson L., «An Enzymatically Synthesized Conducting Molecular Complex of Polyaniline and Poly(vinylphosphonic acid)» Macromolecules, Vol. 33, No. 262, (November 2000), pp. 9542–9547 ISSN0024-9297

55. Hussain A., Kumar A., «Electrochemical synthesis and characterization of chloride doped polyaniline» Bulletin of Material Science, Vol. 26, No. 3, (April 2003), pp. 329-334 ISSN0250-4707

56. Mu S., Chen C., Wan J., «The kinetic behavior for the electrochemical polymerization of aniline in aqueous solution» Synthetic Metals, Vol.88, (April 1997), pp. 249-254, ISSN0379-6779

57. Camalet J., Lacroix J., Ngyen T., Aeiyach S., Pham M., Petit Jean J., Lacaze P.-C. «Aniline electropolymerization on platinum and mild steel from neutral aqueous media» Journal of Electroanalytical Chemistry, Vol. 485, No.1 (May 2000) pp. 13-20, ISSN1572-6657

58. Córdova R., del Valle M., Arratia A., Gómez H. Schrelber R., «Effects of anions on the nucleation and growth mechanism of polyaniline» Journal of Electroanalytical Chemistry, Vol. 377, No. 1-2, (October 1994), pp. 75-83, ISSN1572-6657

59. Nunziante P., Pistoia G., «Factors affecting the growth of thick polyaniline films by the cyclic voltmmetry technique» Electrochimica Acta, Vol. 34, No. 2, (February 1989), pp. 223-228, ISSN0013-4686

60. Okamoto H., Okamoto M., Kotaka T., «Structure and properties of polyaniline films prepared via electrochemical polymerization. II: Structure and properties of polyaniline films prepared via electrochemical polymerization» Polymer, Vol. 39, No. 18, (1998), pp. 4359-367 ISSN0032-3861

61. Karyakin A., Strakhova A., Yatsimirsky A., «Self-doped polyanilines electrochemically active in neutral and basic aqueous solutions.: Electropolymerization of substituted anilines» Journal of

Electroanalytical Chemistry, Vol. 371, No. 1-2, (June 1994), pp. 259-265, ISSN1572-6657

62. Mattoso L., Bulhões L., «Synthesis and characterization of poly(o-anisidine) films» Synthetic Metals, Vol. 52, No. 2, (October 1992), pp. 171-181, ISSN0379-6779

63. Fedorko P., Trznadel M., Pron A., Djurado D., Planès J., Travers J. «New analytical approach to the insulator–metal transition in conductive polyaniline» Synthetic Metals, Vol. 160, No. 15-16, (August 2010), pp. 1668-1671, ISSN0379-6779

64. Pron A., Rannou P., «Processible conjugated polymers: from organic semiconductors to organic metals and superconductors» Progress in Polymer Science, Vol. 27, No. 1, (February 2002), pp. 135-190, ISSN0079-6700

65. Stejskal J., Kratochvíl, Jenkins A., «The formation of polyaniline and nature of its structures» Polymer, Vol. 37, No. 2, pp. 367-369, (February 1996), ISSN0032-3861

66. S. Kango, «Progress in Polymer Science» 38, (2013), 1232-1261

67. D. Dragoman, M. Dragoman, «Advanced Optoelectronic Devices» Springer, BerlinHeidelberg, 2000.

68. H. Zimmermann, «Integrated Silicon Optoelectronics» Springer, Berlin Heidel-berg, 2000.

69. N. Daldosso, L. Pavesi, «Low-dimensional silicon as a photonic material» in: V.Kumar (Ed.), Nanosilicon, Elsevier Ltd, Oxford, 2007, pp. 314–333.

70. G. Masini, L. Colace, G. Assanto, Mater. Sci. Eng. B 89 (2002) 2–9

71. G. Reed, A. Kewell, Mater. Sci. Eng. B 40 (1996) 207–215.

72. A.J. Kenyon, Semicon. Sci. Tech. 20 (2005) R65–R84.

73. F. Priolo, G. Franzò, S. Coffa, A. Polman, S. Libertino, R. Barklie, D. Carey, J. Appl.Phys. 78 (1995) 3874–3882.

74. Sambhu Badhra et al., Progress in Polymer Science 34, (2009), 783-810

75. Pawan Kumar et al., Synthetic Metals 160, (2010), 1507–1512

76. R.F. Carvalhal, D.S. Machado, R.K. Mendes, A.L.J. Almeida, N.H. Moreira, M.H.O.Piazetta, A.L. Gobbi, L.T. Kubota, «Development of a disposable amperometricbiosensor for salicylate based on a plastic electrochemical microcell» Biosens.Bioelectron. 25 (2010) 2200

77. I. Willner, R. Baron, B. Willner, «Integrated nanoparticle–biomolecule systemsfor biosensing and bioelectronics» Biosens. Bioelectron. 22 (2007) 1841.

78. Y. Xiao, F. Patolsky, E. Katz, J.F. Hainfeld, I. Willner, «Plugging into enzymes:nanowiring of redox enzymes by a gold nanoparticle» Science 299 (2003)1877.

79. A. Määttänen, U. Vanamo, P. Ihalainen, P. Pulkkinen, H. Tenhu, J. Bobacka, J.Peltonen, «A low-cost paper-based inkjet-printed platform for electrochemicalanalyses» Sens. Actuators B 177 (2013) 153.

80. P.K. Ivanova-Mitseva, V. Fragkou, D. Lakshmi, M.J. Whitcombe, F. Davis, A.Guerreiro, J.A. Crayston, D.K. Ivanova, P.A. Mitsev, E.V. Piletska, S.A. Piletsky, «Conjugated polymers with pendant iniferter units: versatile materials for grafting» Macromolecules 44 (2011) 1856.

81. F. Xu, W. Shao, T. Abdiryim, R. Jamal, «The study on the application of solid-state method for synthesizing the polyaniline/noble metal (Au or Pt) hybridmaterials» Nanoscale Res. Lett. 8 (2013) 117

82. X. Li, «Improving the electrochemical properties of polyaniline by co-doping with titanium ions and protonic acid» Electrochim. Acta 54 (2009)5634

83. G. Inzelta, M. Pineri, J.W. Schultze, M.A. Vorotyntsev, «Electron and proton con-ducting polymers: recent developments and prospects» Electrochim. Acta 45(2000) 2403

84. H. Su, T. Wang, S. Zhang, J. Song, C. Mao, H. Niu, B. Jin, J. Wu, Y. Tian, «Facile synthesis of polyaniline/TiO2/grapheme oxide composite for high performance supercapacitors», Solid State Sci. 14 (2012) 677.

85. L. Ding, D. Du, J. Wu, H. Ju, «A disposable impedance sensor for electrochemicalstudy and monitoring of adhesion and proliferation of K562 leukemia cells» Electrochem. Commun. 9 (2007) 953.

86. G. Milczarek, «Electrochemical modification of poly-aniline films in the presenceof guaiacol-sulfonic acid» Electrochem. Commun. 9 (2007) 123.

87. A. Morrin, F. Wilbeer, O. Ngamna, A.J. Killard, S.E. Moulton, M.R. Smyth, G.G.Wallace, «Novel biosensor fabrication methodology based on processable conducting polyaniline nanoparticles» Electrochem. Commun. 7 (2005) 317.

88. P.R. Bidez, S.X. Li, A.G. MacDiarmid, E.C. Venancio, Y. Wei, P.I. Lelkes, «Polyaniline, an electroactive polymer, supports adhesion and proliferation of cardiacmyoblasts» J. Biomater. Sci. Polym. Edn. 17 (2006) 199.

89. M. Li, Y. Guo, Y. Wei, A.G. MacDiarmid, P.I. Lelkes, «Electrospinning polyaniline-contained gelatin nanofibers for tissue engineering applications» Biomaterials 27 (2006) 2705.

90. M.P. Prabhakaran, L. Ghasemi-Mobarakeh, G. Jin, S. Ramakrishna, «Electrospunconducting polymer nanofibers and electrical stimulation of nerve stem cells» J. Biosci. Bioeng. 112 (2011) 501.

91. W.K. Oh, S. Kim, K.H. Shin, Y. Jang, M. Choi, J. Jang, «Inkjet-printed polyanilinepatterns for exocytosed molecule detection from live cells» Talanta 105 (2013)333.

92. J. Jang, S. Ko, Y. Kim, «Dual-functionalized polymer nanotubes as substrates formolecular-probe and DNA-carrier applications» Adv. Funct. Mater. 16 (2006)754.

93. T. Ahuja, I.A. Mir, D. Kumar, R. Rajesh, «Biomolecular immobilization onconducting polymers for biosensing applications» Biomaterials 28 (2007)791.

94. H.C. Budnikov, G.A. Evtugyn, A.V. Porfireva, «Electrochemical DNA sensors basedon electropolymerized materials» Talanta 102 (2012) 137.

95. C.C. Hu, C.H. Chu, «Electrochemical impedance characterization of polyaniline-coated graphite electrodes for electrochemical capacitors – effects of filmcoverage: thickness and anions» J. Electroanal. Chem. 503 (2001) 105.

96. K. Aoki, M. Kawase, «Introduction of a percolation threshold potential atpolyaniline-coated electrodes» J. Electroanal. Chem. 377 (1994) 125

97. C. Gabrielli, M. Keddam, N. Nadi, H. Perrot, «Ions and solvent transport acrossconducting polymers investigated by ac electrogravimetry. Application to polyaniline» J. Electroanal. Chem. 485 (2000) 101

98. S. Wang, «Optimum degree of functionalization for carbon nanotubes» Curr. Appl.Phys. 9 (2009) 1146.

99. L.M. Santos, J. Ghilane, C. Fave, P.C. Lacaze, H. Randriamahazaka, L.M. Abrantes, J.C. Lacroix, «Electrografting polyaniline on carbon through the electroreductionof diazonium salts and the electrochemical polymerization of aniline» J. Phys.Chem. C 112 (2008) 16103.

100. L. Pilan, M. Raicopol, A. Pruna, V. Branzoi, «Polyaniline/carbon nanotube composite films electrosynthesis through diazonium salts electroreduction and electrochemical polymerization» Surf. Interface Anal. 44 (2012)1198.

101. C. Deetuam, D. Weise, C. Samthong, P. Praserthdam, R. R. Baumann, A. Somwangthanaroj, J. Appl. Polym. Sci., 2015, 132, 42108-42117

102. S. Rattan, P. Singhal and A. L. Verma, Polym. Eng. Sci., 2013, 53, 2045-2052

103. M. Stavytska-Barba and A.M. Kelley, J. Phys. Chem. C, 2010, 114, 6822-6830

104. T. Y. Wu, Z. Y. Kuo, J. J. Jow, C. W. Kuo, C. J. Tsai, P. R. Chen and H. R. Chen, Int. J.Electrochem. Sci., 2012, 7, 8076-8090

105. Z. Xiong and C. Liu, Org. Electron., 2012, 13, 1532–1540

106. X. Wu, J. Liu, D. Wu, Y. Zhao, X. Shi, J. Wang, S. Huang and G. He, J. Mater. Chem. C, 2014, 2, 4044-4050

107. B. H. Zhang, G. P. Tan, Z. Y. Xie, W. Y. Wong, J. Q. Ding and L. X. Wang, Adv. Mater., 2012, 24, 1873-1877

108. R. Jalili, J. M. Razal, P. C. Innis and G. G. Wallace, Adv. Funct. Mater., 2011, 21, 3363–3370

109. H. Okuzaki, Y. Harashina and H. Yan, Eur. Polym. J., 2009, 45, 256–261

110. H. C. Budnikov, G. A. Evtugyn and A. V. Porfireva, Talanta, 2012, 102, 137–155

111. H. Shi, C. Liu, J. Xu, H. Song, B. Lu, F. Jiang, W. Zhou, G. Zhang and Q. Jiang, ACS Appl. Mater. Interfaces, 2013, 5, 12811−12819

112. L. Zhang, H. Peng, P. A. Kilmartin, C. Soeller, and J. Travas-Sejdic, Macromolecules, 2008,41, 7671-7678

113. H. Shi, C. Liu, J. Xu, H. Song, Q. Jiang, B. Lu, W. Zhou and F. Jiang, Int. J. Electrochem. Sci., 2014, 9, 7629-7643

114. H. Shi, C. Liu, Q. Jiang, J. Xu, B. Lu, F. Jiang and Z. Zhu, Nanotechnology, 2015, 26, 245401-245409

115. T. G. Drummond,M. G. Hill, J. K. Barton, «Bioelectronics. From theory to applications» Nat. Biotechnol., 2003, 21, 1192–1199

116. E. Palecek and F. Jelen, Crit. Rev. Anal. Chem., 2002, 32, 261–270

117. R. J. Lipshutz, D. Morris, M. Chee, E. Hubbell, M. J. Kozal, N. Shah, N. Shen, R. Yang and S. P. Fodor, Biotechniques, 1995, 19, 442–447

118. Guido Mula et al., Nanoscale Res. Lett.7, (2012), 377

119. A.B.Steel, T.M.Herne, M.J.Tarlov, «Electrochemical quatitation of DNA immobilized on gold» Anal. Chem. 1998, 70, 4670-4677

120. Z. Li, L. Zhang, G. Cheng, X. Yang, J. Zhou, Y. Chen, «Effect of Potential Window, Concentration of Hexaammineruthenium (III) and pH on Electrochemical Quantification of Thiol-Modified DNA Monolayers on Gold» Int. J. Electrochem. Sci., 9 (2014) 4241 – 4250

121. G. Zhong, A. Liu, X. Xu, Z. Sun, J. Chen, K. Wang, Q. Liu, X. Lin, J. Lin, «Detection of femtomolar level osteosarcomarelated gene via a chronocoulometric DNA biosensor based on nanostructure gold electrode» International Journal of Nanomedicine 2012:7 527–536

122. M. Khoshroo, A.A. Rostami, «Characterization of the organic molecules depositedat gold surface by the electrochemical reaction of diazonium salts» J. Electroanal.Chem. 647 (2010) 117.

123. K. Darowicki, J. Kawula, «Impedance characterization of the process of polyaniline first redox transformation after aniline electropolymerization» Electrochim. Acta 49 (2004) 4829

124. M. Zic, «The effect of the PANI-free volume on impedance response» J. Electroanal.Chem. 610 (2007) 57.

125. H. Lu, Y. Zhou, S. Vongehra, K. Hu and X. Meng, Synth. Met., 2011, 161, 1368–1376

126. Q. Wang, Q. Yao, J. Chang and L. D. Chen, J. Mater. Chem., 2012, 22, 17612-17618

127. L. Fan, N. Zhang and K. Sun, Chem. Commun., 2014, 50, 6789-6792

128. M. H. Yeh, C.P. Lee, C. Y. Chou, L. Y. Lin, H. Y. Wei, C.W. Chu, R. Vittal and K. C. Ho, Electrochim. Acta, 2011, 57, 277–284

129. P. Danielsson, J. Bobacka, and A. Ivaska, J. Solid State Electrochem., 2004, 8, 809-817

130. J. Bobacka, A. Lewenstam and A. Ivaska, J. Electroanal. Chem., 2000, 489, 17-27

131. J. Y. Ouyang, C. W. Chu, F. C. Chen, Q. Xu, and Y. Yang, J. Macromol. Sci. A, 2004, 41, 1497–1511

132. H. S. Dehsari, E. K. Shalamzari, J. N. Gavgani, F. A. Taromi and S. Ghanbary, RSC Adv., 2014, 4, 55067- 55076

133. A. A. Karyakin, O. A. Bobrova, L. V. Luckachova, and E. E. Karyakina, Sens. Actuators, B:Chem., 1996, 33, 34-38

134. B. Lakard, G. Herlem, S. Lakard, R. Guyetant and B. Fahys, Polymer, 2005, 46, 12233–12239

135. A. Pinna, F. Simbula, D. Marongiu, A. Pezzella, M. d'Ischia, G. Mula, «Boosting, probing and switching-off visible light-induced photocurrents in eumelanin-porous silicon hybrids» RSC Adv., 2015,5, 56704-56710

136. F. Turcu, A. Schulte, G. Hartwich, W. Schuhmann, «Imaging immobilised ssDNA and detecting DNA hybridisation by means of the repelling mode of scanning electrochemical microscopy (SECM) » Biosensors and Bioelectronics 20 (2004) 925–932

137. M. Gebala, L. Stoica, S. Neugebauer, W. Schuhmann, «Label-Free Detection of DNA Hybridization in Presence of Intercalators Using Electrochemical Impedance Spectroscopy» Volume 21, Issue 3-5, pages 325–331, February 2009

138. S. Grützke, S. Abdali, W. Schuhmann, M. Gebala, «Detection of DNA hybridization using electrochemical impedance spectroscopy and surface enhanced Raman scattering» Electrochemistry Communications 19 (2012) 59–62

139. L.V. Hai, S. Reisberg, A. Chevillot-Biraud, V. Noel, M.C. Pham, B. Piro, «Simultaneous Electroreduction of Different Diazonium Salts for Direct Electrochemical DNA Biosensor Development» Electrochimica Acta 140:49-58 September 2014

140. Allen J. Bard, Larry R. Faulkner, Electrochemical Methods: Fundamentals and Applications

Table of symbols

Roman symbols

A	Surface area	cm^2
c_i^{∞}	Concentration of the species *i* in the bulk solution	mol cm^{-3}
c_i^{σ}	Concentration of the species *i* at the electrode surface	mol cm^{-3}
C_{dl}	Double layer capacitance	F cm^{-2}
D	Diffusion coefficient	cm^2 s^{-1}
E	Potential of an electrode vs a reference	V
E^0	Standard potential	V
E_{eq}	Equilibrium potential	V
F	Faraday's constant	C mol^{-1}
i	Current density	A cm^{-2}
i_0	Exchange current density	A cm^{-2}
i_p	Peak current density	A cm^{-2}
I	Current intensity	A
I(Q)	Scattered intensity	-
J_i	Flux of species i	mol cm^{-2} s^{-1}
k	Rate constant for a chemical reaction	cm s^{-1}

k_0	Standard rate constant	cm s^{-1}
K	Equilibrium constant	
m	Moles of electroactive species in electrolysis cell	mol
M	Molar	mol/L
n	Electron numbers	-
Q	Charge	C
Q	Scattered wave vector	-
R	Gas constant	J mol^{-1} K^{-1}
R	Resistance	Ω
t	Time	s
T	Absolute temperature	K
x	Distance perpendicular to the electrode surface	cm

Greek symbols

α	Transfer coefficient	-
η	Overpotential	V
θ	Scattering angle	°
λ	X-ray wave length	-
ν	Potential scan rate	V s^{-1}
τ	Transition time	s

Acronims

ACN	Acetonitrile
Au(111)	Monocrystalline gold
[BMP] [TFSA]	1-butyl-1-methylpyrrolidinium bis(trifluoromethylsulfonyl)imide
C	Carbon
CV	Cyclic Voltammetry
EDC	N-(3-Dimethylaminopropyl)-N′-ethylcarbodiimide
FIB	Focused ion beam
IL	Ionic Liquid
$K_3Fe(CN)_6$	Potassium ferri-cyanide
$K_4Fe(CN)_6$	Potassium ferro-cyanide
KH_2PO_4	Potassium dihydrogenophosphate
K_2HPO_4	Di-potassium hydrogenophosphate
KCl	Potassium chloride
NaCl	Sodium chloride
NBD	4-nitrobenzenediazonium
NHS	N-Hydroxysuccinimide
OCP	Open circuit potential
OHP	Outer Helmholtz Plane
PANI	Polyaniline
PEDOT:PSS	Poly(3,4-ethylenedioxythiophene): poly(styrenesulfonic acid) complex
PB	Phosphate buffer

Pt	Platinum
SCE	Satured Calomel Electrode
SEM	Scanning Electron Microscopy
$TBAPF_6$	tetrabutylammonium hexafluorophosfate

List of figures